STRUCTURAL AND BIOCHEMICAL INSIGHTS INTO METHYLATION SITE AND STATE SPECIFICITY OF JMJD2 LYSINE DEMETHYLASES

by

Swathi Krishnan

A dissertation submitted in partial fulfillment
of the requirements for the degree of
Doctor of Philosophy
(Biological Chemistry)
in the University of Michigan
2012

Doctoral Committee:

Associate Professor Raymond C. Trievel, Chair
Professor Carol A. Fierke
Assistant Professor Georgios Skiniotis
Professor John J. G. Tesmer
Associate Professor Xiaochun Yu

To my family

ACKNOWLEDGEMENTS

It has been a valuable learning experience for me at the University of Michigan, Ann Arbor. Firstly, I thank Dr. Ray Trievel for giving me an opportunity to work in his lab. Ray has been helpful in many ways and been very generous with many expensive reagents and peptides that have been instrumental in my thesis research. I also thank him for encouraging me to apply for various grants and awards, writing review articles and reviewing manuscripts and helping me become a well-rounded researcher. I thank my thesis committee members for providing valuable suggestions and discussions and for making it all the way to the MSRB buildings for my 9am meetings.

I thank Paul, for helping me with almost everything in the lab and for all the great conversations and Stacie, who taught me crystallography when I knew nothing about it, and helped me get my driver's license! Thanks to Kim for being a vibrant presence in the lab and always encouraging me to smile through tough times. I also thank the Biochem students and staff, particularly, Beth for all the help and support.

I would not be the person I am today without my mom and dad and I am immensely grateful to them for being my source of strength even when they were 9000 miles away. Thanks Preethi for being my moral support, friend and confidante for the past 25 years! You are the best sister anyone can ask for. Lastly, but by no means the least, I thank Rozario who, made me fall in love with New York City and him, showed me how baseball can be fun and changed my life in the most wonderful ways possible. As long as I am with you, I will consider myself the luckiest person in the world.

TABLE OF CONTENTS

LIST OF FIGURES

LIST OF TABLES

LIST OF ABBREVIATIONS

2-OG, 2-oxoglutarate

AR, androgen receptor

BSA, bovine serum albumin

ChIP, chromatin immunoprecipitation

DTT, dithiothreitol

EDTA, ethylenediaminetetraacetic acid

ERα, estrogen receptor α

FAD, flavin adenine dinucleotide

FDH, formaldehyde dehydrogenase

FPLC, fast performance liquid chromatography

HP1, heterochromatin protein 1

HPLC, high-performance liquid chromatography

IC_{50}, apparent inhibitor constant

ICP-HRMS, inductively coupled plasma-high resolution mass spectroscopy

Il12b, interleukin 12b

IMAC, immobilized metal affinity chromatography

ING, inhibitor of growth

IPTG, isopropyl β-D-1-thiogalactopyranoside

JmjC, jumonji C

KDM, lysine demethylase

KLK, kallikrein

KMT, lysine methyltransferase

LSD1, lysine specific demethylase

Mdc, macrophage-derived chemokine

MLL, mixed lineage leukemia

NAD^+, nicotinamide adenine dinucleotide

NADH, nicotinamide adenine dinucleotide-reduced

NOG, N-oxalylyglycine

Oct4, octamer-binding transcription factor 4

pAF, para-aminophenylalanine

PEG, polyethylene glycol

PHD, plant homeodomain

PSA, prostate specific antigen

RFU, relative fluorescence units

RMSD, root mean square deviation

SDS-PAGE, sodium dodecylsulfate polyacrylamide gel electrophoresis

SER, surface entropy reduction

TEV, tobacco etch virus

TFF1, trefoil factor 1

TSS, transcription start site

WT, wildtype

ABSTRACT

The human JMJD2/KDM4 family of histone lysine demethylases comprises four homologs: JMJD2A, JMJD2B, JMJD2C and JMJD2D. These enzymes have been implicated in a number of biological processes such as transcriptional activation, development and cell cycle control. The biological functions of these enzymes are defined by their distinct methylation site and state specificities. JMJD2A, JMJD2B and JMJD2C display dual specificity for trimethylated histone H3 Lys9 and Lys36 (H3K9me3 and H3K36me3), whereas JMJD2D is specific for H3K9me3. Furthermore, while most JMJD2 homologs are predominantly trimethyllysine-specific, JMJD2D can demethylate both tri- and dimethyllysines. To enable quantitative kinetic studies of JMJD2 demethylases, we developed and applied a new affinity purification protocol that minimizes contamination by transition state metals. In order to delineate the molecular basis of site and state specific demethylation by the JMJD2 enzymes, we determined the first crystal structure of JMJD2D in the apoenzyme form and in a ternary complex with 2-OG and an H3K9me3 peptide. Our site specificity studies with JMJD2A and JMJD2D revealed surprising differences in H3K9me3 recognition by these enzymes despite the overall similarity in the substrate binding conformation. In addition, our docking studies with H3K36me3 and biochemical analysis with histone H3 hybrid peptides underscored the role of steric clashes, electrostatic clashes and loss of productive hydrogen bonds in occluding recognition of the H3K36me3 site by JMJD2D. Our structural and biochemical analysis of the active site also revealed the basis for differential state specificity in the JMJD2 enzymes and highlighted the role of CH•••O hydrogen bonds in di- and trimethyllysine substrate recognition. Together, these

structural and biochemical studies elucidate the molecular basis of the different substrate specificities within the JMJD2 family, which is not only key to understanding their distinct biological functions but will also aid in the structure-based design of selective inhibitors of JMJD2 enzymes implicated in disease.

CHAPTER 1

HISTONE LYSINE DEMETHYLASES

Histone Modifications and Regulation of Gene Expression

The genomic DNA of eukaryotes is compacted into a higher-ordered structure termed chromatin. The fundamental unit in chromatin is the nucleosome, which is composed of basic proteins called histones. Histones H2A, H2B, H3 and H4 form an octameric core around which approximately 146bp of DNA is wrapped (corresponding to 1.7 turns of DNA). Linker histone H1 and linker DNA further compact the nucleosome core particles to a 30nm fiber. The crystal structure of the nucleosome core particle revealed that the N-terminal tails of the histone proteins are exposed outside the nucleosome core (Figure 1.1) and are highly disordered [1]. Many amino acid residues on these tails as well as in the core are subject to a number of post-translational modifications such as acetylation, methylation, phosphorylation, ubiquitination, sumoylation, etc. Each of these modifications can 'code' for different functions depending on the type, location and context of the modification [2, 3]. One of the first well characterized modifications, histone lysine acetylation is associated with transcriptional activation because neutralization of the ε amine group of lysines by acetylation dissociates DNA from histones, hence allowing access for the transcriptional machinery [4]. In addition, acetylated lysines recruit chromatin remodeling complexes such as nucleosome remodeling factor (NURF), which can bind to acetyllysines via bromodomain containing reader molecules such as Bromodomain PHD finger transcription factor (BPTF) and lead to an 'open' chromatin state [5]. Correlatively, hypo-

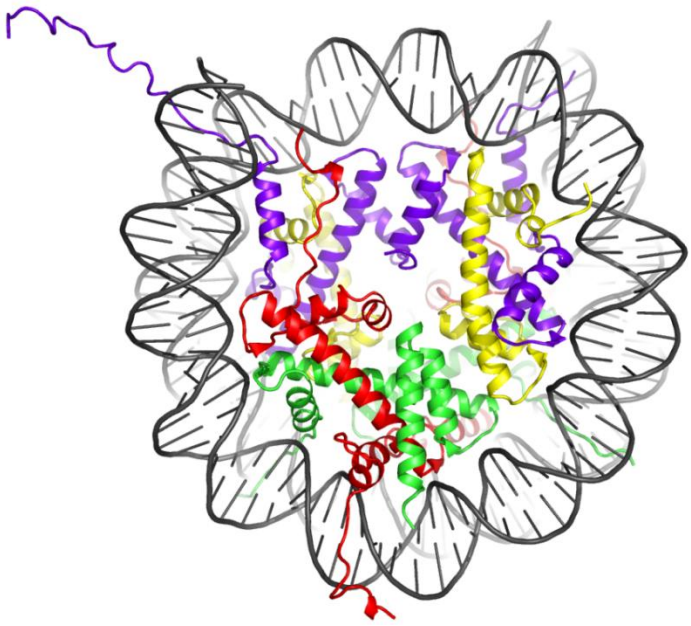

Figure 1.1: Crystal Structure of a Nucleosome Core Particle. Red: H2A; Green: H2B; Purple: H3; Yellow: H4; Black: DNA (PDB ID: 1AOI).

acetylated regions of chromatin are often associated with poor transcribed regions. In summary, histone modifications can modulate the structure and dynamics of chromatin by chemically altering the nucleosomal interactions and recruiting a number of regulatory complexes.

Biological Functions of Histone Lysine Methylation

Lysine methylation is an abundant modification predominantly occurring on histones H3 and H4. Unlike many histone modifications, methylation is unique because it can bring about varied responses based on which residue is methylated (the site) and the extent or state of methylation (mono-, di- or trimethylation in the case of lysines) [6, 7]. For example, methylation of H3K4 is often associated with transcriptional activation and methylation of H3K36 is a mark that is associated with the elongating form of RNA Polymerase II. In contrast, methylation of H3K9 and H3K27 are linked to silent genes or heterochromatin [8]. Similar to the site, the state of methylation can signal for diverse outcomes. For example, tri and dimethylation of H3K9 demarcates repressed genes and heterochromatin while monomethylation of the same residue is seen in actively transcribed genes [9]. These differential effects are often brought about by different 'reader' molecules that are highly state and site specific, and signal for the outcome associated with a particular methylation mark [10]. For example, one of the readers of H3K4me3 is the inhibitor of growth proteins ING3-5. These proteins form a part of the histone acetyl transferase complex and enhance transcription activation via histone acetylation [11, 12]. Similarly, the protein Heterochromatin Protein 1 (HP1) is highly specific for H3K9me3/me2 and is required for the efficient formation and maintenance of heterochromatin [13, 14]. In yeast, the protein Esa1p-associated factor (Eaf3) specifically recognizes H3K36me3 via its chromodomain and recruits the reduced potassium dependency 3 small (Rpd3S) histone deacetylase complex to

H3K36me3 containing coding regions to hypoacetylate histones and prevent spurious transcriptional initiation by RNA Polymersase II [15-18]. A comprehensive list of functions associated with different histone methylation marks on the H3 tail is shown in Table 1.1. These various methylation marks are actively deposited and removed in a very specific manner by enzymes called Lysine Methyltransferases (KMTs) and Lysine Demethylases (KDMs), respectively. The biological functions of these enzymes are in part determined by their methylation site and state specificities.

Mechanisms of Histone Lysine Demethylation

For many years, lysine methylation was thought to be an irreversible modification owing to the strong nature of the C-N covalent bond. This notion was eradicated with the discovery of the first KDM called Lysine Specific Demethylase 1 (LSD1) [19], which catalyzes the demethylation of H3K4me2 and H3K4me1 [19, 20] and has been reported to demethylate non-histone substrates such as p53 [21, 22]. These enzymes are FAD-dependent monoamine oxidases that oxidize the amino group of the methylated lysine (with the concomitant reduction of the cofactor FAD) to generate an imine intermediate. This intermediate spontaneously hydrolyzes to release formaldehyde. Hydrogen peroxide is also a by-product of this reaction and is formed by the re-oxidation of FAD by molecular oxygen. The LSD family of KDMs is highly efficient with turnover numbers (k_{cat}) ranging from 2-12 min^{-1} depending on the length of the histone substrate used and the method by which the enzyme is assayed [20, 23-25]. Although these enzymes can catalyze the demethylation of mono and dimethyllysines, their need for protonated nitrogen (to form the imine intermediate) precludes them from demethylating trimethylated lysines [19, 26, 27].

Table 1.1: Functions of Histone H3 Lysine Methylation

Methylation Site	Methylation State	Functions
H3K4	me3, me2	transcriptional activation (observed in promoter regions), chromatin remodeling [9, 28, 29]
	me1	transcriptional activation (observed in enhancer regions), chromatin remodeling [28, 29]
H3K9	me3, me2	transcriptional silencing, heterochromatin formation [9, 13]
	me1	transcriptional activation (observed in promoter regions) [9], heterochromatin assembly [30], nuclear assembly of newly synthesized histones [31]
H3K27	me3, me2	transcriptional silencing mediated by Polycomb group proteins [9, 32, 33]
	me1	transcriptional activation (observed in promoter regions) [9]
H3K36	me3, me2, me1	transcriptional elongation, prevention of spurious transcription by RNA Polymerase(II), regulation of histone deacetylation [9, 34, 35]

The Jumonji demethylases (JmjC) are a much larger family and are related to the cupin family of dioxygenses. These enzymes use Fe(II), 2-oxogluatrate (2-OG) and molecular oxygen to catalyze the demethylation of tri, di and monomethyllysines [26, 36-38]. The catalytic mechanism of JmjC enzymes is shown in Figure 1.2. In the active site, Fe(II) is first coordinated by a conserved His-Glu/Asp-His triad followed by the binding of 2-OG and molecular oxygen. This results in the formation of a highly reactive oxoferryl (IV) species and the oxidative decarboxylation of 2-OG to succinate. The oxoferryl (IV) species hydroxylates the substrate methyllysine group, and this results in the formation of an unstable carbinolamine intermediate that spontaneously decomposes to formaldehyde and the demethylated product.

The JmjC family encompasses a number of subfamilies such as JHDM1 (KDM2), JMJD1 (KDM3), JMJD2 (KDM4), JARID1, (KDM5), UTX/JMJD3 (KDM6), and PHF8/KIAA1718 (KDM7). These enzymes have been implicated in a number of biological processes such as nuclear hormone signaling (JMJD2), transcriptional repression (JARID) and activation (JMJD2, UTX/JMJD3) and developmental signaling (UTX/JMJD3, JMJD2, PHF8) These enzyme families exhibit distinct methylation site and state specificities (Figure 1.3) which can largely determine their biological functions [26, 27, 37, 39-42]. For example, the UTX/JMJD3 sub-family of enzymes catalyzes the removal of H3K27me3/me2, a repressive mark that is often enriched in developmental gene loci. It has been shown that UTX forms a part of the Mixed Lineage Leukemia (MLL)2/3 complex, an H3K4 methyltransferase complex that is involved in the upregulation of *hox* genes during development. The deposition of H3K4me3 (an activating mark) by the MLL methyltransferase in concert with the removal of the repressive mark H3K27me3/me2 by UTX results in the robust transcription of the *hox* genes [33].

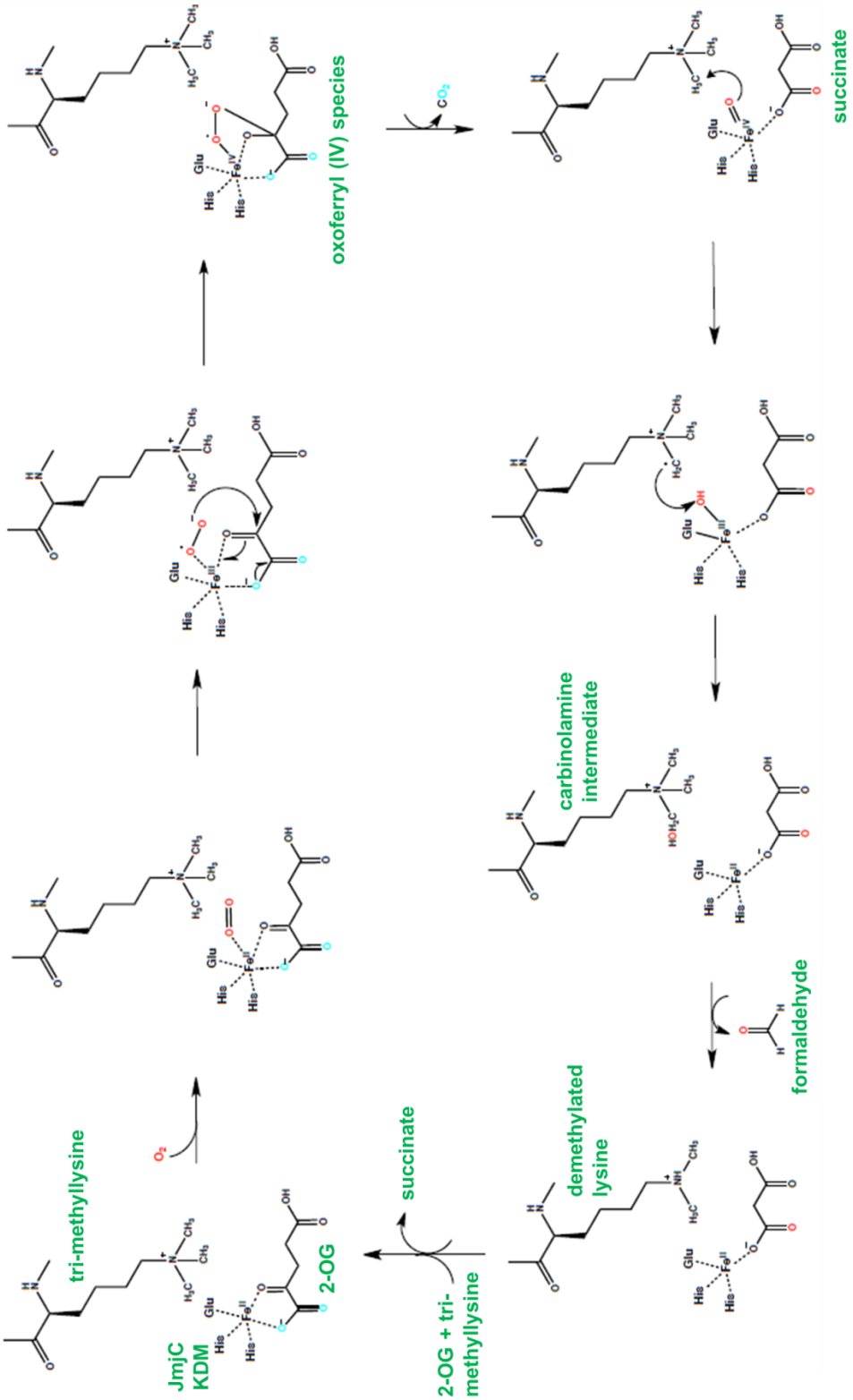

Figure 1.2: Catalytic mechanism of JmjC Lysine Demethylases

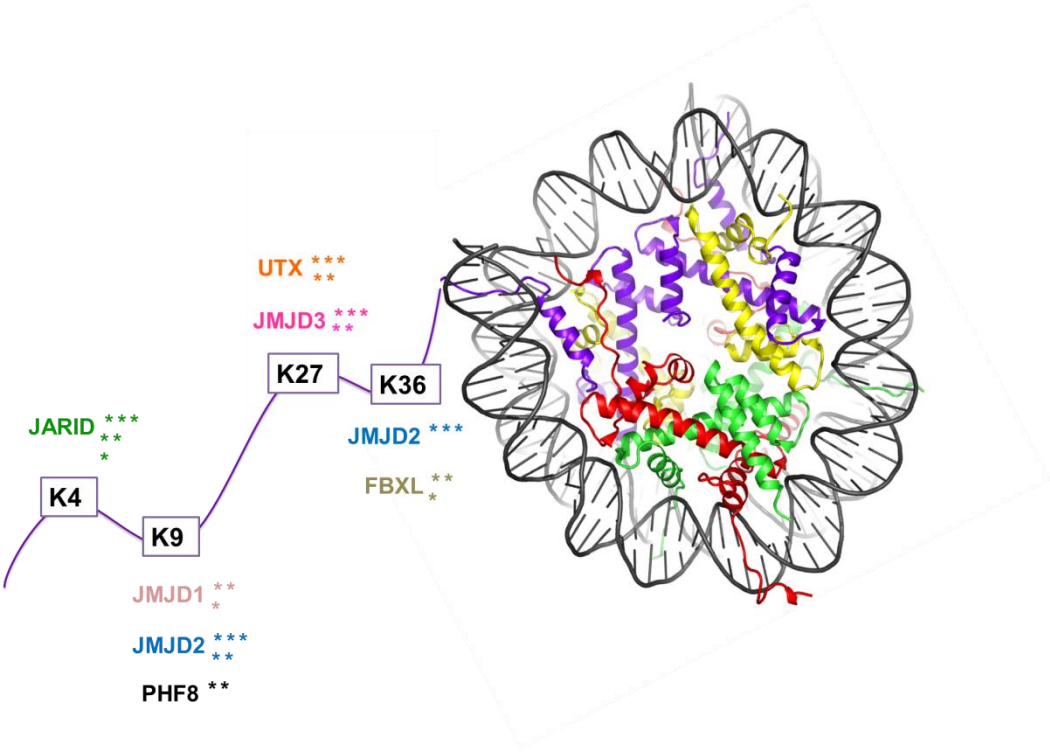

Figure 1.3: Differential Methylation Site and State specificity in JmjC KDMs. Enzymes specific for tri-, di- and monomethyl lysines are depicted with ***, ** and * respectively.

JMJD2 KDMs in Biology and Disease

The JMJD2 family (also denoted as the KDM4 family) of demethylases is highly conserved from yeast to humans [36, 43-49]. The human JMJD2 family includes four homologs: JMJD2A (KDM4A), JMJD2B (KDM4B), JMJD2C (KDM4C) and JMJD2D (KDM4D). These enzymes contain an N terminal JmjN domain followed by the catalytic JmjC domain and a large C terminal region (Figure 1.4). In JMJD2A, JMJD2B and JMJD2C, the C terminal region is followed by tandem PHD and Tudor domains, while these domains are absent in JMJD2D (Figure 1.4). The PHD and Tudor domains are involved in the recognition of other chromatin modifications such as methylated lysines and arginines on histone H3 [10]. Structural studies by Huang *et al* have shown that the double Tudor domain of JMJD2A recognizes H3K4me3 and potentially, H4K20me3 [50]. All JMJD2 KDMs catalyze the demethylation of H3K9me3 and the closely related H1.4K26me3 (a repressive mark seen in linker histones) and some homologs can also demethylate H3K36me3 [27, 45]. These enzymes have been implicated in regulating numerous genomic processes, such as transcription, cell cycle progression, nuclear hormone signaling, embryonic stem cell self-renewal, and development [27, 41, 42, 51-57]. JMJD2A, JMJD2C and JMJD2D form stable complexes with the Androgen Receptor (AR) and upregulate the expression of downstream targets such as the Prostate Specific Antigen (PSA) and Kallikrein (KLK) by removing H3K9me3 at the *PSA* and *KLK* promoters [58, 59]. JMJD2C is also a target of the transcription factor Oct4, and is required for the maintenance of stem cell pluripotency [55]. JMJD2A has been implicated in regulating cell cycle progression and DNA replication timing by antagonizing the occupancy of the heterochromatin protein HP1γ [51]. JMJD2B has been shown to associate with the MLL-2 complex and Estrogen Receptor-α (ERα) and upregulate the expression of ERα target genes such as Trefoil factor 1 (TFF1) and cathepsin D

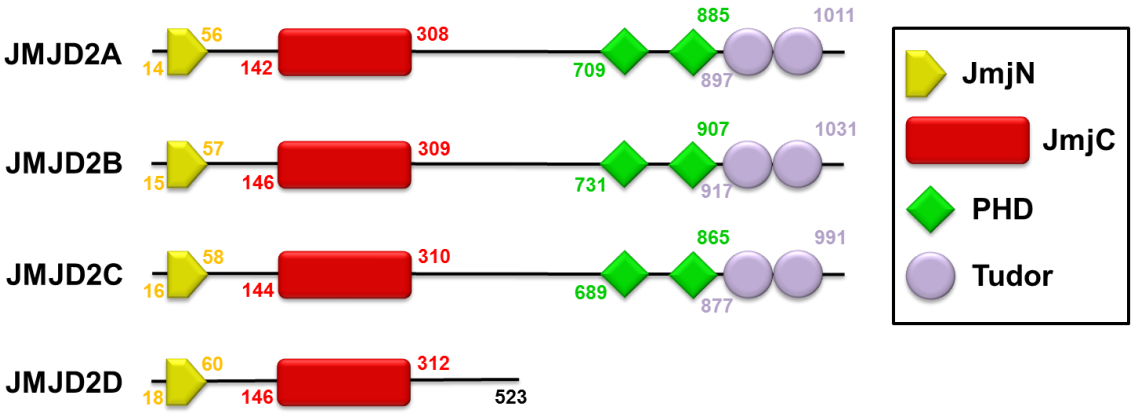

Figure 1.4: Domain architecture of the human JMJD2 enzymes. Domain boundaries were obtained from UniProt (http://www.uniprot.org): JMJD2A (O75164), JMJD2B (O94953), JMJD2C (Q9H3R0), JMJD2D (Q6B0I6).

[60-62]. Although the biological functions of JMJD2D are still being explored, recent studies have shown that JMJD2D demethylates H3K9me3 in upstream enhancer elements of the macrophage-derived chemokine (*Mdc*) and Interleukin 12B (*Il12b*) loci and regulates the expression of these genes in a cell type specific manner [63]. Functional studies on the JMJD2 enzymes have also been performed in lower eukaryotes. Knockdown of the single JMJD2 homolog in *C.elegans* increased H3K9me3 and H3K36me3 levels in the pachytene regions and resulted in germ line apoptosis and altered progression of double strand break repair [45]. In addition, depletion of JMJD2A in chick embryos resulted in neural crest specification defects primarily due to impaired demethylation of the repressive mark H3K9me3 from neural crest specifier genes such as *Sox10* and *Snail2* [57].

The involvement of JMJD2 enzymes in tumorogenesis and other diseases is generally better understood than their biological functions. Because of their important roles in AR signaling, not surprisingly, JMJD2A, JMJD2C and JMJD2D have been implicated in the onset and progression of prostate cancers [58, 59]. JMJD2B has been shown to promote breast, colon and gastric cancers [60-62, 64-66]. In addition, JMJD2B removes H3K9me3 at pericentric heterochromatin and increases chromosomal instability, a hallmark of most cancers [44]. JMJD2D has been described as a 'pro-proliferative' molecule and shown to promote colon cancer cell proliferation [67]. A comprehensive list of the functions and disease implications of JMJD2 enzymes is provided in Table 1.2.

JMJD2 KDMs as Drug Targets

Due to their roles in the onset and progression of different cancers, significant effort has been channeled into developing inhibitors for the JMJD2 enzymes [68-73]. One of the major

Table 1.2: Biological functions, disease implications and specificity of JMJD2 KDMs

ENZYME	KNOWN BIOLOGICAL FUNCTIONS	DISEASE IMPLICATIONS	SUBSTRATE SPECIFICITY
JMJD2A/KDM4A	Neural crest specification [37], Androgen Receptor signaling [38], DNA damage response [53], DNA replication timing and cell cycle progression [31] [54], skeletal muscle differentiation [55]	Overexpressed in Prostate [38], Breast [56], Colon and Bladder [57]. Promotes Cardiac Hypertrophy [58]	H3K9me3 H3K36me3 H1.4K26me3
JMJD2B/KDM4B	Estrogen Receptor signaling [40-42] , Regulation of cyclin-dependent kinases [46]	Overexpressed in breast [40-42], lung [46], bladder and gastric cancers [44, 45]. Promotes chromosomal instability [25, 59]	H3K9me3 H3K36me3 H1.4K26me3
JMJD2C/KDM4C/GASC1	Androgen Receptor signaling [39], maintenance of embryonic stem cell pluripotency [35] and embryonic development [60], regulation of adipogenesis [61]	Overexpressed in acute myeloid leukemia [62] and in prostate [39], lung and squamous cell cancers [63]. Enhances expression of Murine Double Minute-2 (Mdm2) oncogene [64]	H3K9me3 H3K36me3 H1.4K26me3
JMJD2D/KDM4D	Androgen Receptor Signaling [38], Spermatogenesis [32], modulation of enhancer function [43]	Overexpressed in prostate [38] and colon cancers [47]. Regulates function of p53 tumor suppressor [47]	H3K9me3/me2 H1.4K26me3/me2

challenges in developing inhibitors for these enzymes has been achieving selectivity for the JMJD2 homologs. Many inhibitors that are 2-OG analogs often target a large group of JmjC enzymes and many 2-OG dependent dioxygenases [68-70, 72]. Although these molecules may be viable probes to study enzyme functions *in vitro* and *in vivo*, their use in therapy is questionable due to their lack of selectivity for different JmjC families. Certain JmjC KDMs have differential functions in the context of cancer. For example, most of the JMJD2 KDMs are oncogenes whereas the UTX family of enzymes functions as tumor suppressors. Hence, efforts have been channeled toward designing inhibitors that are more selective to specific families of demethylases by exploiting their different substrate specificities. More recently, a bisubstrate analog fusing 2-OG and an H3K9 peptide has been developed and crystallized with JMJD2A, illustrating the potential of bisubstrate peptido-mimetics to inhibit specific families of JmjC KDMs [73]. The availability of more JmjC-peptide complex structures and understanding the mechanisms of substrate recognition will be highly beneficial in the design of additional, more selective inhibitors.

Methylation Site and State Specificities in the JMJD2 KDMs

The various biological functions of JMJD2 KDMs are largely dependent on their methylation site and state specificities. Despite the high sequence identity within the catalytic domains (>75%), there is a surprising degree of variability in the methylation site and state specificities among JMJD2 homologs. JMJD2A, JMJD2B and JMJD2C display dual specificity in demethylating H3K9me3 and H3K36me3. These methylation marks encode for distinct biological functions – transcriptional repression and transcriptional elongation respectively [27, 45]. Hence it is conceivable that JMJD2A, JMJD2B and JMJD2C might be involved in a subset

of processes, each requiring either demethylation of H3K9me3 or H3K36me3 or both. In contrast, JMJD2D is specific for H3K9me3 and completely lacks activity toward H3K36me3 [45]. An additional level of variation in specificity arises in the methylation state specificity within this family. JMJD2A, JMJD2B and JMJD2C are efficient at demethylating trimethylated H3K9 and H3K36 but have very weak activity toward dimethylated lysines. On the other hand, JMJD2D is efficient toward H3K9me3 and H3K9me2 [45]. Different methylation states can also encode for varied functions. A classic example is the methylation states associated with H3K9 site. High-resolution Chromatin Immunoprecipitation (ChIP) experiments combined with DNA sequencing revealed that H3K9me3 and H3K9me2 are highly prevalent in heterochromatin regions whereas H3K9me1 is more abundant in active promoters near the Transcription Start Sites (TSS) [9]. Differential methylation states can also affect the binding of effector proteins such as HP1 which preferentially recognize H3K9me3 and H3K9me2 and have weak affinity for H3K9me1 [13, 14]. Thus the methylation site and state specificities of the JMJD2 enzymes could largely dictate the biological functions of different members of this family.

Objectives of This Work

The molecular mechanisms by which JMJD2 homologs achieve selectivity for specific methylation sites and states remains poorly understood. Although structures of JMJD2A have been solved by several groups [74-76], a detailed mechanism describing the site and state specificity of the JMJD2 family has remained elusive, primarily due to lack of structural and biochemical elucidations for other JMJD2 homologs, particularly JMJD2D. In this work, we determined the first crystal structure of human JMJD2D in the apoenzyme form and in complex with 2-OG and an H3K9me3 peptide (Chapter 3). We then performed structural comparisons

with JMJD2A, molecular docking analyses with H3K36me3 and biochemical studies with an array of histone peptide substrates to study how JMJD2 enzymes recognized H3K9me3 and why JMJD2D lacked specificity for the H3K36me3 site (Chapter 4). We also explored the active site of JMJD2A and JMJD2D and deciphered the methylation state specificity determinants in these enzymes (Appendix A). We used unnatural amino acids as a tool to manipulate an active site tyrosine and investigate the role of the CH•••O hydrogen bonds formed by this residue in JMJD2A demethylation (Appendix A). A crucial step to performing all the biochemical analyses described in Chapter 4 and Appendix A was the development of a viable biochemical assay that provided reproducible results and allowed for the accurate measurement of kinetic parameters. The development of a Strep-Tactin affinity based purification of recombinant JmjC KDMs along with the optimization of the formaldehyde dehydrogenase (FDH) - coupled demethylase assay is described in Chapter 2. These set of optimization experiments were critical to performing kinetic analyses describing the methylation site (Chapter 4) and state specificities (Appendix A) of JMJD2A and JMJD2D. Together, our studies furnish a fundamental understanding of the molecular mechanisms of site and state specific demethylation within the JMJD2 family of KDMs and these findings will be instrumental in deciphering the biological functions of these enzymes and in the design of JMJD2 specific inhibitors (Chapter 5).

REFERENCES

1. Luger, K., et al., Crystal structure of the nucleosome core particle at 2.8 A resolution. Nature, 1997. 389(6648): p. 251-60.
2. Jenuwein, T. and C.D. Allis, Translating the histone code. Science, 2001. 293(5532): p. 1074-80.
3. Kouzarides, T., Chromatin modifications and their function. Cell, 2007. 128(4): p. 693-705.

4. Shahbazian, M.D. and M. Grunstein, Functions of site-specific histone acetylation and deacetylation. Annu Rev Biochem, 2007. 76: p. 75-100.

5. Ruthenburg, A.J., et al., Multivalent engagement of chromatin modifications by linked binding modules. Nature reviews. Molecular cell biology, 2007. 8(12): p. 983-94.

6. Greer, E.L. and Y. Shi, Histone methylation: a dynamic mark in health, disease and inheritance. Nat Rev Genet, 2012. 13(5): p. 343-57.

7. Kouzarides, T., Histone methylation in transcriptional control. Current opinion in genetics & development, 2002. 12(2): p. 198-209.

8. Sims, R.J., 3rd, K. Nishioka, and D. Reinberg, Histone lysine methylation: a signature for chromatin function. Trends in genetics : TIG, 2003. 19(11): p. 629-39.

9. Barski, A., et al., High-resolution profiling of histone methylations in the human genome. Cell, 2007. 129(4): p. 823-37.

10. Taverna, S.D., et al., How chromatin-binding modules interpret histone modifications: lessons from professional pocket pickers. Nat Struct Mol Biol, 2007. 14(11): p. 1025-40.

11. Shi, X.B. and O. Gozani, The fellowships of the INGs. J Cell Biochem, 2005. 96(6): p. 1127-1136.

12. Ruthenburg, A.J., C.D. Allis, and J. Wysocka, Methylation of lysine 4 on histone H3: intricacy of writing and reading a single epigenetic mark. Mol Cell, 2007. 25(1): p. 15-30.

13. Nakayama, J., et al., Role of histone H3 lysine 9 methylation in epigenetic control of heterochromatin assembly. Science, 2001. 292(5514): p. 110-3.

14. Grewal, S.I. and J.C. Rice, Regulation of heterochromatin by histone methylation and small RNAs. Curr Opin Cell Biol, 2004. 16(3): p. 230-8.

15. Carrozza, M.J., et al., Histone H3 methylation by Set2 directs deacetylation of coding regions by Rpd3S to suppress spurious intragenic transcription. Cell, 2005. 123(4): p. 581-592.

16. Joshi, A.A. and K. Struhl, Eaf3 chromodomain interaction with methylated H3-K36 links histone deacetylation to Pol II elongation. Mol Cell, 2005. 20(6): p. 971-978.

17. Keogh, M.C., et al., Cotranscriptional Set2 methylation of histone H3 lysine 36 recruits a repressive Rpd3 complex. Cell, 2005. 123(4): p. 593-605.

18. Wagner, E.J. and P.B. Carpenter, Understanding the language of Lys36 methylation at histone H3. Nature Reviews Molecular Cell Biology, 2012. 13(2): p. 115-126.

19. Shi, Y., et al., Histone demethylation mediated by the nuclear amine oxidase homolog LSD1. Cell, 2004. 119(7): p. 941-53.

20. Forneris, F., et al., Human histone demethylase LSD1 reads the histone code. J Biol Chem, 2005. 280(50): p. 41360-5.

21. Tsai, W.W., et al., p53-targeted LSD1 functions in repression of chromatin structure and transcription in vivo. Mol Cell Biol, 2008. 28(17): p. 5139-46.

22. Huang, J., et al., p53 is regulated by the lysine demethylase LSD1. Nature, 2007. 449(7158): p. 105-8.

23. Gaweska, H., et al., Use of pH and kinetic isotope effects to establish chemistry as rate-limiting in oxidation of a peptide substrate by LSD1. Biochemistry, 2009. 48(23): p. 5440-5.

24. Schmidt, D.M. and D.G. McCafferty, trans-2-Phenylcyclopropylamine is a mechanism-based inactivator of the histone demethylase LSD1. Biochemistry, 2007. 46(14): p. 4408-16.

25. Szewczuk, L.M., et al., Mechanistic analysis of a suicide inactivator of histone demethylase LSD1. Biochemistry, 2007. 46(23): p. 6892-902.

26. Cloos, P.A., et al., Erasing the methyl mark: histone demethylases at the center of cellular differentiation and disease. Genes Dev, 2008. 22(9): p. 1115-40.

27. Mosammaparast, N. and Y. Shi, Reversal of histone methylation: biochemical and molecular mechanisms of histone demethylases. Annu Rev Biochem, 2010. 79: p. 155-79.

28. Sims, R.J., 3rd and D. Reinberg, Histone H3 Lys 4 methylation: caught in a bind? Genes Dev, 2006. 20(20): p. 2779-86.

29. Heintzman, N.D., et al., Histone modifications at human enhancers reflect global cell-type-specific gene expression. Nature, 2009. 459(7243): p. 108-112.

30. Pinheiro, I., et al., Prdm3 and Prdm16 are H3K9me1 Methyltransferases Required for Mammalian Heterochromatin Integrity. Cell, 2012. 150(5): p. 948-60.

31. Campos, E.I., et al., The program for processing newly synthesized histones H3.1 and H4. Nat Struct Mol Biol, 2010. 17(11): p. 1343-51.

32. Cao, R., et al., Role of histone H3 lysine 27 methylation in Polycomb-group silencing. Science, 2002. 298(5595): p. 1039-43.

33. Lee, M.G., et al., Demethylation of H3K27 regulates polycomb recruitment and H2A ubiquitination. Science, 2007. 318(5849): p. 447-50.

34. Lee, J.S. and A. Shilatifard, A site to remember: H3K36 methylation a mark for histone deacetylation. Mutation Research-Fundamental and Molecular Mechanisms of Mutagenesis, 2007. 618(1-2): p. 130-134.

35. Butler, J.S. and S.Y.R. Dent, Chromatin 'resetting' during transcription elongation: a central role for methylated H3K36. Nat Struct Mol Biol, 2012. 19(9): p. 863-864.

36. Klose, R.J., E.M. Kallin, and Y. Zhang, JmjC-domain-containing proteins and histone demethylation. Nat Rev Genet, 2006. 7(9): p. 715-27.

37. Shi, Y. and J.R. Whetstine, Dynamic regulation of histone lysine methylation by demethylases. Mol Cell, 2007. 25(1): p. 1-14.

38. Tsukada, Y., et al., Histone demethylation by a family of JmjC domain-containing proteins. Nature, 2006. 439(7078): p. 811-6.

39. Allis, C.D., et al., New nomenclature for chromatin-modifying enzymes. Cell, 2007. 131(4): p. 633-6.

40. Krishnan, S., S. Horowitz, and R.C. Trievel, Structure and Function of Histone H3 Lysine 9 Methyltransferases and Demethylases. Chembiochem, 2011.

41. Nottke, A., M.P. Colaiacovo, and Y. Shi, Developmental roles of the histone lysine demethylases. Development, 2009. 136(6): p. 879-89.

42. Shi, Y., Histone lysine demethylases: emerging roles in development, physiology and disease. Nat Rev Genet, 2007. 8(11): p. 829-33.

43. Cloos, P.A., et al., The putative oncogene GASC1 demethylates tri- and dimethylated lysine 9 on histone H3. Nature, 2006. 442(7100): p. 307-11.

44. Fodor, B.D., et al., Jmjd2b antagonizes H3K9 trimethylation at pericentric heterochromatin in mammalian cells. Genes Dev, 2006. 20(12): p. 1557-62.

45. Whetstine, J.R., et al., Reversal of histone lysine trimethylation by the JMJD2 family of histone demethylases. Cell, 2006. 125(3): p. 467-81.

46. Katoh, M., Identification and characterization of JMJD2 family genes in silico. International journal of oncology, 2004. 24(6): p. 1623-8.

47. Kim, T. and S. Buratowski, Two Saccharomyces cerevisiae JmjC domain proteins demethylate histone H3 Lys36 in transcribed regions to promote elongation. J Biol Chem, 2007. 282(29): p. 20827-35.

48. Klose, R.J., et al., The transcriptional repressor JHDM3A demethylates trimethyl histone H3 lysine 9 and lysine 36. Nature, 2006. 442(7100): p. 312-6.

49. Tu, S., et al., Identification of histone demethylases in Saccharomyces cerevisiae. J Biol Chem, 2007. 282(19): p. 14262-71.

50. Huang, Y., et al., Recognition of histone H3 lysine-4 methylation by the double tudor domain of JMJD2A. Science, 2006. 312(5774): p. 748-751.

51. Black, J.C., et al., Conserved antagonism between JMJD2A/KDM4A and HP1gamma during cell cycle progression. Mol Cell, 2010. 40(5): p. 736-48.

52. Iwamori, N., et al., The testis-enriched histone demethylase, KDM4D, regulates methylation of histone H3 lysine 9 during spermatogenesis in the mouse but is dispensable for fertility. Biol Reprod, 2011. 84(6): p. 1225-34.

53. Lin, C.H., et al., Heterochromatin protein 1a stimulates histone H3 lysine 36 demethylation by the Drosophila KDM4A demethylase. Mol Cell, 2008. 32(5): p. 696-706.

54. Lin, C.H., et al., HP1a Targets the Drosophila KDM4A Demethylase to a Subset of Heterochromatic Genes to Regulate H3K36me3 Levels. PLoS One, 2012. 7(6): p. e39758.

55. Loh, Y.H., et al., Jmjd1a and Jmjd2c histone H3 Lys 9 demethylases regulate self-renewal in embryonic stem cells. Genes Dev, 2007. 21(20): p. 2545-57.

56. Lorbeck, M.T., et al., The histone demethylase Dmel\Kdm4A controls genes required for life span and male-specific sex determination in Drosophila. Gene, 2010. 450(1-2): p. 8-17.

57. Strobl-Mazzulla, P.H., T. Sauka-Spengler, and M. Bronner-Fraser, Histone demethylase JmjD2A regulates neural crest specification. Dev Cell, 2010. 19(3): p. 460-8.

58. Shin, S. and R. Janknecht, Activation of androgen receptor by histone demethylases JMJD2A and JMJD2D. Biochem Biophys Res Commun, 2007. 359(3): p. 742-6.

59. Wissmann, M., et al., Cooperative demethylation by JMJD2C and LSD1 promotes androgen receptor-dependent gene expression. Nat Cell Biol, 2007. 9(3): p. 347-53.

60. Kawazu, M., et al., Histone demethylase JMJD2B functions as a co-factor of estrogen receptor in breast cancer proliferation and mammary gland development. PLoS One, 2011. 6(3): p. e17830.

61. Shi, L., et al., Histone demethylase JMJD2B coordinates H3K4/H3K9 methylation and promotes hormonally responsive breast carcinogenesis. Proc Natl Acad Sci U S A, 2011. 108(18): p. 7541-6.

62. Yang, J., et al., The histone demethylase JMJD2B is regulated by estrogen receptor alpha and hypoxia, and is a key mediator of estrogen induced growth. Cancer Res, 2010. 70(16): p. 6456-66.

63. Zhu, Y., D. van Essen, and S. Saccani, Cell-type-specific control of enhancer activity by H3K9 trimethylation. Mol Cell, 2012. 46(4): p. 408-23.

64. Fu, L., et al., HIF-1alpha-induced histone demethylase JMJD2B contributes to the malignant phenotype of colorectal cancer cells via an epigenetic mechanism. Carcinogenesis, 2012.

65. Li, W., et al., Histone demethylase JMJD2B is required for tumor cell proliferation and survival and is overexpressed in gastric cancer. Biochem Biophys Res Commun, 2011. 416(3-4): p. 372-8.

66. Toyokawa, G., et al., The histone demethylase JMJD2B plays an essential role in human carcinogenesis through positive regulation of cyclin-dependent kinase 6. Cancer Prev Res (Phila), 2011. 4(12): p. 2051-61.

67. Kim, T.D., et al., Regulation of tumor suppressor p53 and HCT116 cell physiology by histone demethylase JMJD2D/KDM4D. PLoS One, 2012. 7(4): p. e34618.

68. King, O.N., et al., Quantitative high-throughput screening identifies 8-hydroxyquinolines as cell-active histone demethylase inhibitors. PLoS One, 2010. 5(11): p. e15535.

69. Luo, X., et al., A selective inhibitor and probe of the cellular functions of Jumonji C domain-containing histone demethylases. J Am Chem Soc, 2011. 133(24): p. 9451-6.

70. Rose, N.R., et al., Inhibitor scaffolds for 2-oxoglutarate-dependent histone lysine demethylases. J Med Chem, 2008. 51(22): p. 7053-6.

71. Rose, N.R., et al., Selective inhibitors of the JMJD2 histone demethylases: combined nondenaturing mass spectrometric screening and crystallographic approaches. J Med Chem, 2010. 53(4): p. 1810-8.

72. Thalhammer, A., et al., Inhibition of the histone demethylase JMJD2E by 3-substituted pyridine 2,4-dicarboxylates. Org Biomol Chem, 2011. 9(1): p. 127-35.

73. Woon, E.C., et al., Linking of 2-oxoglutarate and substrate binding sites enables potent and highly selective inhibition of JmjC histone demethylases. Angew Chem Int Ed Engl, 2012. 51(7): p. 1631-4.

74. Chen, Z., et al., Structural basis of the recognition of a methylated histone tail by JMJD2A. Proc Natl Acad Sci U S A, 2007. 104(26): p. 10818-23.

75. Couture, J.F., et al., Specificity and mechanism of JMJD2A, a trimethyllysine-specific histone demethylase. Nat Struct Mol Biol, 2007. 14(8): p. 689-95.

76. Ng, S.S., et al., Crystal structures of histone demethylase JMJD2A reveal basis for substrate specificity. Nature, 2007. 448(7149): p. 87-91.

CHAPTER 2

OPTIMIZATION OF THE FORMALDEHYDE DEHYDROGENASE-COUPLED LYSINE DEMETHYLASE ASSAY FOR JUMONJI ENZYMES

The JmjC demethylases have often been considered inherently weak enzymes and many experts have postulated the need for accessory factors to enhance enzymatic activity [1, 2]. Previously reported turnover numbers for these enzymes were ~ 0.01 min^{-1} which is over two orders of magnitude lower than the LSD family of lysine demethylases [3-9]. There are a number of biochemical methods available to assay the JmjC demethylases both qualitatively and quantitatively. Most studies on JmjC enzymes employ immunoblot analysis and mass spectrometry-based assays that can qualitatively assess changes in lysine methylation states [10, 11]. Quantitative methods to measure demethylase activity have also been reported, including an amplified luminescent proximity homogeneous assay that detects changes in lysine methylation state via antibodies [12] and assays that rely on formaldehyde detection such as the Nash reaction [13], nuclear magnetic resonance (NMR) spectroscopy [14], and a formaldehyde dehydrogenase-coupled assay [7].

The Formaldehyde Dehydrogenase (FDH) Coupled Demethylase Assay

One of the most widely used assays to kinetically analyze JmjC enzymes is the FDH-coupled demethylase assay. The scheme of this assay is depicted in Figure 2.1. The demethylation of a methylated lysine by any JmjC enzyme results in the formation of

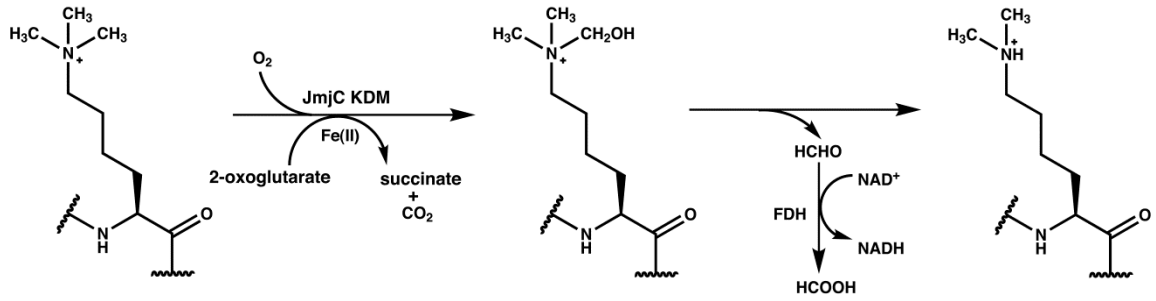

Figure 2.1: Schematic of the FDH-coupled Demethylase Assay. The JmjC KDM hydroxylates the methyllysine substrate using the co-substrates 2-OG, Fe(II) and O_2 to yield the demethylated lysine, formaldehyde, CO_2, and succinate. The formaldehyde released during the reaction is oxidized by FDH, which concomitantly reduces NAD^+ to NADH. The NADH fluorescence is measured using an excitation wavelength of 340 nm and emission wavelength of 490 nm.

formaldehyde and succinate as by-products (Figure 1.2 in Chapter 1). The production of formaldehyde is continuously monitored via FDH, the coupling enzyme. FDH oxidizes formaldehyde to formic acid and the cofactor nicotinamide adenine dinucleotide (NAD^+) is concomitantly reduced to NADH. The fluorescence of NADH (λ_{ex} = 340 nm; λ_{em} = 490 nm) is measured and is used to calculate the rate of demethylation. Previously reported kinetic parameters for JmjC enzymes were determined using the FDH-coupled demethylase assay [7]. In these studies, hexahistidine-tagged JmjC enzyme was recombinantly purified by immobilized metal affinity chromatography (IMAC) and was subsequently used in the FDH-coupled assay. A major caveat with purifying the enzymes in this manner is contamination by transition state metals such as Ni(II) and Co(II).

Inhibition of JmjC KDMs by Transition State Metals

A number of groups have shown that transition state metals can inhibit JmjC demethylases. Chen *et al* have shown that the JmjC KDM, JMJD1A is inhibited by Ni(II) [15, 16]. They determined an IC_{50} of 25 µM for Ni(II) and showed that Ni(II) occupies the active site of JMJD1A. In addition, they reported that the addition of catalytic Fe(II) up to 2 mM was unable to displace the Ni(II) from the active site suggesting that the inhibition by Ni(II) was irreversible. In addition they also provided evidence that Ni(II) inhibits JMJD1A in cells and suggested that Ni(II) inhibition of 2-OG-dependent dioxygenases could lead to metal toxicity and promote carcinogenesis [15]. Sekirnik *et al* reported that JMJD2A was inhibited by a range of transition state metals such Ni(II) [IC_{50}= 10.3 µM],Co(II) [IC_{50}=5.3 µM] , and Cu(II) [IC_{50}=0.5 µM] and the inhibition by these metals was prevalent even with 50-100 µM Fe(II) [17]. Previously reported kinetic analysis of JmjC KDMs was performed using hexa-histidine tagged

enzymes purified on Ni(II) IMAC columns and the turnover numbers for these enzymes were much lower than the FAD-dependent demethylase LSD1 [3-7]. We hypothesized that purification of JmjC KDMs on Ni(II) columns could lead to Ni(II) contaminated enzymes. Since the inhibition by Ni(II) is irreversible and addition of up to 100-fold excess Fe(II) does not displace Ni(II) from the active site, we proposed that the use of Ni(II)-inhibited enzymes in demethylase assays may be incompatible to determining accurate kinetic parameters. To minimize transition state metal contamination, we adopted a Strep-Tactin purification scheme for the JmjC KDMs, JMJD2A and JMJD2D. In addition, we also optimized the various reagents, including the histone substrates, used in FDH-coupled demethylase assay and determined the kinetic parameters of Strep-Tactin column purified JMJD2 KDMs. Together, these results demonstrate that the purification of JMJD2 KDMs using a metal-free Strep-Tactin column yields highly active enzymes and provides a reliable tool for their biochemical characterization.

MATERIALS AND METHODS

Expression and Purification of Strep(II)-Tagged JMJD2A and JMJD2D

The Strep-Tactin method of purification using Strep(II) affinity tags was originally reported by Schmidt and Skerra as a one-step protein purification and detection/capture method [18]. The catalytic domains of human JMJD2A (residues 1–350) and human JMJD2D (residues 12–342) were cloned into the pST4 vector, a variant of pET15b (Novagen) that encodes the enzymes with an N-terminal Strep(II) tag (WSHPQFEK) followed by a tobacco etch virus (TEV) protease cleavage site to facilitate tag removal. KDMs were expressed in *Escherichia coli* Rosetta 2 (DE3) cells (Novagen). Cells were initially grown at 37º C and when the cell density (optical density) was 0.4-0.6, protein expression was induced using 1 mM (final concentration)

isopropyl thiogalactoside (IPTG) overnight at 18º C (for JMJD2A) or 16º C (for JMJD2D). The pelleted cells were re-suspended in Buffer A (100 mM Tris (pH 7.5) and 500 mM NaCl) and stored at -20º C. The KDMs were purified on a refrigerated FPLC system using a 5.0 ml Strep-Tactin affinity column (Qiagen). Prior to a new purification, the column was freshly regenerated with four column volumes of 1X regeneration buffer followed by equilibration with four column volumes of Buffer A for optimal yield. A 150 ml superloop was used to inject the sample onto the column. After sample injection, the column was washed with at least four column volumes of Buffer A to remove unbound sample. The KDMs were eluted with Buffer A containing 2.5 mM desthiobiotin (Sigma). Peak fractions (Figure 2.2) were pooled and incubated with 1 mg/ml TEV protease at 4º C overnight to remove the Strep(II) tag. The KDMs were then concentrated and purified by gel filtration chromatography using a Superdex 200 column (GE Healthcare) equilibrated in 20 mM Tris (pH 7.5) and 150 mM NaCl. The purity of the enzymes was assessed by sodium dodecyl sulfate polyacrylamide gel electrophoresis (SDS–PAGE) (Figure 2.3). The KDMs were concentrated to 10–20 mg/ml, flash frozen in liquid nitrogen, and stored at -80º C. Protein concentration was determined by their absorbance at 280 nm in 6.0 M guanidinium chloride and 100 mM HEPES (pH 7.5) [extinction coefficients were calculated using ExPASy ProtParam (http://web.expasy.org/protparam): JMJD2A, ε280nm = 73,800 M^{-1} cm^{-1}, and JMJD2D, ε280nm =70,820 M^{-1} cm^{-1}].

Expression and Purification of Recombinant Formaldehyde Dehydrogenase

The Zn(II)-dependent glutathione-independent FDH from *Pseudomonas putida* was expressed in *E.coli* Rosetta 2 cells as a His-tagged fusion protein as previously reported [19]. Protein expression was induced at an OD of 0.6 using 500 μM IPTG and cells were allowed to

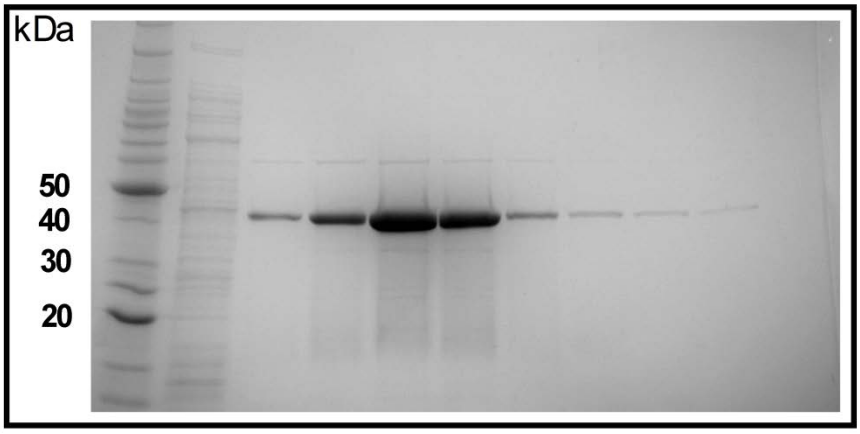

Figure 2.2: Strep-Tactin purification of Strep(II)-tagged JMJD2A. Peak fractions of the Strep(II)-tagged enzyme were eluted from the Strep-Tactin column using desthiobiotin and were analyzed on a 12% SDS-PAGE gel stained with Coomassie Blue. Lane 1: Molecular weight standards; Lane 2: flow through from the Strep-Tactin column; Lanes 3-10: Fractions 5-12 from Strep-Tactin column.

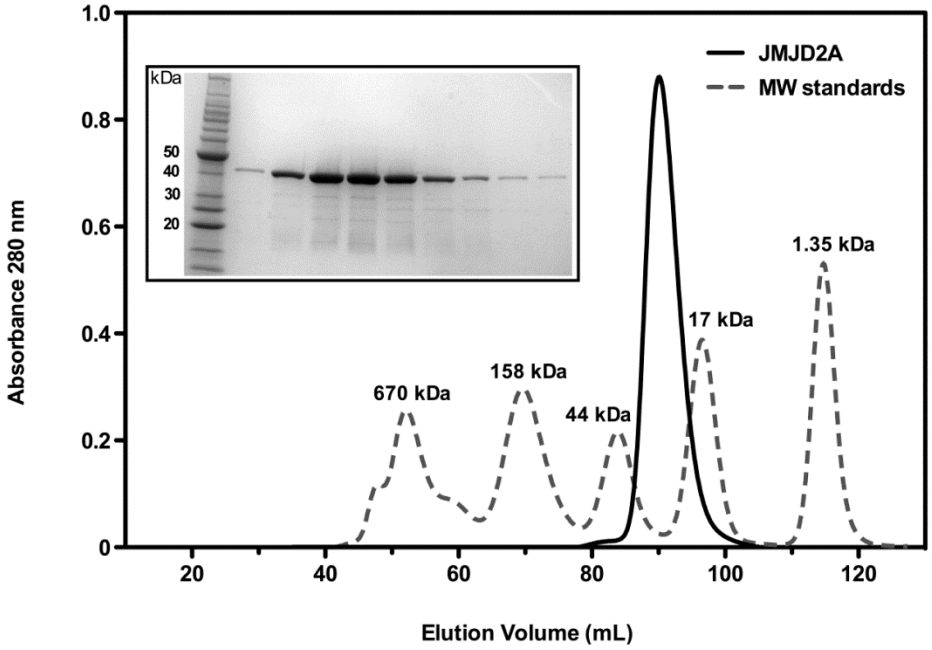

Figure 2.3: Gel Filtration Purification of JMJD2A. Chromatogram of the Superdex 200 gel filtration purification of JMJD2A (solid line) overlaid with the molecular weight standards (dashed line). The JMJD2A catalytic domain elutes at the expected elution volume, corresponding to its molecular mass of 41 kDa. The inset panel depicts the coomasie blue stained SDS-PAGE gel of the peak fractions from the Superdex 200 purification.

grow overnight at 25º C. Cells were harvested in 50 mM HEPES (pH 8.0) and 500 mM NaCl and stored at -20º C. His-FDH was purified using an IMAC Sepharose column (GE Healthcare) charged with Zn(II) followed by Superdex 200 gel filtration chromatography, where the protein eluted as a monomer. The purity of the FDH was assessed by SDS–PAGE (Figures 2.4 and 2.5). Peak fractions were pooled and concentrated to 13 mg/ml, flash frozen in liquid nitrogen, and stored at -80ºC. Protein concentration was determined by absorbance at 280 nm in 6.0 mM guanidinium chloride and 100 mM HEPES (pH 7.5) [extinction coefficients were calculated using ExPASy ProtParam (http://web.expasy.org/protparam): FDH, ε280nm = 73,800 M^{-1} cm^{-1}].

Substrate Histone Peptides

A 15-residue histone H3 peptide with a trimethylated Lys9 and C-terminal amidation (H3K9me3, sequence: ARTKQTAR-Kme3-STGGKA-amide) was synthesized by the Protein Structure Core Facility at the University of Michigan. To assess the efficacy of substrates bearing Methyllysine Analogs (MLAs), an analogous H3K9C peptide was also synthesized. The H3K9C peptide was alkylated with (2-bromoethyl)trimethylammonium bromide (Aldrich) to install a trimethyllysine analog at Cys9 ($H3K9_Cme3$) according to the protocol of Simon and coworkers [20]. The H3K9me3 and $H3K9_Cme3$ peptides were purified by reverse phase high-performance liquid chromatography (HPLC) with chloride as the counter ion, and net peptide content was determined by amino acid analysis.

Determination of Metal Content of JMJD2A and JMJD2D

Analysis of transition metals in JMJD2A and JMJD2D was performed using a Thermo Scientific Element inductively coupled plasma high-resolution mass spectrometer (ICP–HRMS)

in the W. M. Keck Elemental Geochemistry Laboratory in the University of Michigan's Department of Geological Sciences. 200 µl of a 20 µM protein sample was submitted for metal detection and multiple purifications of StrepTactin column purified JMJD2A and JMJD2D were analyzed. As a control, the metal content of different batches of Ni(II) column purified JMJD2D was also determined. The transition metal concentrations in the gel filtration buffer were measured and subtracted from the metal concentrations in the protein samples. The percent metal content was determined by:

$$\textbf{\% metal content} = \frac{\text{metal concentration in sample}(\mu M)\text{-metal concentration in buffer }(\mu M)}{\text{protein concentration }(\mu M)} \times \mathbf{100}\ \%$$

Reagents for the FDH-Coupled Demethylase Assay

In addition to the Strep(II)-tagged KDMs, recombinant FDH and histone peptides, the following reagents were used in the assay: L-Ascorbic acid, NaCl, and HEPES were purchased from Fisher Scientific. Ammonium iron(II) sulfate [$(NH_4)_2Fe(SO_4)_2$] and 2-OG (acid) were obtained from Fluka. NAD^+ and NADH were purchased from Roche. All buffers were prepared using water purified by a Milli-Q Biocel System (Millipore), yielding a resistivity of 18.2 MΩ. L-Ascorbic acid and $(NH_4)_2Fe(SO_4)_2$ were stored in a desiccator under vacuum to minimize oxidation of the reagents. The concentration of all the reagents used in the FDH-coupled demethylase assay was optimized. Sample optimization plots for 2-OG and FDH are shown in Figures 2.6 and 2.7 respectively.

Setting up the FDH-Coupled Demethylase Assay

Coupled fluorescent demethylase assays were performed in a cocktail containing 50 mM

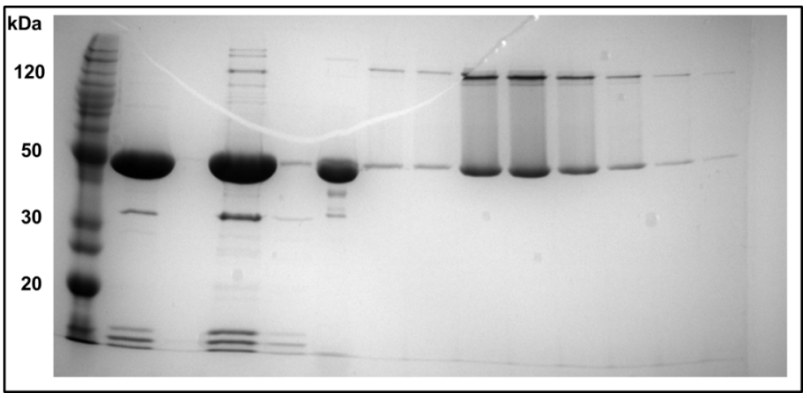

Figure 2.4: Purification of recombinant FDH on S200 column. Lane 1: Molecular Weight Standards; Lane 2: Pooled fractions from Zn column; Lane 3: empty; Lane 4: Fractions from Zn column concentrated to 2 ml; Lane 5: empty; Lane 6: FDH sample from previous purification; Lane 7-Lane 14: Fractions 15-22 from S200 column after sample in Lane 4 was injected into the column. The bands at ~120 kDa are most likely FDH samples that were not properly reduced before gel loading (Figure 2.5).

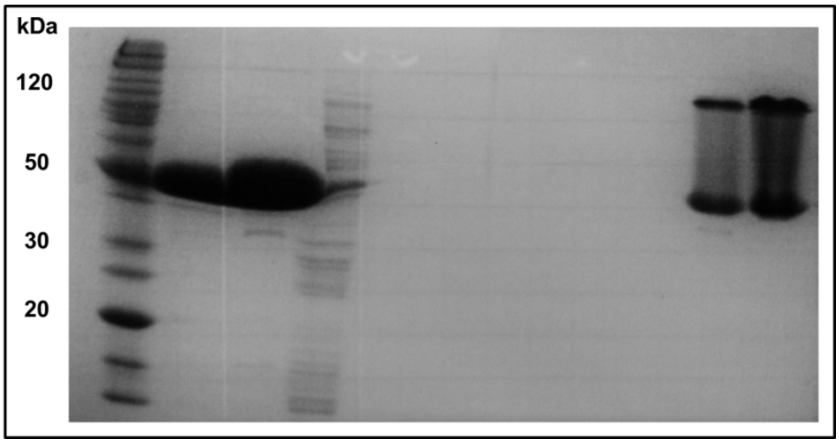

Figure 2.5: FDH samples with excess Dithiothreitol (DTT). FDH samples after gel filtration purification were prepared with excess DTT and heated for 5 min at 90ºC for complete reduction of disulfide linkages. Lane 1: Molecular Weight Standards; Lane 2 and Lane 3: Concentrated FDH samples after S200 purification were reduced using DTT and loaded on the gel. The last two lanes represent the samples on Lanes 2 and 3 loaded without reducing agents. This resulted in bands at ~120 kDa which were also seen in Figure 2.4.

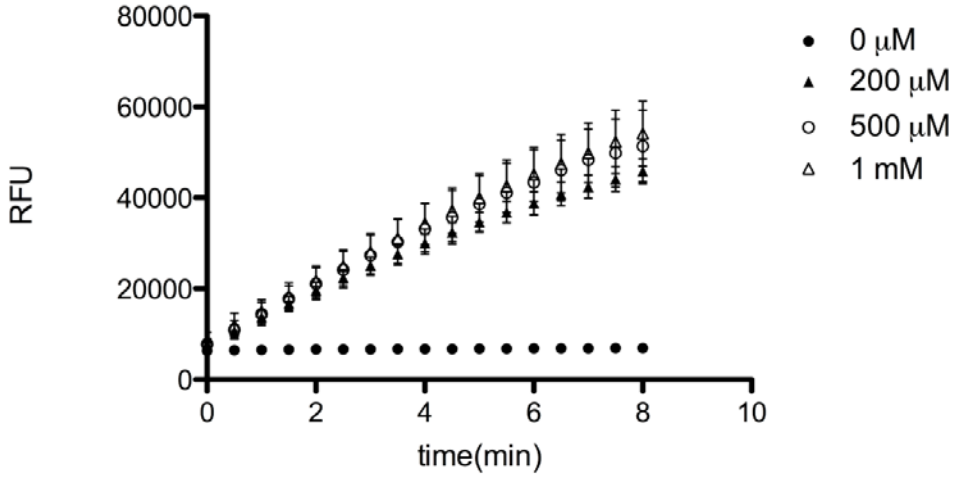

Figure 2.6: Optimization of 2-OG concentration in the coupled demethylase assay. Increasing 2-OG concentrations (0 μM, 200 μM, 500 μM, and 1 mM) were included in the assay cocktail with 1.0 μM JMJD2A and 700 μM H3K9me3 peptide substrate. The optimal assay concentration of 2-OG derived from this experiment was 1 mM.

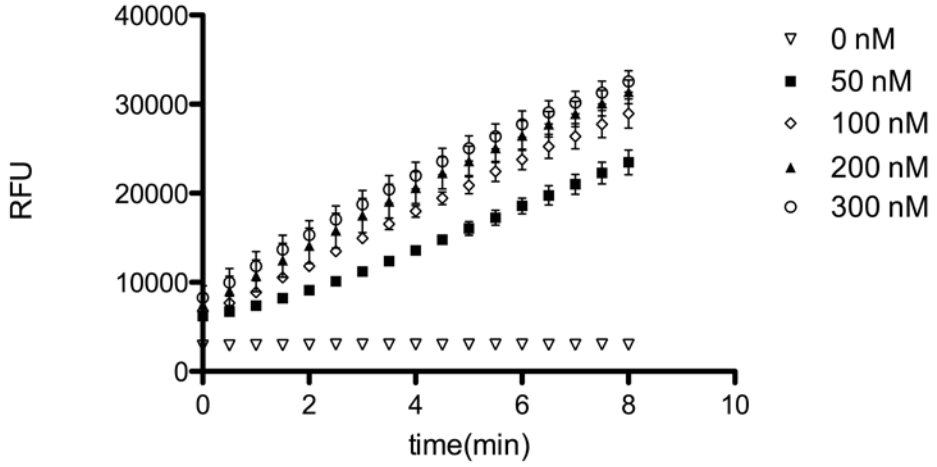

Figure 2.7: Optimization of the FDH concentration in the coupled demethylase assay. Increasing FDH concentrations (0 nM, 50 nM, 100 nM, 200 nM and 300 nM) were included in the assay cocktail with 1.0 μM JMJD2A and 700 μM H3K9me3 peptide substrate. The optimal assay concentration of FDH derived from this experiment was 100nM.

HEPES (pH 7.5), 50 mM NaCl, 50 µM $(NH_4)_2Fe(SO_4)_2$, 1 mM L-ascorbic acid, 1 mM NAD^+, 0.1 µM FDH, 1 mM 2-OG and variable concentrations of JMJD2 enzyme and H3K9me3 peptide substrate. The concentrations mentioned above were for a total assay volume of 100 µL. For determining the linear range of enzyme concentration, 700 µM H3K9me3 peptide was used and the concentration of the KDM was varied from 0.0-2.0 µM for JMJD2A and 0.0-1.0µM for JMJD2D. For performing the Michaelis–Menten kinetics, the KDM concentration was kept constant (1 µM JMJD2A and 0.5 µM JMJD2D) and the H3K9me3 peptide concentration was varied from 0-700 µM. To maintain optimal and reproducible activity in the assay, the $(NH_4)_2Fe(SO_4)_2$ and L-ascorbic acid stock solutions were prepared fresh every 2 hours to reduce their oxidation. For a 100 µL assay, 75 µL of the assay cocktail containing HEPES (pH 7.5), NaCl, $(NH_4)_2Fe(SO_4)_2$, L-ascorbic acid, NAD^+, FDH and KDM was prepared separately from 25 µl of the substrate cocktail containing H3K9me3 peptide and 2-OG. The assay and substrate cocktails were pipetted into 96-well black polypropylene plates (Corning Scientific) and incubated at 37º C in the plate reader for 3-4 min. Reactions were initiated by the addition of the substrate cocktail into the assay cocktail to produce a final volume of 100 µl. Care was taken to avoid any air bubbles in the wells and the plate was gently tapped before insertion into the plate reader. NADH fluorescence was measured every 30 sec for a period of 5–10 min using a Tecan Safire2 microplate reader with excitation and emission wavelengths of 340 and 490 nm, respectively. Table 2.1 provides a detailed template outlining the assay setup.

NADH Calibration Assay

To determine the gain setting for the plate reader and to calculate the rate of demethylation, an NADH calibration assay was performed prior to/alongside the KDM assay.

Table 2.1: Step-wise protocol for performing the FDH-coupled demethylase assay

Step	Reagent
75µL of assay cocktail is added to a well in a black 96 well plate	HEPES 7.5 (50 mM) NaCl (50 mM) $(NH_4)_2Fe(SO_4)_2$ (50 µM)* L-Ascorbic Acid (1 mM)* NAD^+ (1 mM) FDH (100 nM) KDM (variable) Water (to adjust volume to 75 µL) * Prepared fresh
25µL of substrate cocktail is added to a separate well	H3K9me3 peptide (variable) 2-OG (1 mM) Water (to adjust volume to 25 µL)
Incubate the cocktails in the microplate at 37 ºC for at least 3-4 min.	
Initiate the assay by pipetting substrate cocktail into assay cocktail and avoiding bubbles.	
Continuously monitor NADH fluorescence for 5-10 min in 30 sec intervals.	
Plot relative fluorescence units (RFUs) versus time and calculate the slope (RFU/min) by linear regression.	

All reagent concentrations represent the final concentration in the 100 µL assay volume. Depending on the type of microplate reader, the gain and Z-position are optimized using the NADH calibration assay (next section). For all the assays used in this study, a gain setting of 86 and Z position of 7220 µm was used.

The stock concentration of NADH was accurately determined by measuring the absorbance at 340 nm in a spectrophotometer (NADH ε_{340nm} = 6220 M^{-1} cm^{-1}). To perform the calibration assay, the assay cocktail from Table 2.1 was used in the absence of the KDM. A range of NADH concentrations (0.0-10.0 µM) was used in place of the substrate cocktail. After adding NADH to the assay cocktail, fluorescence was measured using the 'endpoint' setting in the plate reader. If the gain setting of the instrument was to be measured, the NADH calibration assay was performed under the 'optimal' gain setting and the gain setting determined by the instrument was used in all subsequent assays by inputting this gain under the 'manual' gain setting. The detailed set up of the NADH calibration curve and a sample plot are shown in Table 2.2 and Figure 2.8 respectively.

Determination of Kinetic Parameters

The FDH-coupled demethylase assay was performed in 30 sec intervals for at least 5 min. Relative fluorescence units (RFU) versus time was plotted and the slope (RFU/min) was calculated by linear regression. The initial velocity v_0 was calculated using the following equation:

$$v_0 = \text{rate of NADH formation (µM NADH min}^{-1}) = \frac{\text{slope of KDM assay (RFU/min)}}{\text{slope of NADH calibration curve (RFU/µM NADH)}}$$

Initial velocities (v_0) were then plotted as a function of substrate concentration, and the following Michaelis–Menten equation was fit to the data using Prism (GraphPad Software) to calculate the k_{cat} and K_m values:

Table 2.2: Step-wise protocol for performing the NADH calibration assay

Step	Reagent
75µL of assay cocktail is added to a well in a black 96 well plate	HEPES 7.5 (50 mM) NaCl (50 mM) $(NH_4)_2Fe(SO_4)_2$ (50 µM)* L-Ascorbic Acid (1 mM)* NAD^+ (1 mM) FDH (100 nM) 2-OG (1 mM) Water (to adjust volume to 85 µL) * Prepared fresh
25µL of NADH cocktail is added to a separate well	NADH (use a range from 0-10 µM) Example: (0 µM, 3.3 µM, 6.6 µM, 10 µM) Water (to adjust volume to 15µL)
Incubate the cocktails in the microplate at 37 ºC for at least 3-4 min.	
Pipet NADH cocktail into assay cocktail and avoiding bubbles.	
Monitor NADH fluorescence using Endpoint mode in the plate reader. Determine gain setting of the instrument.	
Plot relative fluorescence units (RFUs) versus NADH concentration and calculate the slope (RFU/µM NADH) by linear regression.	

.
All reagent concentrations represent the final concentration in the 100 µL assay volume

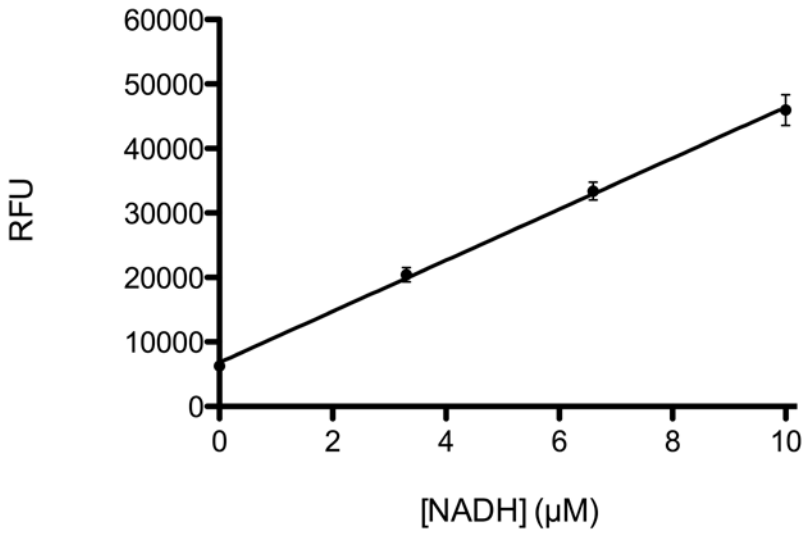

Figure 2.8: NADH calibration curve. RFUs were plotted as function of NADH concentration. The calibration curve data were measured just before or concomitantly with the KDM assays. The calibration curve shown here represents the fluorescence values measured at time = 0 min. Error bars represent standard deviation calculated from triplicate measurements.

$$v_0 = k_{cat}\,[E_{Total}][S] / (K_m + [S])$$

where

v_0 = initial velocity, µM NADH min^{-1}

k_{cat} = turnover number, min^{-1}

E_{Total} = total enzyme concentration, µM

[S] = substrate concentration, µM

K_m = substrate concentration yielding half-maximal velocity, µM

For peptides with high background drift, a control assay was run in the absence of KDM and the slope of RFUs versus time was determined. This was subtracted from the slope of RFUs versus time for all subsequent assays performed in the presence of KDM.

RESULTS

Purity of Recombinant Formaldehyde Dehydrogenase

Previous kinetic analyses using the FDH-coupled demethylase assay were carried out using commercially available FDH (Sigma). However, we had observed that these samples usually contain a large amount of bovine serum albumin (BSA) most likely added to stabilize the FDH. Many groups have shown that BSA has a propensity to chelate divalent metal ions and can catalyze the oxidation of Fe(II) to Fe(III) [21-24]. We hypothesized that using commercial FDH contaminated with BSA might be incompatible with the demethylase assay because the BSA could potentially deplete Fe(II) in the assay cocktail, and decrease the amount of Fe(II) available for the KDM. To circumvent this issue, we purified recombinant FDH from *P.putida* using

Zn(II) affinity column and gel filtration chromatography (Figures 2.4 and 2.5). We used a Zn(II) affinity column because FDH is a Zn(II) dependent metalloenzyme. Recombinant FDH purified by this method was not only of high purity, but was highly active and very compatible with the demethylase assay (Figure 2.7).

Purity of Strep(II)-Tagged JMJD2A and JMJD2D

We purified Strep(II)-tagged JMJD2A and JMJD2D using a two-step protocol : an affinity chromatography step on a Strep-Tactin column followed by gel filtration after tag removal. We noticed that the purity of the samples (as seen on an SDS PAGE gel) was high following the first affinity purification step (Figure 2.2). Hence, the Strep-Tactin column could be used as a one –step purification protocol to obtain highly pure recombinant protein. We purified the protein samples by gel filtration chromatography after overnight Strep(II)-tag cleavage by TEV protease and this yielded highly pure protein (Figure 2.3).

Metal Content Analysis of Strep(II)-Tagged JMJD2A and JMJD2D

We adopted a Strep-Tactin purification system to reduce the amounts of inhibitory transition state metals and obtain reliable kinetic parameters. To verify whether switching the conventional hexahistidine-Ni(II) sepharose purification to a Strep(II)-Strep-Tactin purification reduced the transition state metal content, we analyzed multiple Strep-Tactin purifications of JMJD2A and JMJD2D by ICP-HRMS (Table 2.3). As a control, we also analyzed the metal content of a three samples of Ni(II) column purified JMJD2D. The data clearly revealed that the Strep-Tactin purified enzymes have substantially lower amounts of transition state metals such as Co, Ni, Cu, Mn and Ca. The Zn content in these samples ranged from 84-90% which was

Table 2.3: Transition state metal content analysis of JMJD2A and JMJD2D

	JMJD2A Batch 1	**JMJD2A Batch 2**	**JMJD2D Batch 1**	**JMJD2D Batch 2**	**Ni column purified JMJD2D**
Metal Content (%)					
Zn	98	93	84	90.3	92
Fe	16	14	5.8	5.9	8.1
Ni	5.6	5.4	2.4	1.8	40-100*
Mg	0.50	0.50	N.D.	1.4	N.D.
Ca	0.50	0.50	N.D.	N.D.	N.D.
Co	0.17	0.09	0.15	0.19	N.D.
Mn	5.7	2.5	0.51	0.41	0.47
Cu	0.010	0.13	0.79	0.50	0.17

* Ni content range for three different batches of Ni(II) column purified JMJD2D.
N.D.- Not Detected.

consistent with the fact that JMJD2 KDMs contain a structural Zn-finger (Chapter 3). The percentage of other transition state metals except Fe was lower than 6%. We observed up to 16% Fe content in the JMJD2A samples suggesting that minor quantities of residual Fe co-purified with the enzyme. We also analyzed the metal content of three samples of Ni(II)-column purified JMJD2D. We observed close to 100% Zn corresponding to the structural Zn-finger and the percentage of Co, Cu, Ca and Mn were less than 6%. Strikingly however, the amount of Ni in these samples ranged from 40-100% suggesting that a significant amount of the metal had leached from the column. We concluded that Ni(II) was potentially bound in the active site with very high affinity because 40-100% Ni was prevalent even after extensive dialysis and gel filtration. The metal analysis data clearly showed that purifying KDMs on a Ni(II) column led to increased inhibitory metal contamination and adopting the Strep-Tactin column purification helped us overcome this issue.

Kinetic Analysis

We performed extensive kinetic analysis on JMJD2A and JMJD2D that were purified using the Strep-Tactin affinity system using the optimized FDH-coupled demethylase assay. In all the assays, the substrate used was an H3K9me3 peptide spanning residues 1-15 of histone H3, trimethylated at Lys 9. We first tested the linearity of enzyme concentration with initial velocity using 0.0-2.0 µM JMJD2A and 0.0-1.0 µM JMJD2D. We observed a linear relationship between enzyme concentration and initial velocity for both enzymes (Figure 2.9). Based on this test, we used 1.0 µM JMJD2A and 0.5 µM JMJD2D and measured the kinetic parameters for demethylation of an H3K9me3 peptide substrate. We performed this analysis with replicate purifications of JMJD2A and JMJD2D (Table 2.4) and observed a K_m of ~100 µM for the

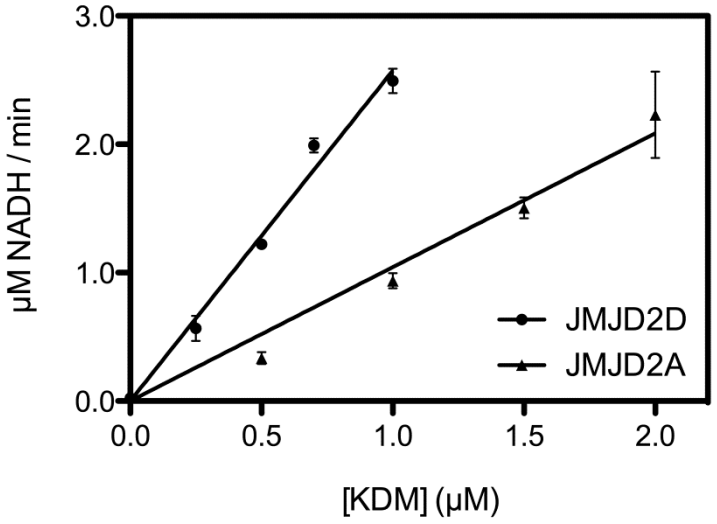

Figure 2.9: Linearity between JMJD2 enzyme concentration and initial velocity. Initial velocities were plotted as a function of JMJD2A (▲, 0.0–2.0 µM) and JMJD2D (●, 0.0–1.0 µM) concentration under conditions with a fixed substrate concentration (700 µM H3K9me3 peptide). The error bars represent standard deviations calculated from triplicate measurements for each data point. A linear regression was calculated for the data points corresponding to each enzyme. For the concentration ranges tested, both enzymes exhibited a linear relationship between concentration and initial velocity.

H3K9me3 peptide for both the enzymes (Figure 2.10 and 2.11). These values were within 2-fold of the K_m values previously reported for hexahistidine-tagged JMJD2A and JMJD2D assayed with the same-length H3K9me3 peptide substrate [7]. In contrast, the average k_{cat} values of Strep(II)-tagged JMJD2A were 1.8 min^{-1} and that of Strep(II)-tagged JMJD2D was 4.0 min^{-1} which were approximately 100- and 50-fold higher, respectively, than those previously measured for hexahistidine-tagged enzymes [7]. Our kinetic data clearly illustrate that the reduction in inhibitory transition state metals combined with the optimized assay resulted in enhanced enzymatic activity for the JMJD2 KDMs.

Use of Methyllysine Analog Bearing Substrates

Simon *et al* designed a method to site specifically install methyl-lysine analogs (MLAs) in full length histones and histone peptides [20] for use in biochemical analysis. This technique involves mutating the lysine of interest to a cysteine followed by alkylation via a halogenated ethylamine that is mono-, di-, or trimethylated (Figure 2.12). Using this protocol, we alkylated an H3K9C peptide to form an H3K9$_C$me3 peptide. After alkylation, the product was HPLC purified and homogeneity of the product was analyzed by Electrospray Ionization-Mass Spectrometry (ESI-MS). When we assayed the activity of JMJD2A for the H3K9$_C$me3 peptide, we observed 4-fold increase in the K_m and 9-fold decrease in k_{cat}/K_m compared to the H3K9me3 peptide of same length bearing a *bona fide* trimethyllysine (Figure 2.13 and Table 2.4). These findings illustrate that histone peptides bearing MLAs are suboptimal substrates for the JMJD2 enzymes compared to their *bona fide* methyllysine counterparts. Hence, biochemical studies and kinetic parameters obtained from the use of MLA bearing substrates may not be truly reflective of *in vivo* conditions.

Table 2.4: Kinetic constants of replicate purifications of Strep-Tactin column purified JMJD2A and JMJD2D

	JMJD2A Batch1	**JMJD2A Batch2**	**JMJD2D Batch1**	**JMJD2D Batch2**
K_m (μM)	96 ± 13	96 ± 7.9	102 ± 9.5	120 ± 18
k_{cat} (min^{-1})	1.7 ± 0.081	1.9 ± 0.05	3.3 ± 0.05	4.7 ± 0.12
k_{cat} / K_m (min^{-1} μM^{-1})	0.018 ± 0.002	0.019 ± 0.002	0.032 ± 0.003	0.038 ± 0.006

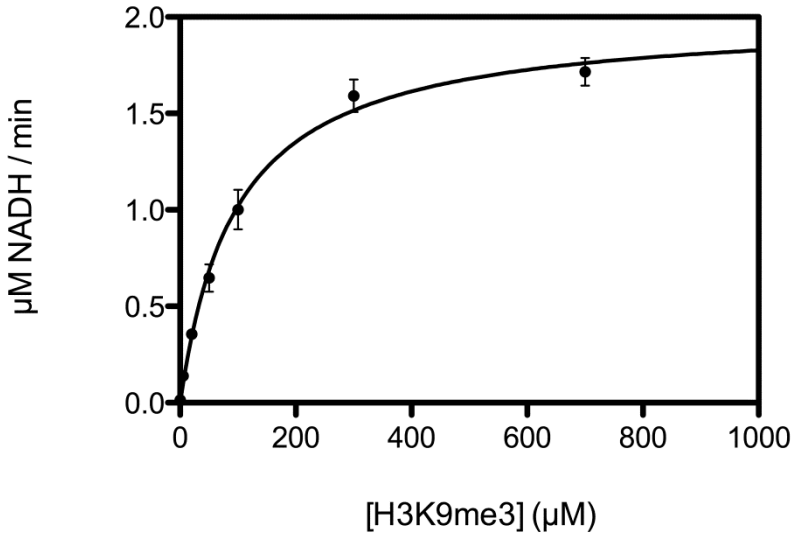

Figure 2.10: Kinetic analysis of JMJD2A and H3K9me3. Michaelis–Menten plot of initial velocity as a function of H3K9me3 peptide concentration for JMJD2A. 1.0 µM enzyme was used in this assay. The error bars represent standard deviation calculated from triplicate measurements. A hyperbolic fit to the data was calculated to determine k_{cat} and K_m values (Table 2.4).

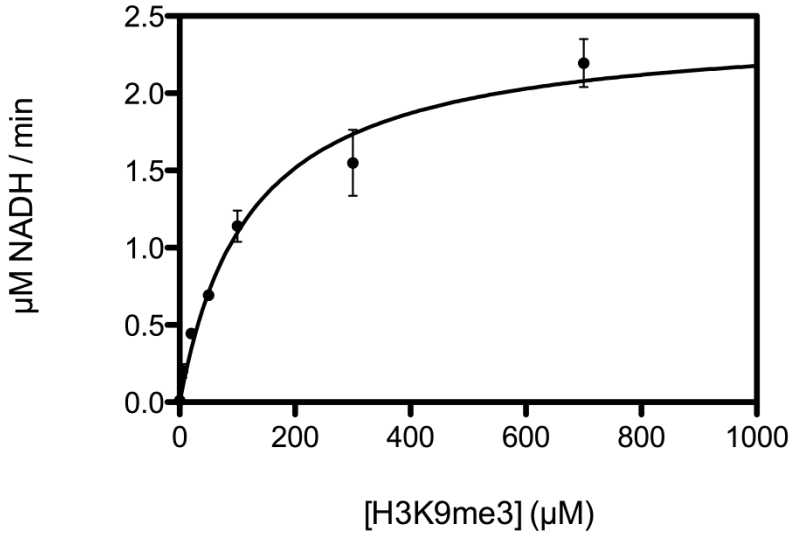

Figure 2.11: Kinetic analysis of JMJD2D and H3K9me3. Michaelis–Menten plot of initial velocity as a function of H3K9me3 peptide concentration for JMJD2D. 0.5 µM enzymes was used in this assay. The error bars represent standard deviation calculated from triplicate measurements. A hyperbolic fit to the data was calculated to determine k_{cat} and K_m values (Table 2.4).

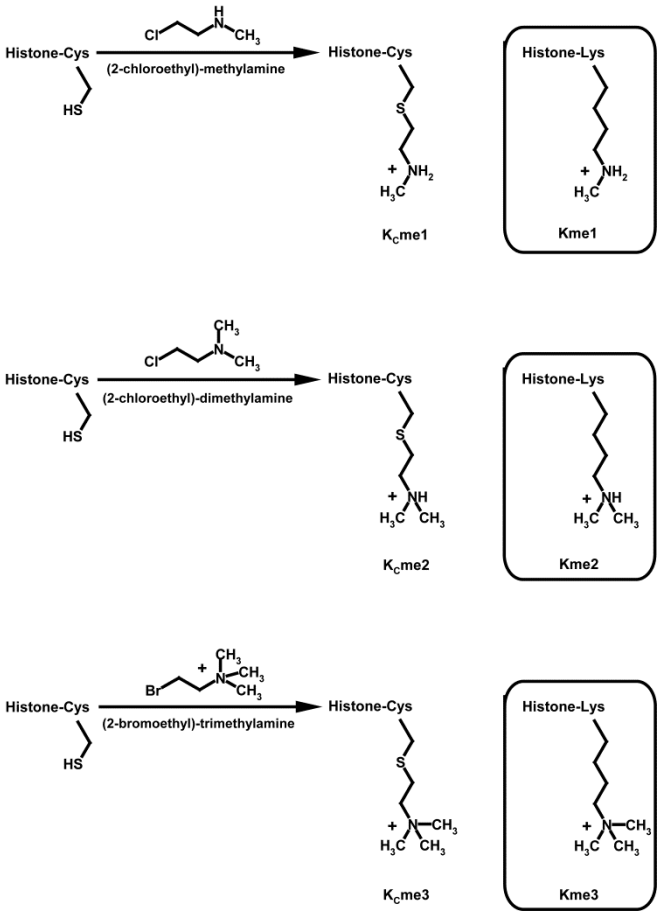

Figure 2.12: Schematic of site-specific installation of methyllysine analogs in histones.

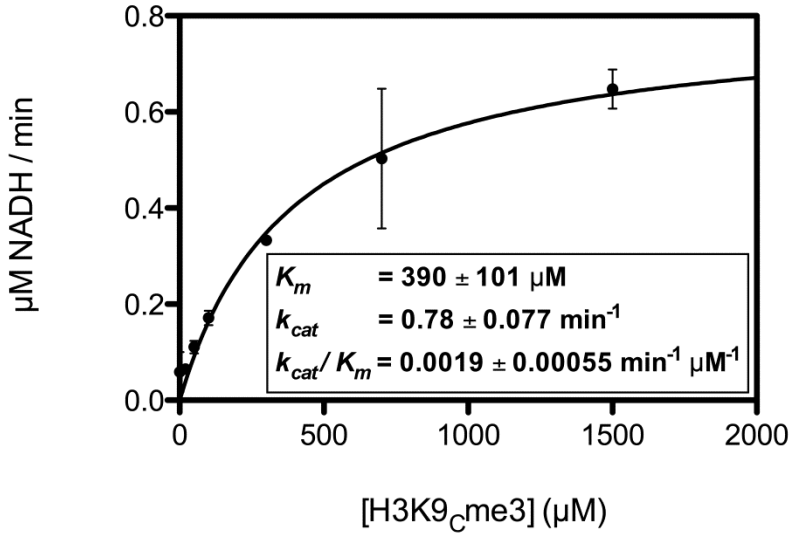

Figure 2.13: Kinetic analysis of JMJD2A and H3K9$_C$me3. Michaelis Menten plot of JMJD2A assayed with the H3K9$_C$me3 peptide substrate. The kinetic parameters for the H3K9$_C$me3 peptide are shown in the inset panel.

DISCUSSION

Since their discovery, relatively low enzymatic activities have been reported for the JmjC KDMs and this has opened questions concerning their biological activities and the possibility that they may need posttranslational modifications and other accessory factors or act on alternative substrates [1, 2]. Turnover numbers reported for these enzymes generally ranged from 0.01 to 0.5 min^{-1} [7-9]. By comparison, the k_{cat} values for the FAD dependent demethylase, LSD1 ranged from 2 to 12 min^{-1} toward H3K4me2 peptide substrates, according to kinetic studies published by several groups [3-6]. Previous studies on the JmjC enzymes have employed hexahistidine-tagged KDMs, which may have contained sub-stoichiometric concentrations of transition metals introduced during IMAC purification. Indeed, many studies have illustrated the susceptibility of JmjC enzymes to inhibition by these metal ions. For example JMJD2E is inhibited by transition metals used in IMAC, such as Ni(II), Co(II), Zn(II), and Cu(II), with IC_{50} values ranging between 0.5 and 15 μM, depending on the metal type [25]. These findings are consistent with *in vitro* and *in vivo* studies reporting inhibition of JMJD1A and JMJD2A by Ni(II) and Co(II), respectively [15, 25-28]. Transition metal ions can competitively inhibit JmjC KDMs through binding to the His-Glu/Asp-His triad that coordinates Fe(II) within the active site [7, 29, 30]. Furthermore, certain transition metal ions, such as Co(II) and Ni(II), can indirectly inhibit JmjC enzymes by catalyzing the oxidation of ascorbic acid, that maintains the redox balance in the demethylase assay. To overcome these issues, we employed a Strep-Tactin affinity purification system that yielded highly active recombinant JmjC KDMs. Notably, the Strep-Tactin purification provided a convenient method for isolating JmjC KDM apoenzymes that could be reconstituted with Fe(II) or other divalent transitional metal ions for biochemical studies. In addition, this approach minimized contamination by divalent transition metal ions as

shown by the ICP-HRMS data (Table 2.3). The turnover numbers for Strep-Tactin purified JMJD2A and JMJD2D measured using our optimized FDH-coupled demethylase assay were ~50-100 fold greater than those reported for their Ni(II) column purified counterparts [7]. Our findings emphasize that KDMs from the JmjC and LSD1 families display comparable lysine demethylase activity *in vitro* and suggest that these enzymes may possess similar activity profiles toward chromatin in living cells. These protocols can be extended to other families of JmjC demethylases such as the UTX and JMJD3 enzymes and other dioxygenases. In summary, these findings highlight the advantages of using affinity tags that are compatible with transition metal-free purification, such as the Strep(II)-tags, when isolating recombinant JmjC KDMs for functional studies as described in Chapters 4 and Appendix A.

ACKNOWLEDGEMENTS

The expression vector for *P. putida* FDH was obtained from Dr.Ashok Bhagwat at the Wayne State University and I thank him for his generosity. I also thank Particia Ortiz-Tello for starting the optimizations of the FDH assay and Evys Collazo for cloning pST4 JMJD2A and optimizing the Strep-Tactin purification. I thank Dr. Henriette Remmer at the Protein Structure Facility at the University of Michigan for synthesizing the H3K9me3 peptides. Finally, I thank Ted Huston at the Department of Geology, University of Michigan for performing the ICP-MS experiments on our JMJD2 enzyme samples.

REFERENCES

1. Culhane, J.C. and P.A. Cole, LSD1 and the chemistry of histone demethylation. Current opinion in chemical biology, 2007. 11(5): p. 561-8.

2. Mosammaparast, N. and Y. Shi, Reversal of histone methylation: biochemical and molecular mechanisms of histone demethylases. Annu Rev Biochem, 2010. 79: p. 155-79.

3. Forneris, F., et al., Human histone demethylase LSD1 reads the histone code. J Biol Chem, 2005. 280(50): p. 41360-5.

4. Gaweska, H., et al., Use of pH and kinetic isotope effects to establish chemistry as rate-limiting in oxidation of a peptide substrate by LSD1. Biochemistry, 2009. 48(23): p. 5440-5.

5. Schmidt, D.M. and D.G. McCafferty, trans-2-Phenylcyclopropylamine is a mechanism-based inactivator of the histone demethylase LSD1. Biochemistry, 2007. 46(14): p. 4408-16.

6. Szewczuk, L.M., et al., Mechanistic analysis of a suicide inactivator of histone demethylase LSD1. Biochemistry, 2007. 46(23): p. 6892-902.

7. Couture, J.F., et al., Specificity and mechanism of JMJD2A, a trimethyllysine-specific histone demethylase. Nat Struct Mol Biol, 2007. 14(8): p. 689-95.

8. Horton, J.R., et al., Enzymatic and structural insights for substrate specificity of a family of jumonji histone lysine demethylases. Nat Struct Mol Biol, 2010. 17(1): p. 38-43.

9. Kristensen, J.B., et al., Enzyme kinetic studies of histone demethylases KDM4C and KDM6A: towards understanding selectivity of inhibitors targeting oncogenic histone demethylases. FEBS Lett, 2011. 585(12): p. 1951-6.

10. Hillringhaus, L., et al., Structural and evolutionary basis for the dual substrate selectivity of human KDM4 histone demethylase family. J Biol Chem, 2011. 286(48): p. 41616-25.

11. Klose, R.J., E.M. Kallin, and Y. Zhang, JmjC-domain-containing proteins and histone demethylation. Nat Rev Genet, 2006. 7(9): p. 715-27.

12. Kawamura, A., et al., Development of homogeneous luminescence assays for histone demethylase catalysis and binding. Anal Biochem, 2010. 404(1): p. 86-93.

13. Tsukada, Y., et al., Histone demethylation by a family of JmjC domain-containing proteins. Nature, 2006. 439(7078): p. 811-6.

14. Hopkinson, R.J., et al., Monitoring the activity of 2-oxoglutarate dependent histone demethylases by NMR spectroscopy: direct observation of formaldehyde. Chembiochem, 2010. 11(4): p. 506-10.

15. Chen, H. and M. Costa, Iron- and 2-oxoglutarate-dependent dioxygenases: an emerging group of molecular targets for nickel toxicity and carcinogenicity. Biometals : an international journal on the role of metal ions in biology, biochemistry, and medicine, 2009. 22(1): p. 191-6.

16. Chen, H., et al., Nickel ions inhibit histone demethylase JMJD1A and DNA repair enzyme ABH2 by replacing the ferrous iron in the catalytic centers. J Biol Chem, 2010. 285(10): p. 7374-83.

17. Sekirnik, R., et al., 2-Oxoglutarate oxygenases are inhibited by a range of transition metals. Metallomics : integrated biometal science, 2010. 2(6): p. 397-9.

18. Schmidt, T.G. and A. Skerra, The Strep-tag system for one-step purification and high-affinity detection or capturing of proteins. Nat Protoc, 2007. 2(6): p. 1528-35.

19. Roy, T.W. and A.S. Bhagwat, Kinetic studies of Escherichia coli AlkB using a new fluorescence-based assay for DNA demethylation. Nucleic Acids Res, 2007. 35(21).

20. Simon, M.D., et al., The site-specific installation of methyl-lysine analogs into recombinant histones. Cell, 2007. 128(5): p. 1003-12.

21. Bar-Or, D., et al., Characterization of the Co2+ and Ni2+ binding amino-acid residues of the N-terminus of human albumin - An insight into the mechanism of a new assay for myocardial ischemia. European Journal of Biochemistry, 2001. 268(1): p. 42-47.

22. Masuoka, J., et al., Intrinsic Stoichiometric Equilibrium-Constants for the Binding of Zinc(Ii) and Copper(Ii) to the High-Affinity Site of Serum-Albumin. Journal of Biological Chemistry, 1993. 268(29): p. 21533-21537.

23. Masuoka, J. and P. Saltman, Zinc(Ii) and Copper(Ii) Binding to Serum-Albumin - a Comparative-Study of Dog, Bovine, and Human Albumin. Journal of Biological Chemistry, 1994. 269(41): p. 25557-25561.

24. Xu, X.L., et al., Oxygen-dependent oxidation of Fe(II) to Fe(III) and interaction of Fe(III) with bovine serum albumin, leading to a hysteretic effect on the fluorescence of bovine serum albumin. Journal of Fluorescence, 2008. 18(1): p. 193-201.

25. Thalhammer, A., et al., Inhibition of the histone demethylase JMJD2E by 3-substituted pyridine 2,4-dicarboxylates. Org Biomol Chem, 2011. 9(1): p. 127-35.

26. Chen, V.B., et al., MolProbity: all-atom structure validation for macromolecular crystallography. Acta Crystallographica Section D-Biological Crystallography, 2010. 66: p. 12-21.

27. Chen, Z., et al., Structural basis of the recognition of a methylated histone tail by JMJD2A. Proc Natl Acad Sci U S A, 2007. 104(26): p. 10818-23.

28. Li, Q., Q. Ke, and M. Costa, Alterations of histone modifications by cobalt compounds. Carcinogenesis, 2009. 30(7): p. 1243-51.

29. Elkins, J.M., et al., Structure of factor-inhibiting hypoxia-inducible factor (HIF) reveals mechanism of oxidative modification of HIF-1 alpha. J Biol Chem, 2003. 278(3): p. 1802-6.

30. Ng, S.S., et al., Crystal structures of histone demethylase JMJD2A reveal basis for substrate specificity. Nature, 2007. 448(7149): p. 87-91.

CHAPTER 3

METHYLATION SITE SPECIFICITY STUDIES - CRYSTAL STRUCTURE OF HUMAN JMJD2D

The human JMJD2 family comprises four members- JMJD2A, JMJD2B, JMJD2C and JMJD2D. These enzymes are characterized by an N-terminal JmjN domain followed by the catalytic JmjC domain and a large C-terminal region. Most homologs possess addition Tudor and PHD domains (Figure 1.4 from Chapter 1). This family of enzymes has been implicated in a wide range of biological functions including neuronal development (JMJD2A), androgen receptor signaling and prostate development (JMJD2A, JMJD2C and JMJD2D), estrogen receptor signaling (JMJD2B) [1-10]. Despite the high degree of sequence identity (>75%) within their catalytic domains (Figure 3.1), the JMJD2 KDMs are quite distinct in their substrate specificities. All members of the JMJD2 family can demethylate H3K9me3, a repressive mark and corroboratively these enzymes have been implicated in transcriptional activation [1, 5, 10-25]. In addition, JMJD2A, JMJD2B and JMJD2C can also demethylate H3K36me3, a chromatin modification that is associated with the elongating form of RNA Polymerase II [7, 26-31]. JMJD2D, on the other hand, lacks specificity for the H3K36me3 site and is highly specific for H3K9me3/me2 [32]. The molecular mechanisms by which these enzymes achieve selectivity for specific sites have not been well studied. Although a number of crystal structures of JMJD2A in complex with both H3K9me3 and H3K36me3 were solved [33-35], these studies do not provide insights into why JMJD2D lacked specificity for the H3K36me3 site. To address this question,

Figure 3.1: Sequence Alignment of the JMJD2 family of KDMs. The residues in different domains are colored: Purple: JmjN domain; Orange: Mixed domain; Red: JmjC domain and Green: C-terminal domain. Residues involved in metal coordination, 2-OG binding and Zn-finger are highlighted in yellow, cyan and gray respectively [32, 34, 35].

we determined the crystal structure of JMJD2D (this chapter) and performed structural comparisons, docking studies and biochemical analysis with an array of mutant and hybrid peptide substrates (Chapter 4). Our results yield new insights into the site-specific demethylation by JMJD2 enzymes and these studies will aid in understanding the biological functions of H3K9me3 and H3K36me3 demethylation.

MATERIALS AND METHODS

Cloning, Expression and Purification of His-JMJD2D

The catalytic domain of human JMJD2D (residues 12-342) was cloned into a variant of pET15b (Millipore EMD Biosciences) with a tobacco etch virus (TEV) protease cleavage site to facilitate removal of the N-terminal hexahistidine tag [34]. The enzyme was overexpressed in *E. coli* BL21 DE3 Rosetta 2 cells. Protein expression was induced by the addition of 1 mM IPTG and cells were allowed to grow at 16º C overnight. Cell pellets were re-suspended in Buffer A (100 mM Tris (pH 7.5) and 500 mM NaCl) and stored at -20ºC. Purification was performed using a refrigerated FPLC system and the enzyme sample was kept on ice at all other times to prevent protein precipitation. 150 µL of EDTA-free Halt protease inhibitor cocktail (Thermo) was added to each cell pellet (obtained from 1 liter of culture) before sonication to prevent proteolysis. Cell lysate was injected into a pre-equilibrated Ni(II) sepharose column (GE Healthcare) using a 150 ml superloop. After washing the column extensively (at least 4 column volumes), the protein was eluted using a linear gradient of Buffer B (Buffer A + 500 mM imidazole). Peak fractions (Figure 3.2) were pooled and 1 mg/ml TEV protease was added to facilitate removal of the hexahistidine tag. After tag removal, the sample was subject to batch binding for 1 h using 5 ml Ni(II) sepharose resin (to remove uncleaved protein), concentrated

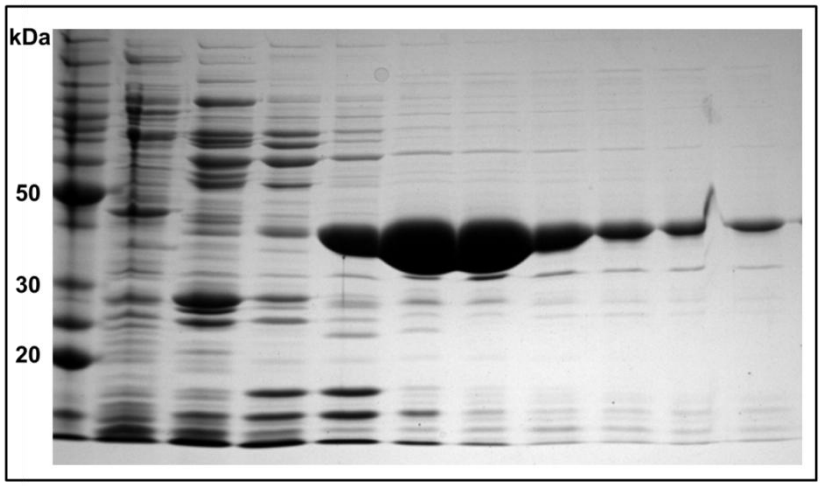

Figure 3.2: Ni(II) column purification of JMJD2D. Lane 1: Molecular Weight Standards; Lane 2: Flow through from column; Lane 3-Lane10 : Fractions 5-13. The protein was purified using an FPLC system.

and loaded on a Superdex 200 gel filtration column (GE Healthcare) pre-equilibrated with 20 mM Tris (pH 7.5) and 150 mM NaCl. Peak fractions (Figure 3.3) were concentrated to 10-20 mg/ml as determined by absorbance at 280 nm, flash frozen, and stored at –80° C.

Crystallization of JMJD2D•2-OG•H3K9me3 Ternary Complex

All crystallization experiments and crystal harvesting were performed at 4º C. Initial crystallization trials were set up using the commercially available sparse-matrix screening kits which included Index (Hampton), JCSG+ (Qiagen), Wizard (Emerald Biosystems), Structure Screen (Molecular Dimensions), PEGs I and II screens (Qiagen), Ammonium Sulfate screen (Qiagen), Cation Screen (Qiagen) and Anion Screen (Qiagen). Crystal drops were set up using 1 µl of protein sample and 1 µl of mother liquor. Two protein samples were used in the crystallization screens- one sample was prepared with 10-12 mg/ml JMJD2D, 1.5 mM 2-OG and 1.5 mM H3K9me3 peptide (New England Peptide) and the second sample was prepared without the peptide. To ensure the presence of the peptide in crystals, only conditions that yielded crystals in the presence of the peptide and not in its absence were pursued. Plate clusters were obtained in 0.3M Potassium Nitrate (KNO_3) and 16% PEG 3350. To further optimize this condition and obtain diffraction quality crystals, we performed an additive screen (Hampton) and the manufacturers' protocol was followed. The additive sodium thiocyanate produced the highest quality crystals which contained a combination of 'flame' and 'diamond' shaped crystals (Figure 3.4). These conditions were further optimized in a 24-well hanging drop set up and we obtained reproducible crystals in 7% PEG 3350, 0.1 M sodium thiocyanate and 0.35M KNO_3. Crystals were harvested by serial transfer into the crystallization solution supplemented with 5%, 15% and 25% 1,3-propanediol and subsequently flash frozen in liquid nitrogen.

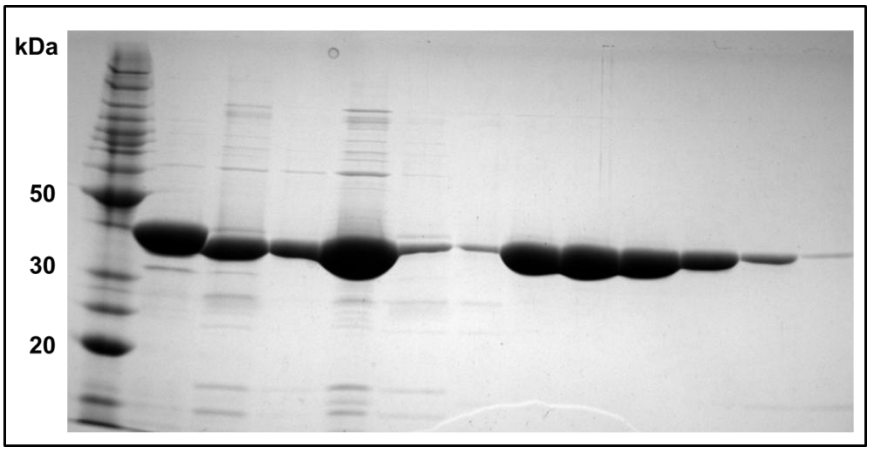

Figure 3.3: S200 purification of JMJD2D. Lane 1: Molecular Weight Standards; Lane 2: Before TEV cleavage; Lane 3: After TEV Cleavage, before batch binding; Lane 4: After batch binding; Lane 5: After concentration; Lane 7: Fraction 24 Lane 8: Fraction 26 Lane 9: Fraction 27 Lane 10: Fraction 28; Lane 11: Fraction 29; Lane 12: Fraction 30; Lane 13: Fraction 32.

Figure 3.4: Crystals of the JMJD2D•2-OG•H3K9me3 ternary complex. 'Flame' and 'diamond' shaped crystals were grown in 7% PEG 3350, 0.1 M sodium thiocyanate and 0.35M KNO_3.

Optimization of Crystals by Surface Entropy Reduction

Few crystallographic conditions were obtained in the sparse matrix screens with JMJD2D in the absence of the peptide. To enhance the crystallizability of the enzyme, the Surface Entropy Reduction (SER) method was used [36-39]. In the SER technique, high entropy amino acid residues (such as Lysines and Glutamates) that are surface exposed are mutated to smaller amino acids such as alanines which have low entropy side chains. High entropy amino acids on the surface are disfavored at protein-protein interfaces and could potentially diminish the chances of forming stable crystals. When we submitted the sequence of JMJD2D to the SER server [39], the top hit was four lysines in the enzyme- K91, K92, K93 and K94. These lysines were clustered into two groups of mutations- (i) K91A/K92A and (ii) K93A/K94A. The enzymatic activity of these mutations was also verified prior to crystallization to ensure these mutations did not perturb catalysis. Crystal screens were set up using the commercially available spare-matrix screens listed above using 10 mg/ml protein and 1.5 mM 2-OG. Both mutation sets had a marked improvement in crystallizability of JMJD2D compared to the WT counterpart. Among the two mutation sets, the K93A/K94A mutant produced best quality crystals and only this mutant was pursued. 'Diamond' shaped crystals were obtained in 0.2 M calcium acetate, 0.1 M HEPES 7.5 and 10% PEG 8000 (Figure 3.5). The crystals were optimized by vapor diffusion and were harvested by serial transfer into the crystallization solution supplemented with 5%,15%, and 25% glycerol and then flash frozen in liquid nitrogen.

X-Ray Diffraction Data Collection, Processing and Structure Determination

Diffraction data were collected at the Life Sciences-Collaborative Access Team (LS-CAT) beamline 21-ID-G at the Advanced Photon Source Synchrotron (Argonne, IL). Crystals of

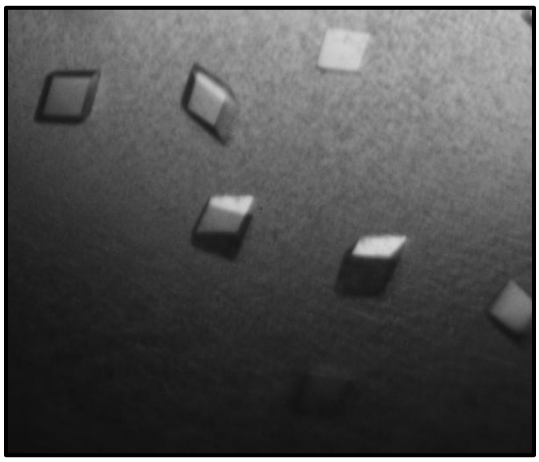

Figure 3.5: Crystals of JMJD2D apoenzyme (K93A/K94A). ‘Diamond’ shaped crystals were grown at 0.2 M calcium acetate, 0.1 M HEPES 7.5 and 10% PEG 8000.

the JMJD2D ternary complex diffracted to 1.8 Å and those from the K93A/K94A mutant (hereon referred to as apoenzyme) diffracted to 2.5 Å. The crystallographic statistics for both structures are listed in Table 3.1. Data was processed and scaled using HKL2000 [40]. Molecular replacement was performed using MOLREP [41] with a JMJD2A structure (PDB entry: 2Q8C) used as the search model for the JMJD2D ternary complex. The structure of the complex was subsequently used as a search model for the JMJD2D apoenzyme. Model building and refinement were conducted using Coot and Refmac, respectively [42, 43]. TLS refinement was used to improve the electron density maps of the JMJD2D apoenzyme [44, 45]. Simulated annealing omit maps were calculated using CNS [46, 47]. After refinement, structures were validated using MOLPROBITY [48]. Structural figures were rendered using PyMOL (Schrodinger, LLC).

Note: For the remainder of Chapter 3, and the whole of Chapters 4 and 5, amino acid residues from the histone peptide substrates are denoted using the one letter code and enzyme residues are denoted using the three letter code.

RESULTS

Structure of JMJD2D Apoenzyme

The crystal structure of the JMJD2D apoenzyme is shown in Figure 3.6. Although 2-OG was added to the protein solution during crystallization, we did not observe any appreciable electron density for the cofactor. However, strong density for the active site metal was seen. We modeled this metal as Ni(II), because the JMJD2D protein sample was purified on a Ni column chromatography and we usually observed >50% Ni(II) content in these samples (Table 2.3).

Table 3.1: Crystallographic Data and Refinement Statistics of JMJD2D

		JMJD2D•2-OG•H3K9me3	JMJD2D apoenzyme
RCSB PDB ID		4HON	4HOO
Data Collection			
Beamline		APS 21-ID-G	APS 21-ID-G
Wavelength (Å)		0.9786	0.9786
Space Group		$P2_12_12_1$	$P3_2$
Cell Dimensions *a,b,c* (Å)		72.2, 79.7, 176.0	73.1, 73.1, 136.0
Resolution Range (Å)[a]		25.0-1.80 (1.84-1.80)	25.0-2.50 (2.57-2.50)
R_{merge} (%)[a]		6.00 (41.80)	5.90 (43.20)
$I/\sigma I$ [a]		31.27 (5.25)	18.60 (2.40)
Completeness (%)[a]		94.50 (100.0)	91.50 (87.0)
Unique Reflections		89,438	25,850
Redundancy[a]		13.70 (10.60)	5.30 (3.10)
Refinement & Validation[b]			
No. of Reflections		84,616	24,508
No. of Atoms		5891	5347
Protein Atoms		5347	5182
Ligand Atoms		133	4
Solvent Atoms		411	161
R_{work}/R_{free} [c]		18.9/ 21.4	20.7/24.6
B-factors (Å^2)			
Overall		20.5	39.0
Protein		19.7	39.5
Ligands		33.5	46.9
Waters		26.3	21.0
Root Mean Square Deviation			
Bond Length (Å)		0.015	0.013
Bond Angles (°)		1.43	1.49
MolProbity Scores			
Clashscore (all atoms)[d]		6.85 (90th percentile N=837)	7.94 (98th percentile N=271)
Molprobity Score		1.41 (96th percentile N=11444)	2.23 (89th percentile N=6960)
Resolution Range (Å)		1.80 ± 0.25	2.50 ± 0.25
Ramachandran			
Favored (%)		98.5	95.7
Allowed (%)		1.5	4.3
Outliers (%)		0	0

[a] Values in parentheses correspond to the highest-resolution shell. [b] Structures were refined in Refmac [42] using isotropic temperature-factor refinement [c] $R_{work} = \Sigma \, ||F_o|-|F_c|| \, / \, \Sigma \, |F_o|$; R_{free} = 5% of the total reflections. [d] Clashscore is the number of serious steric overlaps (> 0.4 Å) per 1000 atoms.

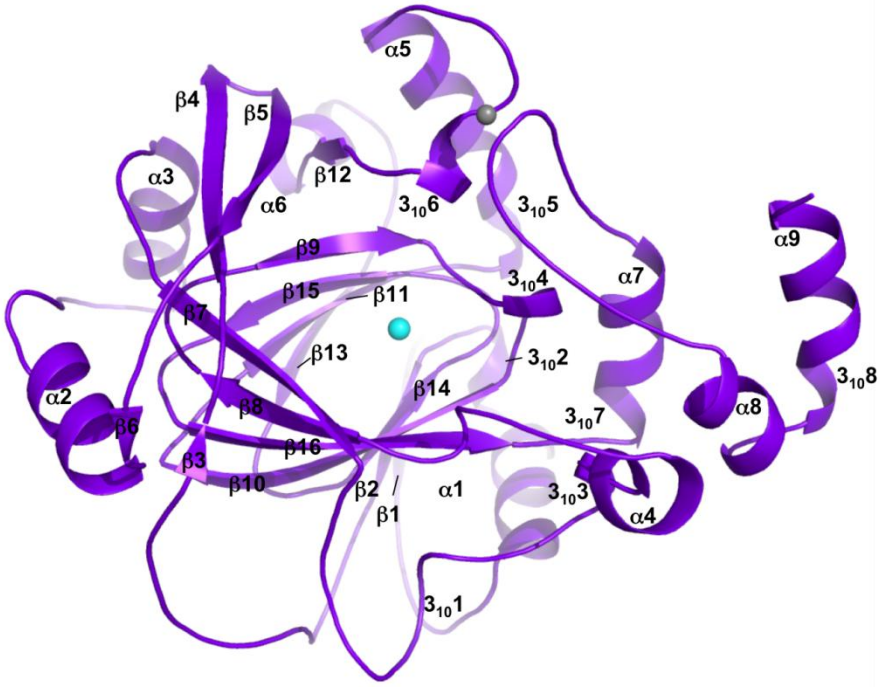

Figure 3.6: Structure of JMJD2D apoenzyme at 2.5Å resolution. The secondary structure elements are defined as: α-helices; β-sheets; 3_{10}-3_{10} helices. Cyan and gray spheres represent Ni(II) and Zn(II) respectively.

The JmjC domain (residues 146-312) of the enzyme adopts a β-barrel fold that is highly homologous to the structures of other JMJD2 KDMs [33-35, 49]. The C-terminal region of the enzyme (312-342) harbors a Zn-binding motif composed of residues His244, Cys238, Cys310 and Cys312 (Figure 3.6), a structural feature conserved throughout the JMJD2 family. The overall structure and domains of JMJD2D are very similar to JMJD2A and JMJD2C with an RMSD Cα (261 atoms) of ~ 0.4Å (Figure 3.7).

Structure of the JMJD2D•2-OG•H3K9me3 Complex

The overall structure of the JMJD2D ternary complex and apoenzyme were very similar and there were no major structural changes upon peptide binding (RMSD Cα = 0.26 Å for all aligned Cα atoms) (Figure 3.8). Simulated annealing omit maps illustrate clear electron density for the co-factor 2-OG, the active site Ni(II) that is bound in the Fe(II) coordination site and residues 6-15 in the H3K9me3 peptide substrate (Figures 3.9 and 3.10). Prior to the solution of our structures, two unpublished structures of the JMJD2D catalytic domain were deposited in the Protein Data Bank (PDB entry: 3DXT and 3DXU) and had been cited in previous studies [49]. In these structures, the C-terminal region adopts an alternative conformation that is not observed in JMJD2A, JMJD2C, or the JMJD2D structures reported here (Figure 3.11). This alternative conformation is presumably stabilized by crystal packing forces as there some crystal contacts observed at the C-terminal region of JMJD2D (Figure 3.12). Structural alignment with the JMJD2D ternary complex illustrates that this alternate conformation results in steric clashes with the N-terminal region of the H3K9me3 substrate (Figure 3.13). In addition, Gly174, which forms part of the trimethyllysine binding pocket (Figure 3.11) is shifted ~12 Å out of the active site in the previously deposited JMJD2D structures. These results indicate that this alternate

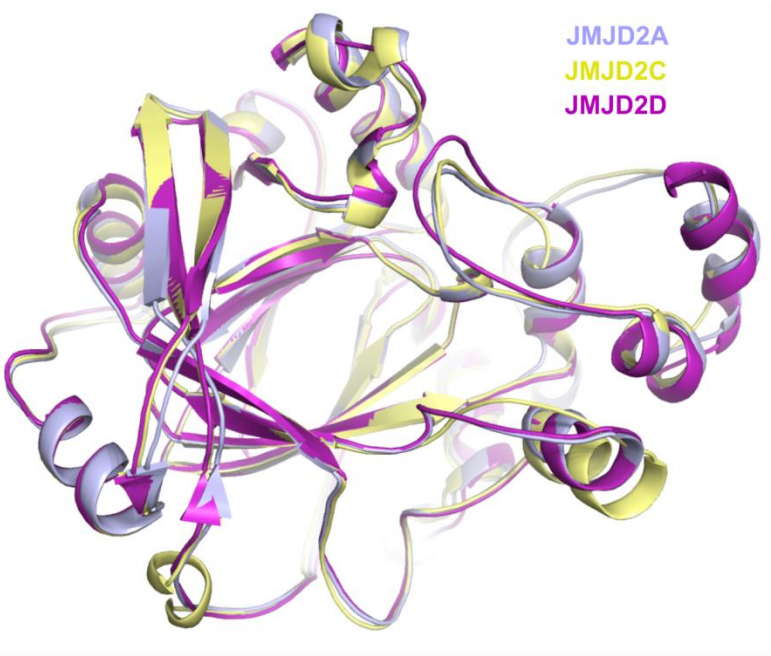

Figure 3.7: Structural conservation among JMJD2 KDMs. Alignment of the apoenzyme structures of JMJD2A (blue), JMJD2C (yellow) and JMJD2D (purple). RMSD Cα (261 atoms)= 0.4Å.

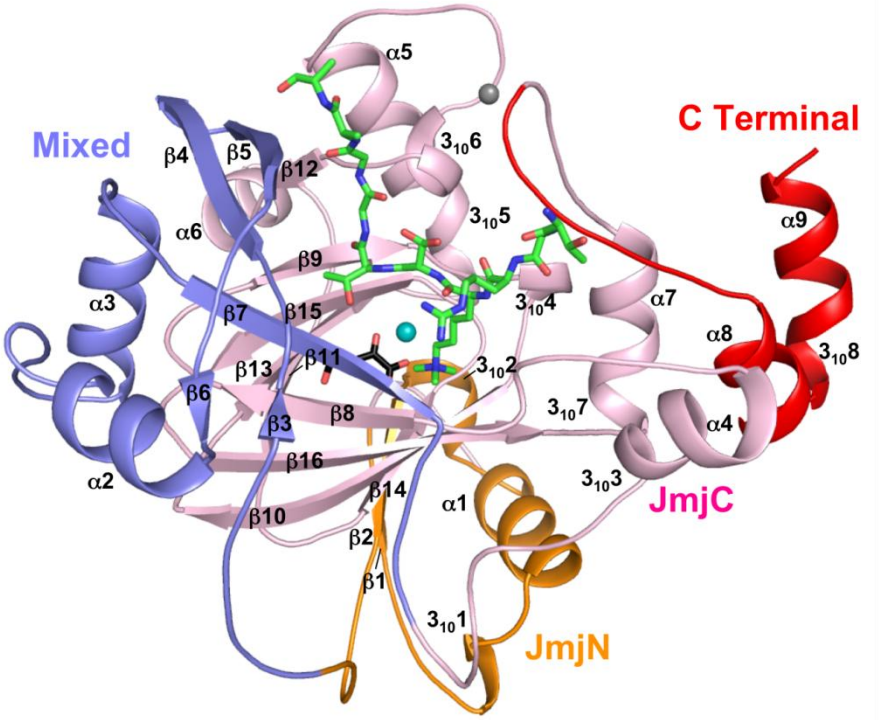

Figure 3.8: Structure of the JMJD2D•2-OG•H3K9me3 ternary complex at 1.8Å resolution. The JmjN domain (orange), JmjC domain (pink), Mixed domain (blue) and C terminal domain (red) are depicted in cartoon representation with the secondary structural elements labeled. Cyan and gray spheres represent Ni (II) in the active site and Zn(II) in the C-terminal Zn motif, respectively. Stick representation of the cofactor 2-OG (black) and the substrate H3K9me3 peptide (green) are shown

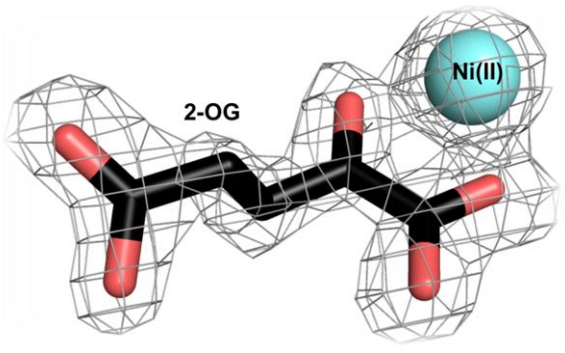

Figure 3.9: Simulated annealing omit map of 2-OG and Ni(II). F_o-F_c omit map of are contoured at 3.0 σ for 2-OG (black) and Ni(II) (cyan)

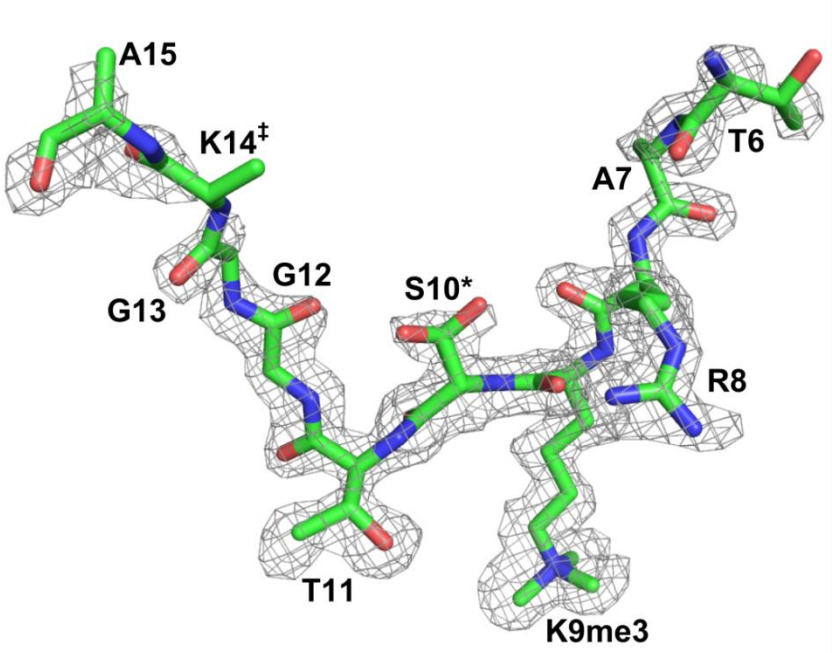

Figure 3.10: Simulated annealing omit map of the H3K9me3 peptide. F_o-F_c omit maps are contoured at 2.0 σ for the H3K9me3 peptide (green). *Two conformations were observed for S10 and each was modeled with an occupancy of 0.5. ‡ The side chain of K14 was not modeled due to a lack of electron density.

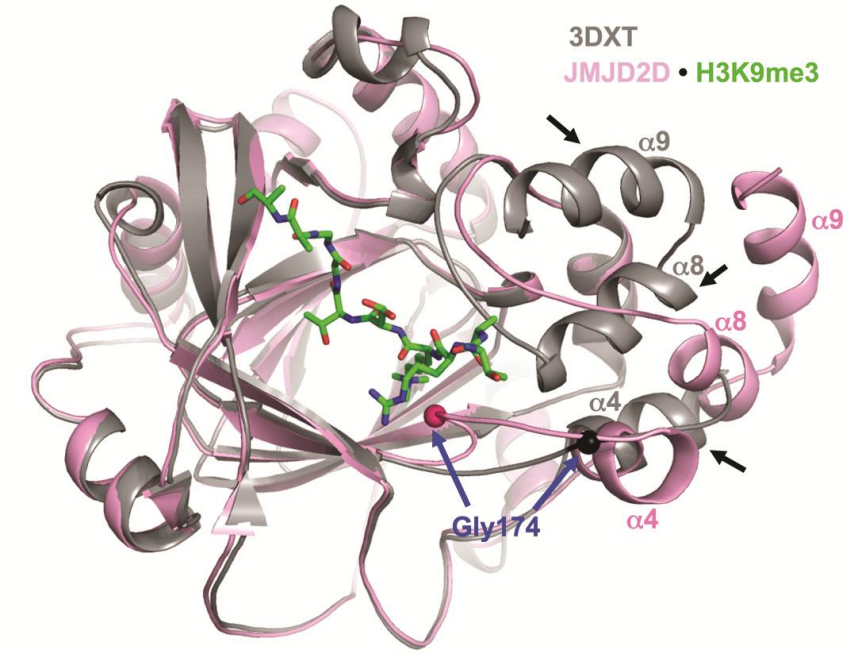

Figure 3.11: Comparison of the JMJD2D•2-OG•H3K9me3 structure and 3DXT. Superimposition of the structures JMJD2D•2-OG•H3K9me3 ternary complex (pink and green) and an unpublished structure of the JMJD2D catalytic domain that was previously deposited into the Protein Data Bank (3DXT.pdb, gray). The dark pink and black spheres represent the position of the active site Gly174 in the JMJD2D•2-OG•H3K9me3 and 3DXT structures, respectively. The positions of helices α4, α8 and α9 (denoted by black arrows) in the 3DXT structure are shifted into different orientations relative to their positions in the JMJD2D ternary complex.

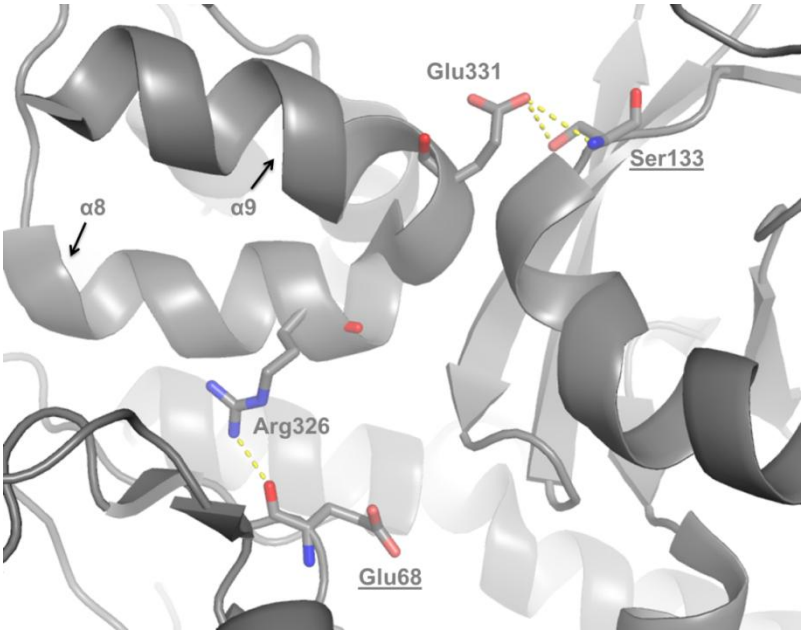

Figure 3.12: Crystal contacts in 3DXT. The alternate C-teminal conforamtion observed in the 3DXT structures could be stabilized by crystal contacts (yellow dashes). Residues from neighbouring asymmetric units are underlined.

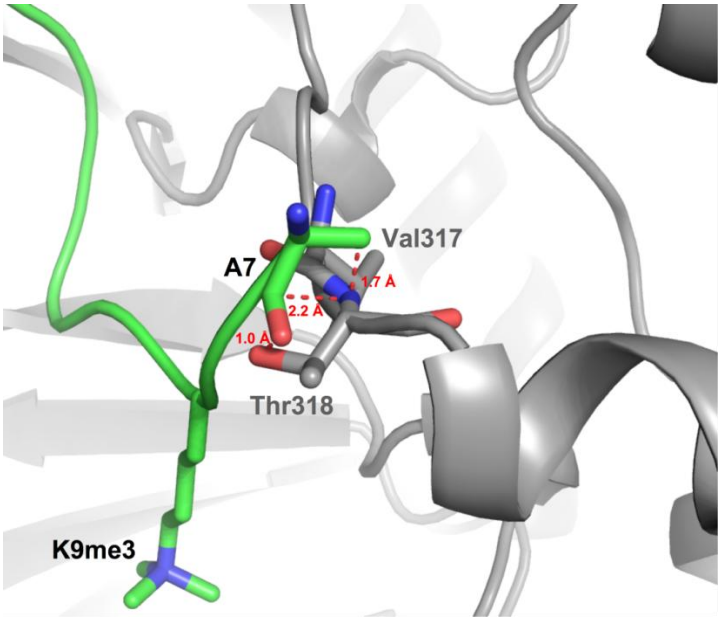

Figure 3.13: Steric clashes in the 3DXT structure. Docking of the H3K9me3 peptide (green carbons) into the 3DXT structure (gray) based on its superimposition with the JMJD2D ternary complex illustrates steric clashes (denoted by red dashes) between A7 in the peptide and Val317 and Thr318 in the 3DXT structure. The clashes are a consequence of the alternate conformation adopted by the C-terminal region in the 3DXT structure.

conformation is incompatible for trimethyllysine recognition and demethylation.

In the active site of JMJD2D, Ni(II) occupies the Fe(II) binding site and is coordinated by His192, Glu194, and His280 (Figure A.3 in Appendix A). The methyl groups of K9me3 in the H3 peptide are coordinated by a network of CH•••O hydrogen bonds to residues Tyr181, Glu194 and Gly174 in JMJD2D. This binding mode is conserved in JMJD2A, with the exception that Ala292 in JMJD2D is substituted by Ser288 in JMJD2A (Figure A.3 in Appendix A) [34]. The H3K9me3 peptide adopts a "W"-shaped conformation with two sharp bends when bound in the histone binding cleft of JMJD2D, analogous to the H3K9me3 binding mode observed in JMJD2A [34, 35]. The first bend occurs at K9me3 and deposits the trimethyllysine substrate into a narrow channel leading to the active site, whereas the second bend at T11 positions the threonyl side chain into a shallow pocket adjacent to the active site (Figure 3.8).

Interactions of JMJD2D with Substrate H3K9me3

A combination of main chain and side chain hydrogen bonds and van der Waals contacts between the H3K9me3 peptide and JMJD2D facilitate optimal recognition of the substrate (Figure 3.14). Most of the side chain interactions occur close to the demethylation site i.e. K9. At the -1 position, R8 is recognized by an intricate network of hydrogen bonds to Asp135 and Tyr179 in JMJD2D. With respect to residues in the C-terminal half of the H3K9me3 peptide, S10, T11 and G12, corresponding to the +1, +2 and +3 positions, adopt a bent conformation that enables these amino acids to bind efficiently inside a pocket adjacent to the active site. This bent conformation is maintained through two hydrogen bond networks: (1) S10 adopts two alternate side chain conformations that enable intra-peptide hydrogen bonding to either the G12 carbonyl oxygen and amide nitrogen or to the R8 carbonyl oxygen and (2) A hydrogen bond between the

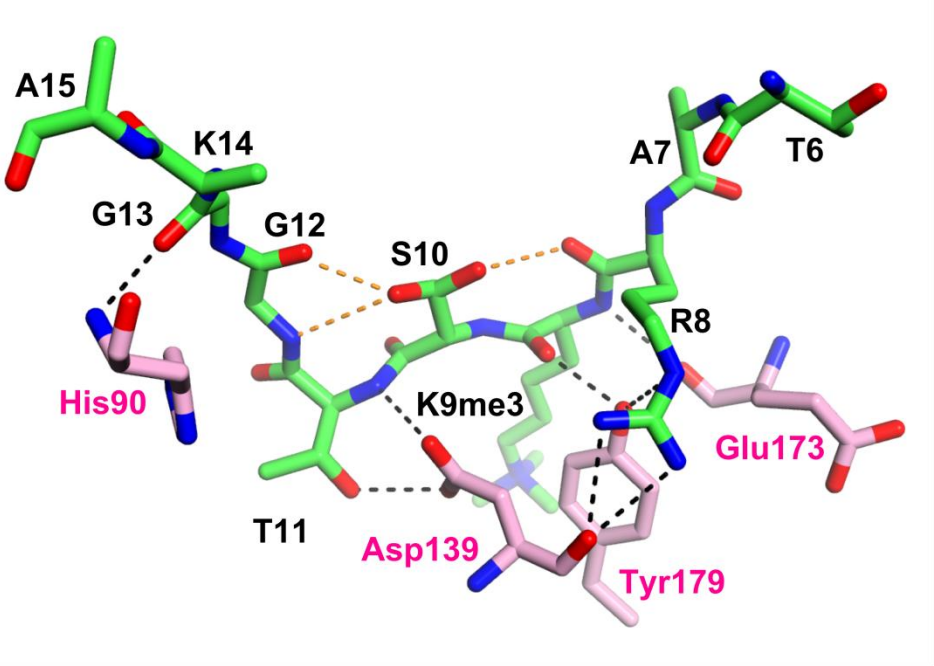

Figure 3.14: Recognition of the H3K9me3 peptide by JMJD2D. Interactions between the H3K9me3 peptide substrate (green) and JMJD2D (pink) showing intra-peptide and enzyme-peptide hydrogen bonds as orange and black dashes, respectively.

side chains of T11 and Asp139 in JMJD2D (Figure 3.14). In addition to these side chain interactions a few main chain interactions are also formed between JMJD2D and the peptide. Hydrogen bonds between the carbonyl oxygen of Glu173 and backbone nitrogen of K9 and between side chain hydroxyl group of Tyr179 and carbonyl oxygen of K9 enable efficient positioning of the K9me3 side chain into the deep acidic pocket that leads into the active site. At the C- terminal region, a hydrogen bond is formed between the backbone nitrogen of His90 and carbonyl oxygen of G13. In summary, a number of main chain and side chain peptide interactions enable efficient recognition of the H3K9me3 site by JMJD2D.

DISCUSSION

The crystal structure of the ternary complex offers insights into how the H3K9me3 site is efficiently recognized by JMJD2D. The apoenzyme structure reveals that JMJD2D does not undergo any major structural changes to accommodate the histone substrate consistent with what has been reported with JMJD2A [34, 35]. The structure of the catalytic domain of JMJD2D is very similar to that of the other human JMJD2 homologs such as JMJD2A and JMJD2C which can demethylate the H3K9me3 site. The JmjC domain structure is also well conserved between JMJD2D and the yeast JmjC KDM, Rph1 with an RMSD of 0.8 Å [50]. Rph1 is exhibits similar substrate specificities to the JMJD2 family wherein it can demethylate both H3K9me3 and H3K36me3 [50, 51]. Although there is no structural data of an Rph1-substrate complex, some of the residues involved in efficient recognition of H3K9me3, such as Asp139 in JMJD2D (Asp135 in JMJD2A) and Tyr179 in JMJD2D (Tyr175 in JMJD2A) are conserved in Rph1 indicating potential similarities in the mode of substrate recognition.

JMJD2D engages in a number of interactions with the H3K9me3 peptide, most of them

being proximal to the K9me3 site. Many of these enzyme-peptide interactions are also conserved in the JMJD2A•H3K9me3 peptide complex, but upon close inspection, several subtle, albeit significant differences were noticed in the H3K9me3 binding modes between JMJD2D and JMJD2A, suggesting differences in recognition of this site (Chapter 4). In addition, using the structures of JMJD2D and a JMJD2A•H3K36me3 complex [33], we delineated the molecular basis for discrimination against the H3K36me3 site by JMJD2D (Chapter 4).

ACKNOWLEDGEMENTS

I would like to thank Stacie Bulfer for the initial cloning of the pHT4-JMJD2D construct. I also thank David Smith and Elena Kondrashkina (LS-CAT, Advanced Photon Source Synchrotron) for assistance in X-ray data collection.

REFERENCES

1. Black, J.C., et al., Conserved antagonism between JMJD2A/KDM4A and HP1gamma during cell cycle progression. Mol Cell, 2010. 40(5): p. 736-48.

2. Iwamori, N., et al., The testis-enriched histone demethylase, KDM4D, regulates methylation of histone H3 lysine 9 during spermatogenesis in the mouse but is dispensable for fertility. Biol Reprod, 2011. 84(6): p. 1225-34.

3. Lin, C.H., et al., Heterochromatin protein 1a stimulates histone H3 lysine 36 demethylation by the Drosophila KDM4A demethylase. Mol Cell, 2008. 32(5): p. 696-706.

4. Lin, C.H., et al., HP1a Targets the Drosophila KDM4A Demethylase to a Subset of Heterochromatic Genes to Regulate H3K36me3 Levels. PLoS One, 2012. 7(6): p. e39758.

5. Loh, Y.H., et al., Jmjd1a and Jmjd2c histone H3 Lys 9 demethylases regulate self-renewal in embryonic stem cells. Genes Dev, 2007. 21(20): p. 2545-57.

6. Lorbeck, M.T., et al., The histone demethylase Dmel\Kdm4A controls genes required for life span and male-specific sex determination in Drosophila. Gene, 2010. 450(1-2): p. 8-17.

7. Mosammaparast, N. and Y. Shi, Reversal of histone methylation: biochemical and molecular mechanisms of histone demethylases. Annu Rev Biochem, 2010. 79: p. 155-79.

8. Nottke, A., M.P. Colaiacovo, and Y. Shi, Developmental roles of the histone lysine demethylases. Development, 2009. 136(6): p. 879-89.

9. Shi, Y., Histone lysine demethylases: emerging roles in development, physiology and disease. Nat Rev Genet, 2007. 8(11): p. 829-33.

10. Strobl-Mazzulla, P.H., T. Sauka-Spengler, and M. Bronner-Fraser, Histone demethylase JmjD2A regulates neural crest specification. Dev Cell, 2010. 19(3): p. 460-8.

11. Kauffman, E.C., et al., Role of androgen receptor and associated lysine-demethylase coregulators, LSD1 and JMJD2A, in localized and advanced human bladder cancer. Mol Carcinog, 2011. 50(12): p. 931-44.

12. Mallette, F.A., et al., RNF8- and RNF168-dependent degradation of KDM4A/JMJD2A triggers 53BP1 recruitment to DNA damage sites. EMBO J, 2012. 31(8): p. 1865-78.

13. Shin, S. and R. Janknecht, Activation of androgen receptor by histone demethylases JMJD2A and JMJD2D. Biochem Biophys Res Commun, 2007. 359(3): p. 742-6.

14. Van Rechem, C., et al., The SKP1-Cul1-F-box and leucine-rich repeat protein 4 (SCF-FbxL4) ubiquitin ligase regulates lysine demethylase 4A (KDM4A)/Jumonji domain-containing 2A (JMJD2A) protein. J Biol Chem, 2011. 286(35): p. 30462-70.

15. Zhang, Q.J., et al., The histone trimethyllysine demethylase JMJD2A promotes cardiac hypertrophy in response to hypertrophic stimuli in mice. J Clin Invest, 2011. 121(6): p. 2447-56.

16. Fodor, B.D., et al., Jmjd2b antagonizes H3K9 trimethylation at pericentric heterochromatin in mammalian cells. Genes Dev, 2006. 20(12): p. 1557-62.

17. Kawazu, M., et al., Histone demethylase JMJD2B functions as a co-factor of estrogen receptor in breast cancer proliferation and mammary gland development. PLoS One, 2011. 6(3): p. e17830.

18. Shi, L., et al., Histone demethylase JMJD2B coordinates H3K4/H3K9 methylation and promotes hormonally responsive breast carcinogenesis. Proc Natl Acad Sci U S A, 2011. 108(18): p. 7541-6.

19. Toyokawa, G., et al., The histone demethylase JMJD2B plays an essential role in human carcinogenesis through positive regulation of cyclin-dependent kinase 6. Cancer Prev Res (Phila), 2011. 4(12): p. 2051-61.

20. Yang, J., et al., The histone demethylase JMJD2B is regulated by estrogen receptor alpha and hypoxia, and is a key mediator of estrogen induced growth. Cancer Res, 2010. 70(16): p. 6456-66.

21. Ishimura, A., et al., Jmjd2c histone demethylase enhances the expression of Mdm2 oncogene. Biochem Biophys Res Commun, 2009. 389(2): p. 366-71.

22. Wang, J., et al., The histone demethylase JMJD2C is stage-specifically expressed in preimplantation mouse embryos and is required for embryonic development. Biol Reprod, 2010. 82(1): p. 105-11.

23. Wissmann, M., et al., Cooperative demethylation by JMJD2C and LSD1 promotes androgen receptor-dependent gene expression. Nat Cell Biol, 2007. 9(3): p. 347-53.

24. Kim, T.D., et al., Regulation of tumor suppressor p53 and HCT116 cell physiology by histone demethylase JMJD2D/KDM4D. PLoS One, 2012. 7(4): p. e34618.

25. Zhu, Y., D. van Essen, and S. Saccani, Cell-type-specific control of enhancer activity by H3K9 trimethylation. Mol Cell, 2012. 46(4): p. 408-23.

26. Guenther, M.G., et al., A chromatin landmark and transcription initiation at most promoters in human cells. Cell, 2007. 130(1): p. 77-88.

27. Li, J.X., D. Moazed, and S.P. Gygi, Association of the histone methyltransferase Set2 with RNA polymerase II plays a role in transcription elongation. Journal of Biological Chemistry, 2002. 277(51): p. 49383-49388.

28. Nimura, K., et al., A histone H3 lysine 36 trimethyltransferase links Nkx2-5 to Wolf-Hirschhorn syndrome. Nature, 2009. 460(7252): p. 287-U157.

29. Shilatifard, A., Chromatin modifications by methylation and ubiquitination: implications in the regulation of gene expression. Annu Rev Biochem, 2006. 75: p. 243-69.

30. Xiao, T.J., et al., Phosphorylation of RNA polymerase II CTD regulates H3 methylation in yeast. Genes Dev, 2003. 17(5): p. 654-663.

31. Yoh, S.M., J.S. Lucas, and K.A. Jones, The Iws1:Spt6:CTD complex controls cotranscriptional mRNA biosynthesis and HYPB/Setd2-mediated histone H3K36 methylation. Genes Dev, 2008. 22(24): p. 3422-3434.

32. Whetstine, J.R., et al., Reversal of histone lysine trimethylation by the JMJD2 family of histone demethylases. Cell, 2006. 125(3): p. 467-81.

33. Chen, Z., et al., Structural basis of the recognition of a methylated histone tail by JMJD2A. Proc Natl Acad Sci U S A, 2007. 104(26): p. 10818-23.

34. Couture, J.F., et al., Specificity and mechanism of JMJD2A, a trimethyllysine-specific histone demethylase. Nat Struct Mol Biol, 2007. 14(8): p. 689-95.

35. Ng, S.S., et al., Crystal structures of histone demethylase JMJD2A reveal basis for substrate specificity. Nature, 2007. 448(7149): p. 87-91.

36. Cieslik, M. and Z.S. Derewenda, The role of entropy and polarity in intermolecular contacts in protein crystals. Acta Crystallogr D Biol Crystallogr, 2009. 65(Pt 5): p. 500-9.

37. Cooper, D.R., et al., Protein crystallization by surface entropy reduction: optimization of the SER strategy. Acta Crystallographica Section D-Biological Crystallography, 2007. 63: p. 636-645.

38. Derewenda, Z.S. and P.G. Vekilov, Entropy and surface engineering in protein crystallization. Acta Crystallographica Section D-Biological Crystallography, 2006. 62: p. 116-124.

39. Goldschmidt, L., et al., Toward rational protein crystallization: A Web server for the design of crystallizable protein variants. Protein Science, 2007. 16(8): p. 1569-1576.

40. Otwinowski, Z. and W. Minor, Processing of X-ray diffraction data collected in oscillation mode. Macromolecular Crystallography, Pt A, 1997. 276: p. 307-326.

41. Vagin, A. and A. Teplyakov, MOLREP: an automated program for molecular replacement. Journal of Applied Crystallography, 1997. 30: p. 1022-1025.

42. Murshudov, G.N., A.A. Vagin, and E.J. Dodson, Refinement of macromolecular structures by the maximum-likelihood method. Acta Crystallographica Section D-Biological Crystallography, 1997. 53: p. 240-255.

43. Emsley, P. and K. Cowtan, Coot: model-building tools for molecular graphics. Acta Crystallographica Section D-Biological Crystallography, 2004. 60: p. 2126-2132.

44. Winn, M.D., M.N. Isupov, and G.N. Murshudov, Use of TLS parameters to model anisotropic displacements in macromolecular refinement. Acta Crystallogr D Biol Crystallogr, 2001. 57(Pt 1): p. 122-33.

45. Winn, M.D., G.N. Murshudov, and M.Z. Papiz, Macromolecular TLS refinement in REFMAC at moderate resolutions. Methods Enzymol, 2003. 374: p. 300-21.

46. Brunger, A.T., et al., Crystallography & NMR system: A new software suite for macromolecular structure determination. Acta Crystallogr D Biol Crystallogr, 1998. 54(Pt 5): p. 905-21.

47. Brunger, A.T., Version 1.2 of the Crystallography and NMR system. Nat Protoc, 2007. 2(11): p. 2728-33.

48. Chen, V.B., et al., MolProbity: all-atom structure validation for macromolecular crystallography. Acta Crystallographica Section D-Biological Crystallography, 2010. 66: p. 12-21.

49. Hillringhaus, L., et al., Structural and evolutionary basis for the dual substrate selectivity of human KDM4 histone demethylase family. J Biol Chem, 2011. 286(48): p. 41616-25.

50. Chang, Y.Y., et al., Crystal structure of the catalytic core of Saccharomyces cerevesiae histone demethylase Rph1: insights into the substrate specificity and catalytic mechanism. Biochemical Journal, 2011. 433: p. 295-302.

51. Klose, R.J., et al., Demethylation of histone H3K36 and H3K9 by Rph1: a vestige of an H3K9 methylation system in Saccharomyces cerevisiae? Mol Cell Biol, 2007. 27(11): p. 3951-61.

CHAPTER 4

METHYLATION SITE SPECIFICITY STUDIES-DIFFERNTIAL SPECIFICITY OF JMJD2D AND JMJD2A

Functional diversity within the JMJD2 family of demethylases has been attributed in part to their differential substrate specificities. Despite their high sequence identity (>75%, Figure 3.1 in Chapter 3) and structural homology, members of the JMJD2 family exhibit striking differences in their substrate specificities with respect to the recognition of H3K36me3. Most JMJD2 KDMs can efficiently demethylate H3K9me3 and H3K36me3, with the exception of JMJD2D which is an H3K9me2/3-specific demethylase [1, 2]. To delineate the molecular mechanisms of site specific demethylation in the JMJD2 family, we determined the crystal structure of JMJD2D in the apoenzyme form and in complex with its cognate H3K9me3 substrate (Chapter 3). Using this structural data, we performed structural comparisons with JMJD2A and biochemical analysis with an array of mutant histone peptides to understand how these enzymes recognized H3K9me3. We also analyzed the role of T11 phosphorylation on H3K9me3 demethylation by the JMJD2 enzymes. To understand why JMJD2D lacked specificity for the H3K36me3 site, we performed docking studies using JMJD2A•H3K36me3 and our JMJD2D structures. Lastly, we corroborated our docking predictions by performing a series of biochemical analysis on hybrid peptide substrates. These studies furnish a clear understanding of how JMJD2 enzymes recognize the H3K9me3 site and the molecular basis by which JMJD2D occludes the H3K36me3 site.

MATERIALS AND METHODS

Protein Expression and Purification

For demethylase assays, the catalytic domains of JMJD2A (residues 1-350), JMJD2C (residues 1-350) and JMJD2D (residues 12-342) were expressed and purified using the Strep-Tactin affinity method combined with an S200 column purification as described in Chapter 2. As JMJD2B (residues 9-357) was unstable after gel filtration chromatography, enzyme assays were performed with concentrated fractions of the enzyme from the Strep-Tactin column. Protein concentration was determined by their absorbance at 280 nm in 6.0 M guanidinium chloride and 100 mM HEPES (pH 7.5) [extinction coefficients were calculated using ExPASy ProtParam (http://web.expasy.org/protparam): JMJD2A, ε280nm = 73,800 M^{-1} cm^{-1}, JMJD2B, ε280nm = 72,685 M^{-1} cm^{-1}, JMJD2C, ε280nm = 81,290 M^{-1} cm^{-1} and JMJD2D, ε280nm =70,820 M^{-1} cm^{-1}]. Protein samples were flash frozen in liquid N_2 and stored at -80º C.

Histone Substrate Peptides

Methylated histone H3 peptide substrates used in the kinetic analyses of JMJD2A and JMJD2D were purchased from Anaspec Inc., and were purified with a chloride counter ion. The peptide were dissolved in MilliQ water , vortexed for 10 sec and the peptide vials were centrifuged at 1500 rpm for 2 min. This was done to ensure accurate peptide concentration, particularly for peptides weighed by net peptide content. Peptide concentrations were quantified by amino acid analysis, with the exception of peptides containing a tyrosine, whose concentrations were measured by their absorbance at 274 nm (Molar extinction coefficient of Tyrosine ε274nm = 1,440 $M^{-1}cm^{-1}$). The sequences of the peptides used in kinetic experiments are listed in Table 4.1.

FDH-Coupled Demethylase Assay

KDM activity was measured using the FDH-coupled demethylase assay as described in Chapter 2. All peptides were dissolved in Milli-Q water. The assay was initiated by the addition of 1.0 mM 2-OG and a variable concentration of peptide substrate into the assay cocktail containing 50 mM HEPES buffer (pH 7.5), 50 mM NaCl, 50 µM $(NH_4)_2Fe(SO_4)_2$, 1.0 mM L-ascorbic acid, 1.0 mM NAD^+, 0.1 µM recombinant FDH and 1.0 µM JMJD2 KDM. NADH fluorescence was continuously monitored (λ_{ex} 340/λ_{em} 490) at 30 sec intervals using a Sapphire 2 microplate reader. Kinetic data were processed using GraphPad Prism.

Molecular Docking of JMJD2D and H3K36me3

Docking analysis was performed using PyMOL. The PDB files of JMJD2A•H3K36me3 complex structure (PDB ID: 2P5B) and that of JMJD2D•H3K9me3 were modified as follows: since both structures contained two molecules in the asymmetric unit, one of the molecules was removed from the PDB file using the Text Wrangler software. In addition, water, other solvent and cofactor atoms were removed. Using these modified PDB files, the align function in PyMOL was used to align the two structures. This resulted in a close alignment of JMJD2A and JMJD2D protein molecules (RMSD Cα (261 atoms) = 0.42Å). The trimethyllysine side-chains of the H3K9me3 peptide from the JMJD2D structure and the H3K36me3 peptide from the JMJD2A structures were nearly superimposed suggesting that the H3K36me3 peptide was modeled in the correct direction. To analyze the JMJD2D•H3K36me3 docked structure using MOLPROBITY, the PDB files were generated as follows: from the previous alignment, all atoms of JMJD2A and H3K9me3 were removed. The resultant PDB file contained the coordinates of JMJD2D and the docked H3K36me3 peptide and was used for MOLPROBITY analysis. All structural figures

Table 4.1: List of the H3 peptides used in the kinetic analysis of JMJD2D and JMJD2A

1	H3K9me3	ARTKQTARK(me3)STGGKA-amide
2	H3K9me3_R8A	ARTKQTAAK(me3)STGGKA-amide
3	H3K9me3_S10A	ARTKQTARK(me3)ATGGKA-amide
4	H3K9me3_T11A	ARTKQTARK(me3)SAGGKA-amide
5	H3K9me3_S10A_T11A	ARTKQTARK(me3)AAGGKA-amide
6	H3K9me3_T11S	ARTKQTARK(me3)SSGGKA-amide
7	H3K9me3T11ph	ARTKQTARK(me3)ST(ph)GGKA-amide
8	H3K36me3	acetyl-SAPATGGVK(me3)KPHRYR-amide
9	H3K36me3_R40A	acetyl-SAPATGGVK(me3)KPHAYR-amide
10	H3K9K36me3	ARTKQTARK(me3)KPHRYR-amide
11	H3K36K9me3	acetyl-SAPATGGVK(me3)STGGKA-amide
12	H3K36K9me3_V35R	acetyl-SAPATGGRK(me3)STGGKA-amide

Peptides with the H3K9me3 site were synthesized with C-terminal amide groups, whereas peptides encompassing the H3K36me3 site were synthesized with N-terminal acetyl and C-terminal amide groups.

were rendered using PyMOL (Schrodinger, LLC) and the electrostatic surface was calculated using the Adaptive Poisson-Boltzmann Solver (APBS) plugin for PyMOL (Baker et al., 2001).

RESULTS

Comparison of H3K9me3 Recognition by JMJD2D and JMJD2A

The H3K9me3 binding mode appears to be conserved between JMJD2A and JMJD2D, consistent with the similar catalytic efficiencies (k_{cat}/K_m values) they display toward an H3K9me3 peptide substrate (Table 2.4 from Chapter 2). The recognition of H3K9me3 site by JMJD2A and JMJD2D involves hydrogen bonds or van der Waals contacts to residues R8, S10, T11 and G12 at the -1, +1, +2 and +3 positions in the H3K9 sequence (Figure 3.14 from Chapter 3). We first examined the interactions involving R8 recognition that were not characterized in previous studies involving JMJD2 enzymes [3-5]. R8 corresponds to the -1 position in the peptide sequence relative to K9 and is recognized by an intricate network of hydrogen bonds to Asp135 and Tyr179 in JMJD2D and to Glu169 in JMJD2A (Figure 4.1). Mutation of R8 to alanine (R8A) in the H3K9me3 peptide resulted in 6-10 fold decreases in the catalytic efficiencies compared to the demethylation of the WT peptide for both enzymes (Table 4.2 and Figure 4.1). These decreases were predominantly due to an increase in the K_m values for the H3K9me3_R8A peptide that is indicative of impaired binding to JMJD2A and JMJD2D, highlighting the importance of the interactions at the -1 position in the overall recognition of H3K9me3. The residues that interact with R8 are conserved among all JMJD2 homologs (Figure 4.2), implying that recognition of R8 in the -1 position of the H3K9 sequence is a universal mode of recognition among the JMJD2 KDMs.

With respect to residues in the C-terminal half of the H3K9me3 peptide, S10, T11 and G12, corresponding to the +1, +2 and +3 positions, adopt a bent conformation that enables these

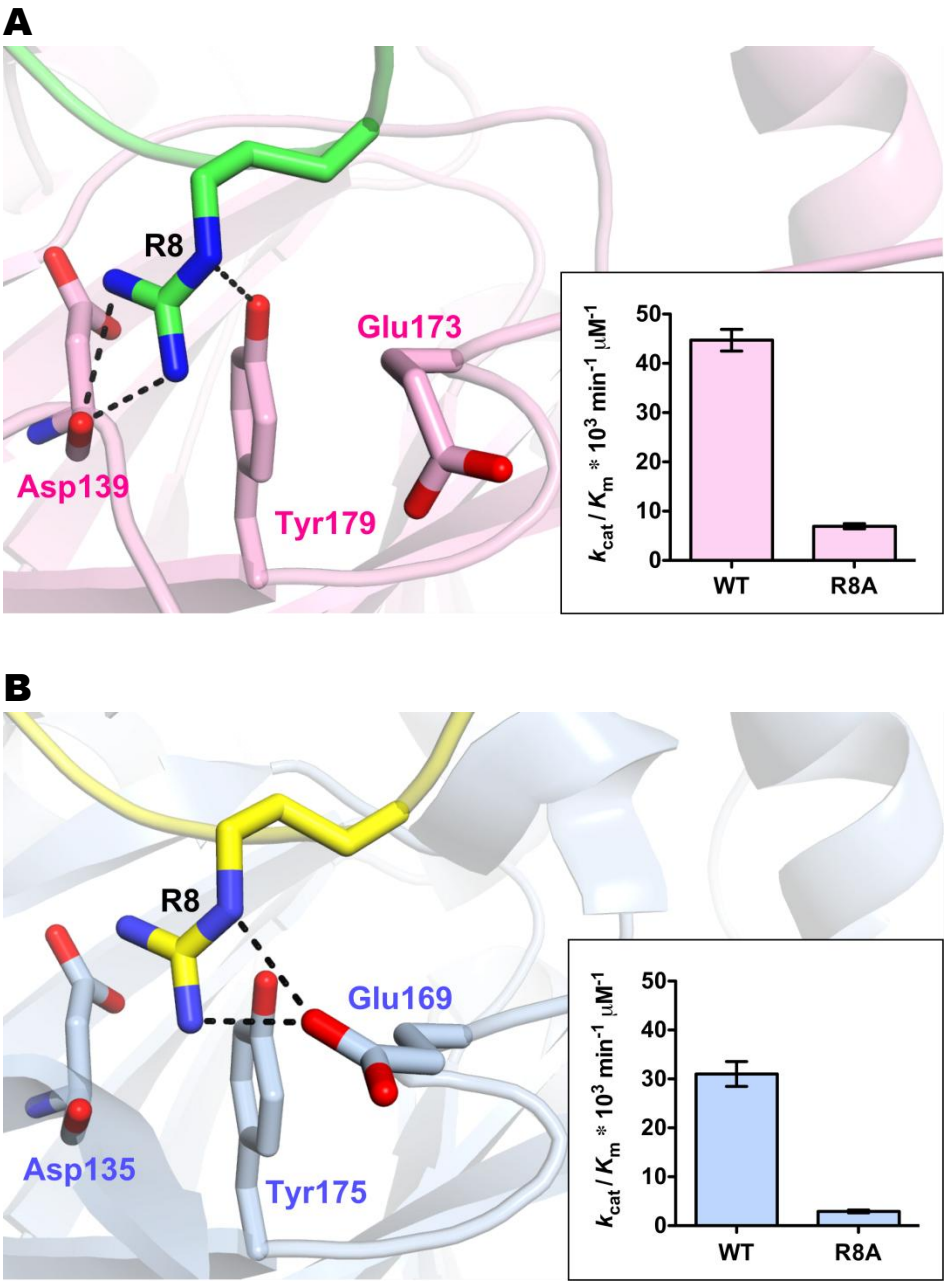

Figure 4.1: Recognition of R8 in the H3K9me3 substrate. (A) JMJD2D•H3K9me3 complex and (B) JMJD2A•H3K9me3 complex. The catalytic efficiencies (k_{cat}/K_m values) of the WT H3K9me3 and H3K9me3_R8A peptide substrates are shown as bar graphs in the insets.

Table 4.2: Kinetic Characterization of JMJD2D and JMJD2A with mutant peptides

	JMJD2D			JMJD2A		
	K_m (μM)	k_{cat}(min^{-1})	$k_{cat}/K_m * 10^3$ (min^{-1} μM^{-1})	K_m (μM)	k_{cat}(min^{-1})	$k_{cat}/K_m * 10^3$ (min^{-1} μM^{-1})
H3K9me3	53 ± 9	2.3 ± 0.2	45 ± 4	56 ± 9	1.7 ± 0.1	31 ± 4
H3K9me3_R8A	240 ± 27	1.6 ± 0.1	6.9 ± 0.9	340 ± 110	0.94 ± 0.19	2.9 ± 0.5
H3K9me3_S10A	96 ± 15	1.6 ± 0.2	17 ± 3	420 ± 19	1.0 ± 0.1	2.5 ± 0.1
H3K9me3_T11A	100 ± 13	2.5 ± 0.2	25 ± 2	40 ± 8	1.6 ± 0.1	43 ± 10
H3K9me3_S10A_T11A	110 ± 31	0.73 ± 0.13	6.8 ± 0.8	430 ± 32	1.1 ± 0.1	2.6 ± 0.1
H3K9me3_T11S	16 ± 1	3.6 ± 0.1	230 ± 22	9.4 ± 1.4	2.9 ± 0.2	320 ± 37
H3K36me3	N.A.	N.A.	N.A.	130 ± 6	1.2 ± 0.2	9.3 ± 1.4
H3K36me3_R40A	N.A.	N.A.	N.A.	830 ± 81	2.2 ± 0.2	2.7 ± 0.2
H3K9K36me3	N.A.	N.A.	N.A.	920 ± 150	0.57 ± 0.03	0.63 ± 0.07
H3K36K9me3	1400 ± 200	1.0 ± 0.1	0.75 ± 0.08	320 ± 28	0.82 ± 0.01	2.6 ± 0.3
H3K36K9me3_V35R	280 ± 12	2.2 ± 0.2	7.9 ± 0.3	19 ± 8.8	1.0 ± 0.1	62 ± 19

The amino acid sequences of the peptides used in the assay are listed in Table 4.1.
N.A. - No Activity detected.

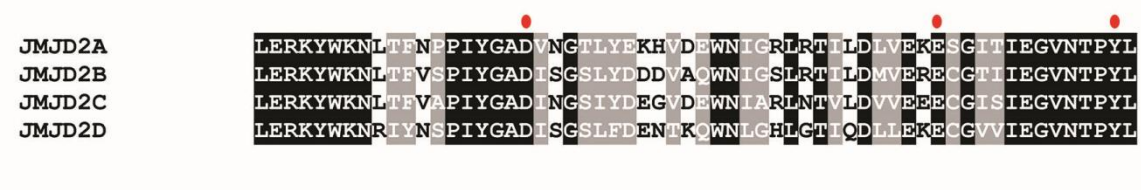

Figure 4.2: Conservation of R8-recognizing residues. Alignment of the amino acid sequence of the human JMJD2 homologs illustrating the sequence identity of residues involved in the recognition of R8 in the H3K9me3 substrate (●). Identical residues are depicted with black background and homologous residues are shown in gray background.

amino acids to bind efficiently inside a pocket adjacent to the active site, as observed in JMJD2A (Figure 4.3) [3, 5]. As described in Chapter 3, in JMJD2D, the bent conformation in the C-terminal half of H3K9me3 is maintained through two hydrogen bond networks: (1) S10 adopts two alternate side chain conformations that enable intra-peptide hydrogen bonding to either the G12 carbonyl oxygen and amide nitrogen or to the R8 carbonyl oxygen and (2) a hydrogen bond between the side chains of T11 and Asp139 in JMJD2D (Figure 4.3A). Mutation of S10 to alanine (S10A) or T11 to alanine (T11A) resulted in only a two-fold reduction in the catalytic efficiency compared to the WT peptide with JMJD2D (Table 4.2 and Figure 4.3A). A double S10A_T11A mutation however, resulted in a six-fold decrease in catalytic efficiency, indicating that a combination of interactions to S10 and T11 is important for optimal recognition of the H3K9me3 site by JMJD2D. Interestingly, this decrease was predominantly due to a decrease in the k_{cat} values while the K_m values were identical to the individual S10A and T11A mutations (Table 4.2). This suggests that the bent conformation at the C terminus might play an important role in JMJD2D catalysis, potentially by enabling proper positioning of the substrate K9me3 into the active site. The mode of recognition of S10 and T11 by JMJD2D starkly contrasts the recognition of these residues by JMJD2A. In a JMJD2A•H3K9me3 complex, the C-terminal bent conformation in the peptide is stabilized only by intra-peptide hydrogen bonds between the side chain hydroxyl group of S10 and backbone oxygen and nitrogen atoms of G12, whereas T11 is rotated away from Asp135 and does not form hydrogen bonds with JMJD2A, unlike in JMJD2D (Figure 4.3B). An S10A mutation abrogates H3K9me3 recognition by JMJD2A with an ~12-fold decrease in catalytic efficiency compared to the wild type (WT) H3K9me3 peptide (Table 4.2 and Figure 4.3B). This decrease was primarily due to an eight-fold increase in the K_m value for the H3K9me3_S10A peptide, indicative of a defect in substrate binding by JMJD2A. On the

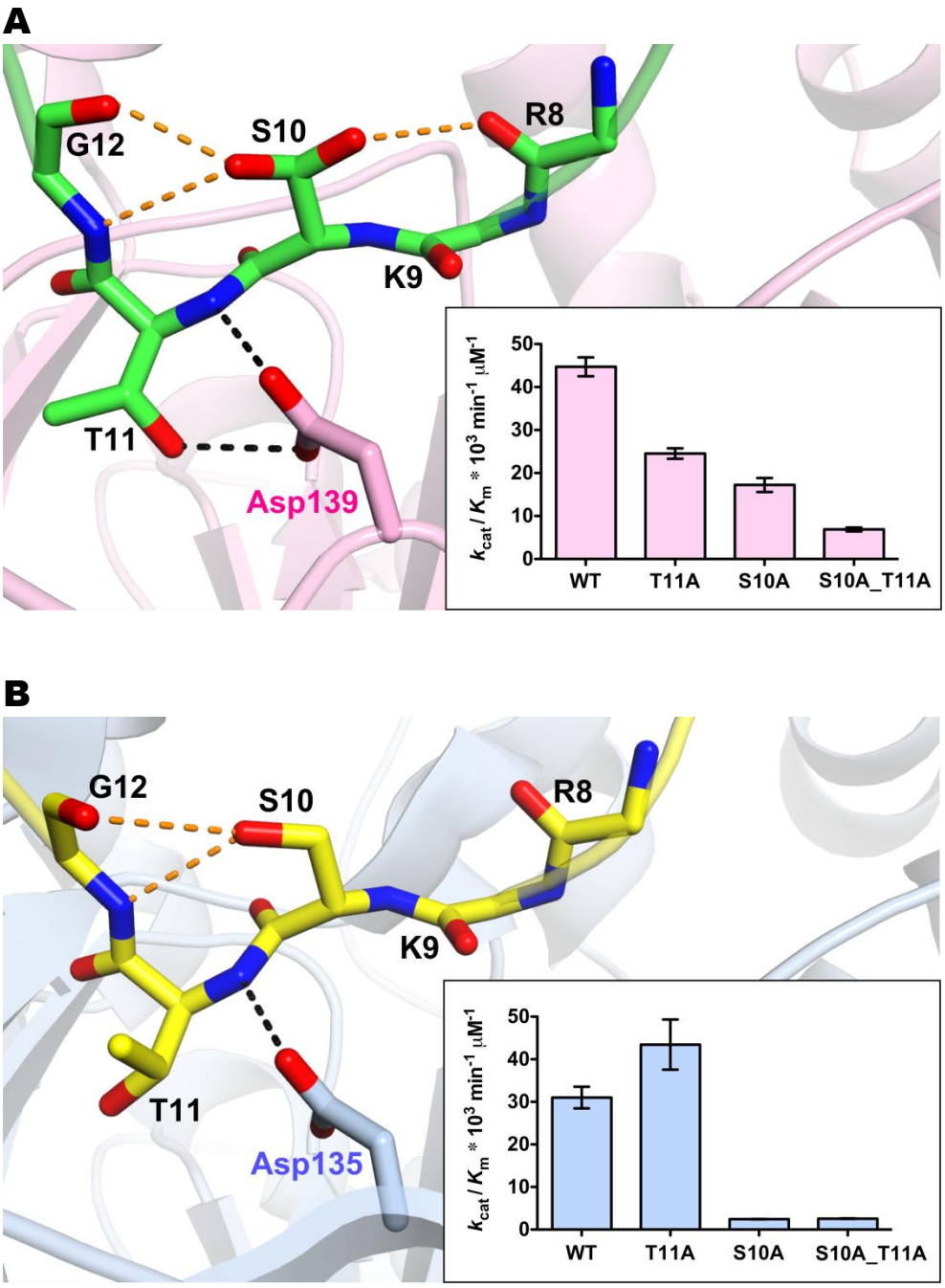

Figure 4.3: Recognition of S10 and T11 in the H3K9me3 substrate. (A) JMJD2D•H3K9me3 complex and (B) JMJD2A•H3K9me3 complex. k_{cat}/K_m values for WT H3K9me3, H3K9me3_S10A, H3K9me3_T11A and H3K9me3_S10A_T11A peptide substrates are shown as bar graphs in the insets.

other hand, a T11A mutation did not affect recognition of the H3K9me3 site, consistent with the lack of hydrogen bonding between T11 and JMJD2A (Table 4.2 and Figure 4.3B). Interestingly, a T11S mutation resulted in a 6-10 fold increase in the k_{cat}/K_m of JMJD2A and JMJD2D compared to WT H3K9me3 (Figure 4.4), primarily due to a decrease in the K_m values for JMJD2A and JMJD2D (Table 4.2). The presence of a serine residue at the +2 position, corresponding to H3T11 may be more amenable to hydrogen bonding to the carboxylate group of Asp139 in JMJD2D (Asp135 in JMJD2A) compared to the bulkier threonyl side chain that has more limited conformational freedom due to steric constraints within +2 binding pocket in the enzymes' substrate binding cleft. In summary, the structural and kinetic data illustrate that R8 is recognized in a highly conserved manner in both JMJD2A and JMJD2D and highlight major variations in the recognition of S10 and T11 by these enzymes, despite the homology of the H3K9me3 peptide conformation and structural conservation of the +1 and +2 binding pockets in these homologs.

Role of H3T11ph in the Recognition of H3K9me3 by JMJD2 KDMs

Previous studies have demonstrated that other post-translational modifications in the residues flanking H3K9me3 can influence demethylation by JMJD2 KDMs. For example, phosphorylation of S10 (S10ph) has been reported to abolish H3K9me3 demethylation by JMJD2A [5], consistent with the importance of this residue in H3K9me3 recognition. Correlatively, protein-kinase-C-related kinase 1 (PRK1) and the cell cycle checkpoint kinase (Chk1) have been shown to phosphorylate T11 in histone H3 (H3T11ph), a modification that has been implicated in regulating androgen receptor (AR) signaling and DNA damage response [6, 7]. In addition, the presence of H3T11ph has been reported to enhance demethylation of

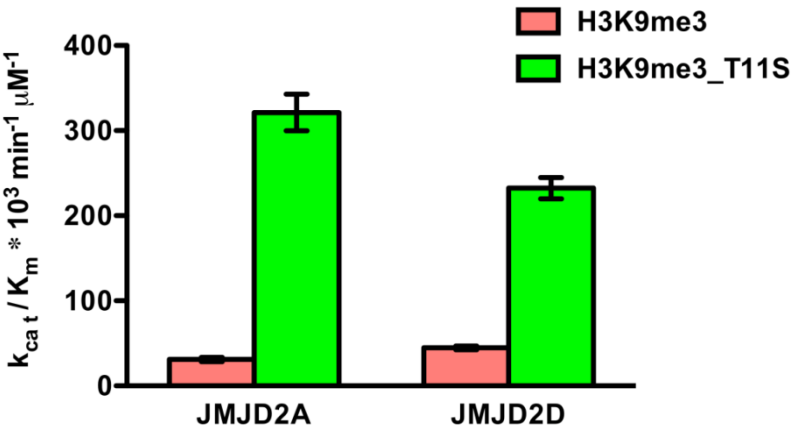

Figure 4.4: Activity of JMJD2A and JMJD2D toward an H3K9me3_T11S peptide. Comparison of the k_{cat}/K_m values of JMJD2A and JMJD2D with WT H3K9me3 and an H3K9me3_T11S peptide substrate showing that substitution of threonine at the +2 position with a serine increases catalytic efficiency by ten-fold for JMJD2A and six-fold for JMJD2D.

H3K9me3 by JMJD2C and promote the upregulation of AR target genes [6]. Contrary to this finding, we observed that JMJD2A, JMJD2B, JMJD2C and JMJD2D are inactive toward an H3K9me3T11ph peptide, indicating T11ph abrogates H3K9me3 demethylation by JMJD2 KDMs (Figure 4.5). When we modeled a phosphorylated threonine residue in the +2 binding pocket of JMJD2D, we observed a number of steric clashes with Ala138, Tyr181 and the potential rotation of the threonyl sidechain could result in clashes with Tyr136, Leu75, His90 and Phe189 (Figure 4.6). Furthermore, the presence of the invariant Asp139 less than 2Å from T11ph could potentially result in electrostatic repulsion (Figure 4.6). In conclusion, our structural and biochemical analysis illustrate that the dimensions of the +2 binding pocket in JMJD2 enzymes sterically and electrostatically preclude the binding of T11ph in the H3K9me3 substrate.

Mode of H3K36me3 Occlusion by JMJD2D

Previous studies have shown that JMJD2A and JMJD2C exhibit dual specificity for both H3K9me3 and H3K36me3 [2]. Our kinetic analysis on JMJD2B revealed that it is also specific for both H3K9me3 and H3K36me3 (Table 4.3). JMJD2D is the only member of the human JMJD2 KDMs that is specific for H3K9me3 and cannot recognize the H3K36me3 site. To understand the molecular determinants underlying this varied specificity, we performed docking studies with a previously solved structure of a JMJD2A•N-oxalylyglycine•H3K36me3 complex [1] with the structure of our JMJD2D ternary complex. First, we identified several regions flanking the substrate binding cleft that differ in either sequence or structural conservation between the enzymes (Figure 4.7). Second, our docking studies revealed severe steric and H39 and R40 in the H3K36me3 peptide and His90 and Leu75 in JMJD2D, respectively (Figure 4.8). The corresponding residues in JMJD2A, Asn86 and Ile71, adopt conformations that

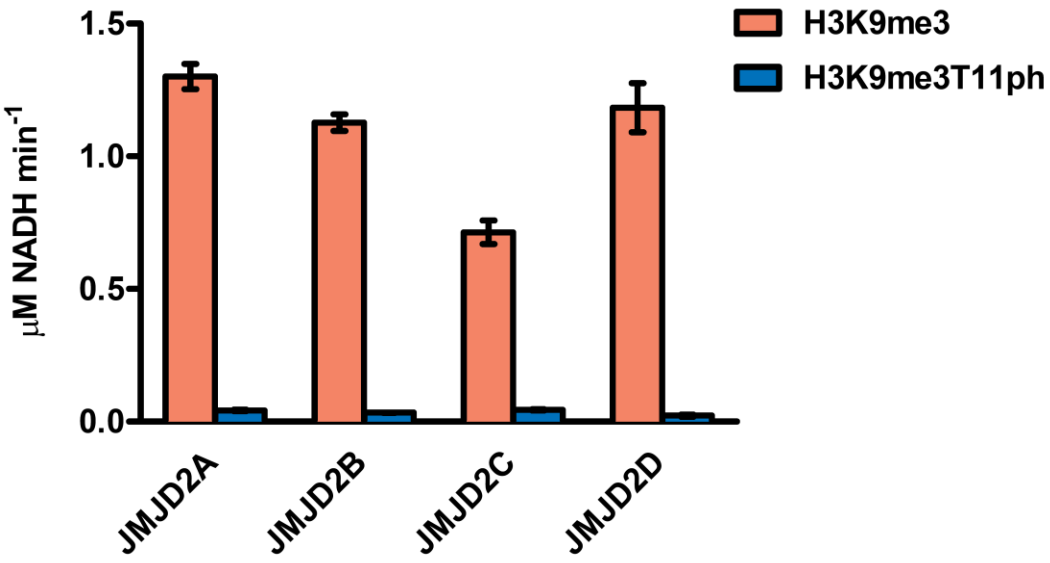

Figure 4.5: Activity of JMJD2 enzymes for an H3K9me3T11ph peptide. Comparison of the initial velocities of JMJD2A, JMJD2C and JMJD2D with WT H3K9me3 and H3K9me3T11ph peptide substrates showing that T11ph inhibits H3K9me3 demethylation by the JMJD2 enzymes.

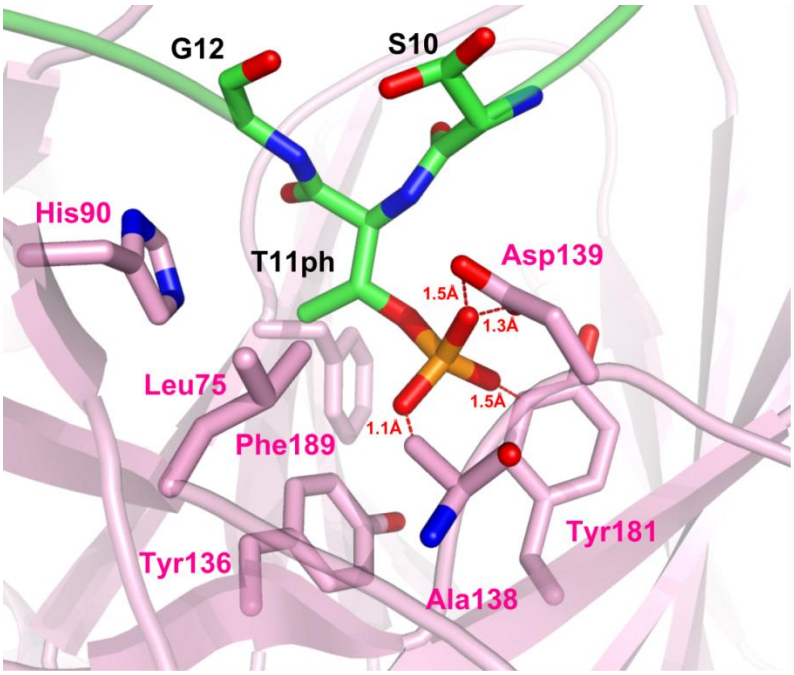

Figure 4.6: T11ph modeled in the JMJD2D peptide binding cleft. The T11 binding pocket in JMJD2D (pink) with a T11ph residue (green and orange) depicting electrostatic repulsion with Asp139 and several steric clashes for the binding of a T11ph residue (red dashes).

Table 4.3: Kinetic Analysis of JMJD2 KDMs

Kinetic Parameters – H3K9me3			
	K_m µM	k_{cat} min^{-1}	$k_{cat} / K_m * 10^3$ min^{-1} $µM^{-1}$
JMJD2A	56 ± 9	1.7 ± 0.1	31 ± 4
JMJD2B	28 ± 3	1.2 ± 0.1	42 ± 3
JMJD2C	25 ± 1	0.66 ± 0.01	26 ± 1
JMJD2D	53 ± 9	2.3 ± 0.2	45 ± 4
Kinetic Parameters – H3K36me3			
	K_m µM	k_{cat} min^{-1}	$k_{cat} / K_m * 10^3$ min^{-1} $µM^{-1}$
JMJD2A	130 ± 6	1.2 ± 0.2	9.3 ± 1.4
JMJD2B	98 ± 16	0.33 ± 0.02	3.4 ± 0.4
JMJD2C	140 ± 31	0.23 ± 0.02	1.7 ± 0.2
JMJD2D	N.A.	N.A.	N.A.

N.A.- No Activity Detected.

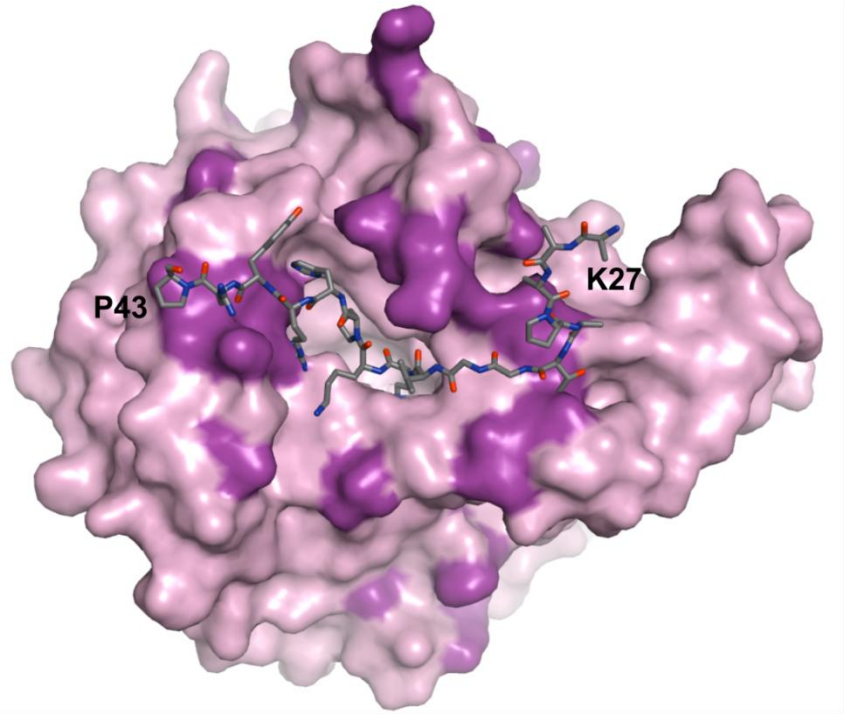

Figure 4.7: JMJD2D docked with the H3K36me3 peptide. Surface representation of JMJD2D (pink) containing the docked H3K36me3 peptide (gray sticks). Purple patches highlight regions in JMJD2D that are not identical in sequence to JMJD2A.

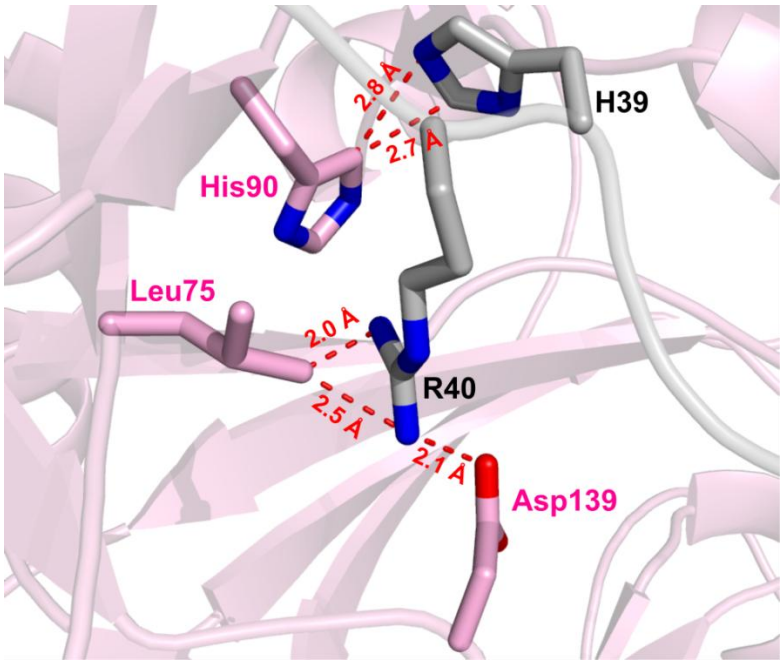

Figure 4.8: Occlusion of H39 and R40 by JMJD2D. Steric clashes between H39 and R40 in H3K36me3 (gray) and Asp139, Leu75 and His90 in JMJD2D (pink) are shown as red dashes.

accommodate H39 and R40 through van der Waals interactions (Figure 4.9). Further, Asp135 in JMJD2A forms a salt bridge with R40, an interaction that is pivotal for efficient demethylation of H3K36me3, as illustrated by the impaired demethylation of an H3K36me3_R40A peptide (Table 4.2 and Figure 4.10). Corroborating these observations, mutation of Ile71 to a leucine (I71L) resulted in a 16-fold decrease in catalytic efficiency of JMJD2A toward H3K36me3, whereas the activity toward H3K9me3 remained unperturbed (Figure 4.11 and Table 4.4). Additionally, the C-terminus of the H3K36me3 peptide harbors a positively charged cluster comprising H39, R40 and R42 that is juxtaposed to a positively charged patch on the surface of JMJD2D that includes Lys91 and Lys92, which may further preclude H3K36me3 binding via electrostatic repulsion (Figure 4.12A). In JMJD2A, Lys91 and Lys92 correspond to neutral amino acids Ile87 and Gln88 (Figure 4.12B).

In addition to accommodating the H3K36me3 substrate without steric or electrostatic clashes, JMJD2A engages in several interactions along the length of the H3K36me3 peptide that promote substrate recognition [1]. At the -1 position of the H3K36me3 site, the amide nitrogen of V35 engages in a hydrogen bond with the backbone carbonyl oxygen of Asp311 in the loop linking helices α9 and α10 in the C-terminal region of JMJD2A (Figure 4.13). This interaction facilitates the proper positioning of K36me3 substrate into the active site [1]. Both the sequence and conformation of the loop that interacts with V35 vary substantially between JMJD2A and JMJD2D. In JMJD2A, residues Arg309, Lys310, Asp311, and Met312 (RKDM motif) form a broad ‘U’-shaped loop that bends sharply near the peptide-binding cleft, positioning the carbonyl oxygen of Asp311 for hydrogen bonding to the V35 amide (Figure 4.13). In JMJD2D, this loop, consisting of residues Gly313, Glu314, Ala315, Arg316 (GEAR motif), is oriented away from the peptide-binding cleft and does not adopt a conformation that is conducive to hydrogen

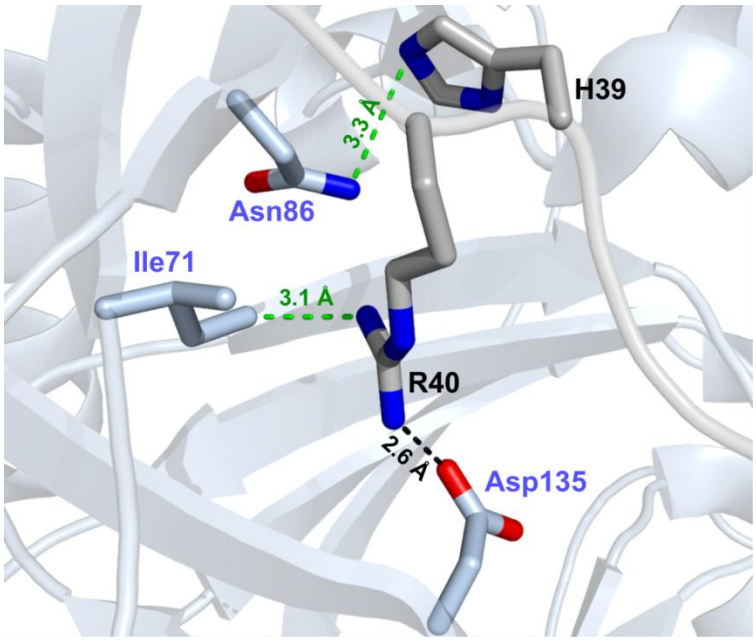

Figure 4.9: Favorable recognition of H39 and R40 by JMJD2A. R40 in H3K36me3 (gray) is recognized by a salt bridge (black dashes) with Asp135 in JMJD2A (blue) [PDB entry: 2P5B]. Green dashes represent interatomic distances favorable for substrate binding.

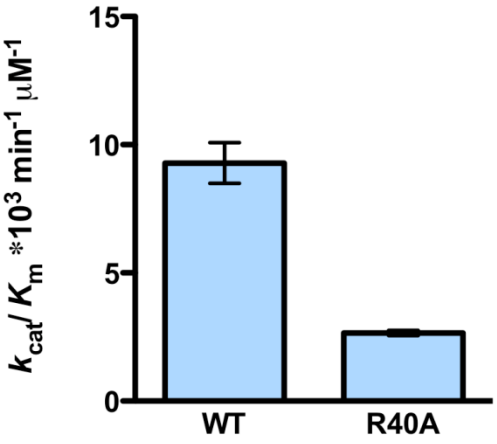

Figure 4.10: Activity of JMJD2A for an H3K36me3_R40A peptide. Mutation of R40 in histone H3 to alanine results in a fourfold decrease in catalytic efficiency of JMJD2A compared to WT H3K36me3. The catalytic parameters are listed in Table 4.2.

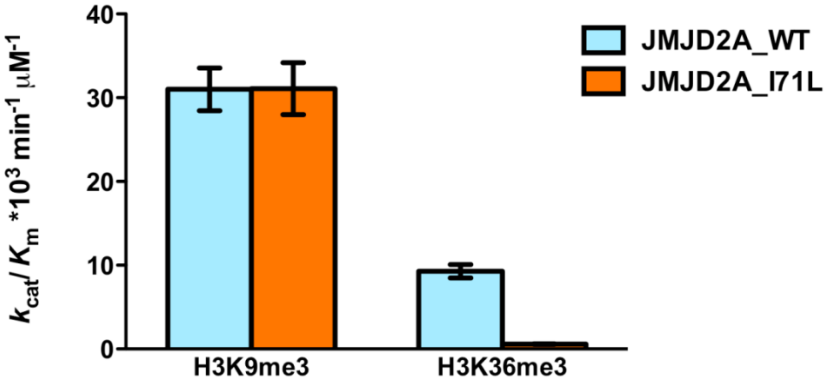

Figure 4.11: Kinetic analysis of JMJD2A_I71L. This mutation results in a 16-fold reduction in catalytic efficiency for H3K36me3 compared to WT JMJD2A (Table 4.4). In contrast, the activity toward H3K9me3 remains unperturbed.

Table 4.4: Comparison of the kinetic parameters of JMJD2A_WT and JMJD2A_I71L

	k_{cat} min^{-1}	K_m µM	$k_{cat} / K_m * 10^3$ min^{-1} $µM^{-1}$
Kinetic Parameters-H3K9me3			
JMJD2A_WT	1.7 ± 0.1	56 ± 9	31 ± 4
JMJD2A_I71L	1.3 ± 0.1	43 ± 6	31 ± 5
Kinetic Parameters-H3K36me3			
JMJD2A_WT	1.2 ± 0.2	130 ± 6	9.3 ± 1.4
JMJD2A_I71L	0.33 ± 0.01	560 ± 39	0.57 ± 0.03

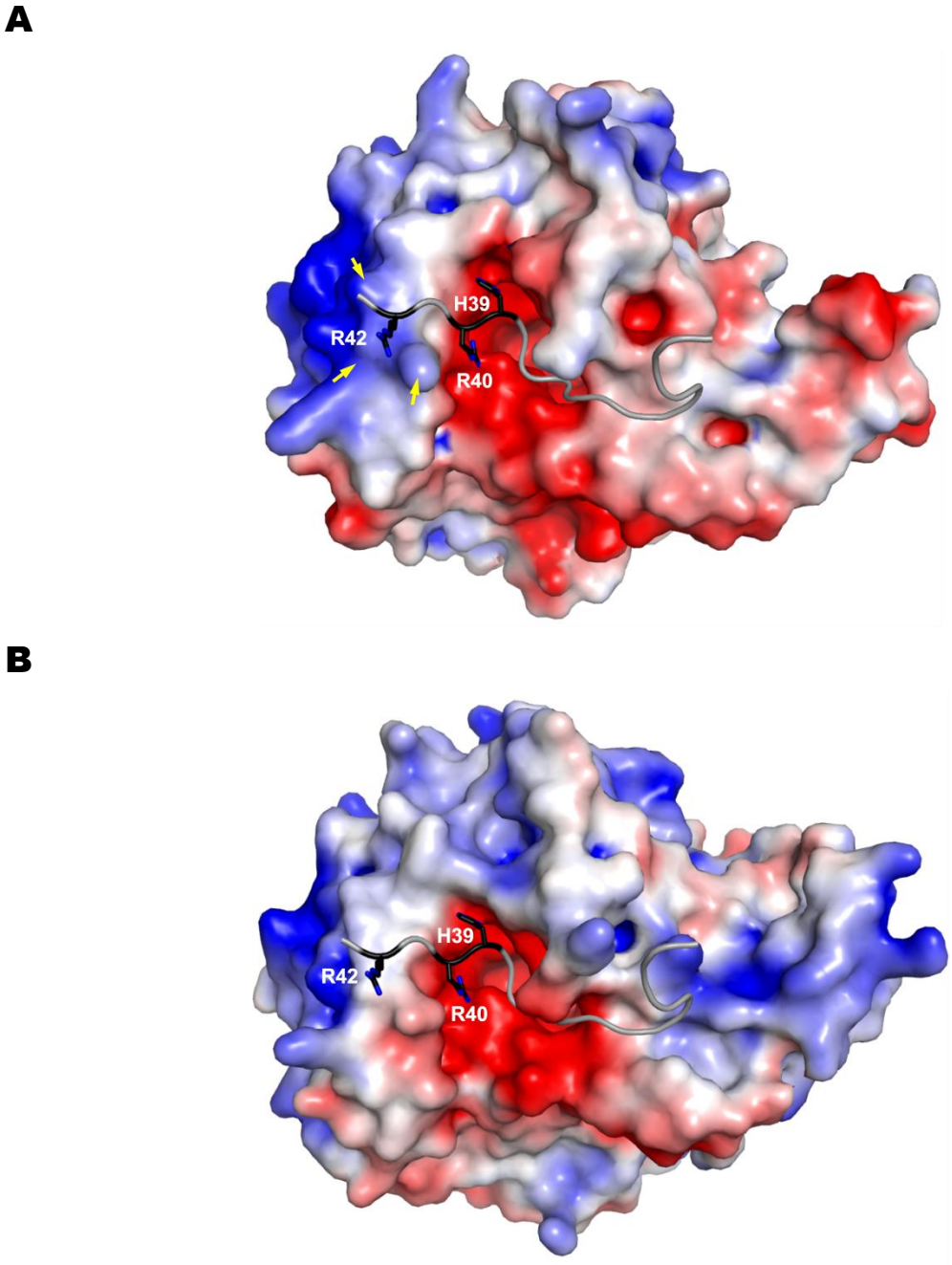

Figure 4.12: Electrostatic surface representations of JMJD2D (A) and JMJD2A (B). Electrostatic potential is contoured from +3 $k_bT \cdot e^{-1}$ (blue) to -3 $k_bT \cdot e^{-1}$ (red). The H3K36me3 peptide (in A and B) is depicted as gray cartoon with the C-terminal basic residues H39, R40 and R42 represented in stick form (black). Yellow arrows refer to the positively charged regions in JMJD2D that electrostatically clash with the H3K36me3 peptide.

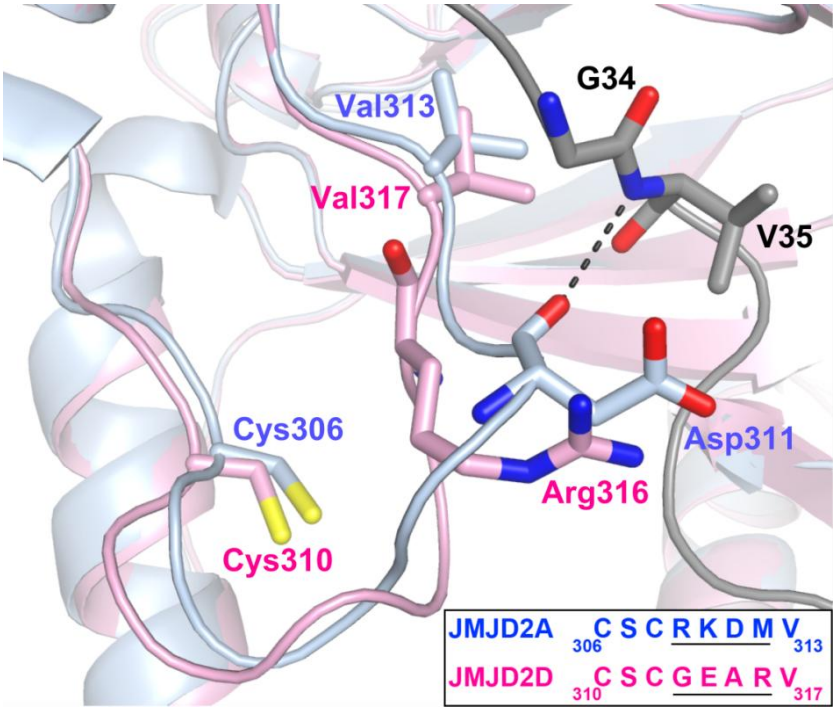

Figure 4.13: Loss of hydrogen bonding between JMJD2D and H3K36me3. Interaction between Asp311 in JMJD2A (blue) and V35 in H3K36me3 (gray) is shown as black dashes. The corresponding residue, Arg316 (pink), in JMJD2D is unable to form this hydrogen bond due to structural variability in the GEAR loop motif (inset).

bonding to V35 in histone H3. Collectively, the structural comparisons between JMJD2A and JMJD2D combined with the JMJD2D•H3K36me3 docking analysis suggest that the loss of productive enzyme-substrate interactions coupled with multiple steric and electrostatic clashes occludes the recognition of the H3K36me3 site by JMJD2D.

Activity of JMJD2D and JMJD2A Toward Hybrid Peptide Substrates

Biochemical analysis of JMJD2D mutants, based on sequence comparison with JMJD2A revealed that individual point mutations in the substrate binding cleft were not sufficient to render JMJD2D with H3K36me3 demethylase activity and clustered mutations significantly diminished enzyme stability (Table 4.5). Hence, to substantiate our docking analysis, we assayed the catalytic activity of JMJD2D with hybrid peptide substrates bearing the N-terminal and C-terminal halves of the H3K9 and H3K36 methylation sites (Figure 4.14). When assayed with a peptide composed of the N-terminal half of the H3K9 site and the C-terminal half of the H3K36 site (H3K9K36me3), JMJD2D exhibited no appreciable activity, consistent with that observed for the H3K36me3 peptide (Figure 4.15). In contrast, JMJD2D displayed a substantial increase in its catalytic efficiency toward an H3K36K9me3 peptide composed of the N- and C-termini of H3K36 and H3K9 sites, respectively (Figure 4.15). These results corroborate our docking studies, indicating that the residues C-terminal to K36 in histone H3 are primarily responsible for the discrimination of JMJD2D against this site. Although JMJD2D was capable of demethylating the H3K36K9me3 hybrid peptide, its catalytic efficiency toward this substrate was relatively weak compared to that of the WT H3K9me3 peptide (Figure 4.15 and Table 4.2). As noted earlier, the loop containing the GEAR motif in JMJD2D does not adopt a conformation that is poised for hydrogen bonding with V35 in histone H3 (Figure 4.13). To introduce a productive

Table 4.5: List of mutations in JMJD2D that were tested for H3K36me3 catalytic activity

MUTATION	RATIONALE
L75I	To relieve steric clash with R40 of H3K36me3 substrate
H90N	To relieve steric clash with H39 of H3K36me3 substrate
Cluster 1: C168S; V171T; F319I	To relieve minor steric clashes at residues N-terminal to H3K36me3
Cluster 2: L75I; H90N	To relieve major steric clashes at residues C-terminal to H3K36me3
Cluster 3: K91I; K92Q	To relieve electrostatic clashes at residues C-terminal to H3K36me3
Cluster 4: L75I; H90N; K91I;K92Q	To relieve steric and electrostatic clashes at residues C-terminal to H3K36me3
Cluster 5: G313R;E314K;A315D;R316M	To introduce hydrogen bond at the -1 position of H3K36me3
L75I; H90N;K91I;K92Q;C168S;V171T; G313R;E314K;A315D;R316M;F319I	Combination of clusters 1-5 mutations

Although most of the mutants were stable (with the exception of Cluster 5 and combination of cluster 1-5 mutant), they did not exhibit any appreciable increase in catalytic activity for H3K36me3 compared to WT JMJD2D.

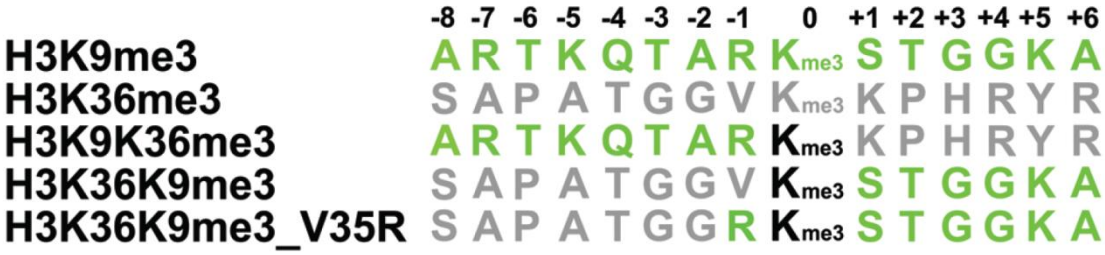

Figure 4.14: Hybrid peptides between H3K9me3 and H3K36me3. Amino acid sequences of the hybrid peptide substrates derived from sequences of the H3K9 and H3K36 methylation sites.

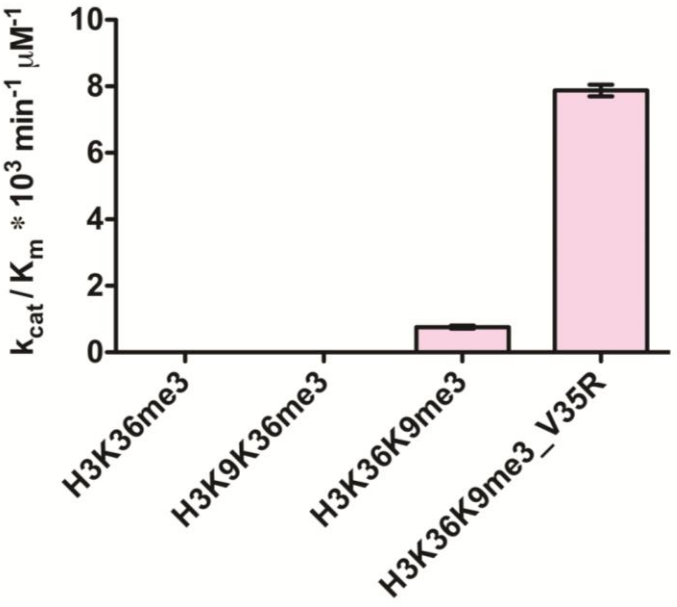

Figure 4.15: Activity of JMJD2D toward hybrid peptides.

interaction at the -1 position of the demethylation site, V35 was mutated to an arginine (V35R) to mimic the interactions of R8 in the H3K9me3 peptide with JMJD2A and JMJD2D (Figure 4.1A and 4.16). When assayed with the H3K36K9me3_V35R peptide, JMJD2D displayed a tenfold increase in the k_{cat}/K_m compared to the H3K36K9me3 hybrid substrate (Figure 4.15 and Table 4.2).

To complement these results, we next analyzed the kinetic parameters of JMJD2A using the H3 hybrid peptides. Consistent with JMJD2D, JMJD2A was inactive toward the H3K9K36me3 peptide, indicating the residues preceding K36 in histone H3 are essential for substrate recognition (Figure 4.17 and Table 4.2). Unexpectedly, when JMJD2A was assayed with the H3K36K9me3 hybrid peptide, we observed a four-fold reduction in the k_{cat}/K_m compared to WT H3K36me3 (Figure 4.17 and Table 4.2). The decrease in catalytic efficiency for the H3K36K9me3 peptide may have been a consequence of the loss of the salt bridge interaction between R40 in histone H3 and Asp135 in JMJD2A (Figure 4.9), as an R40A mutation in the H3K36me3 peptide impairs the catalytic efficiency of JMJD2A by fourfold (Figure 4.10 and Table 4.2). Conversely, JMJD2A exhibited a sevenfold increase in its catalytic efficiency when assayed with the H3K36K9me3_V35R peptide compared to WT H3K36me3 (Figure 4.17 and Table 4.2). This increase in activity presumably reflects a compensatory effect in which the V35R mutation enhances interactions with JMJD2A through hydrogen bonding in the -1 position, as observed for R8 in the H3K9me3 site (Figure 4.1B). This interaction would offset the mutation of R40 to glycine in the H3K36K9me3 hybrid substrate (Figure 4.14) that abolishes a salt bridge interaction with Asp135 in the substrate binding cleft (Figures 4.9 and 4.10). In summary, the kinetic data corroborate our structural alignment and docking analysis of JMJD2A and JMJD2D, underscoring that steric and electrostatic clashes combined with the loss

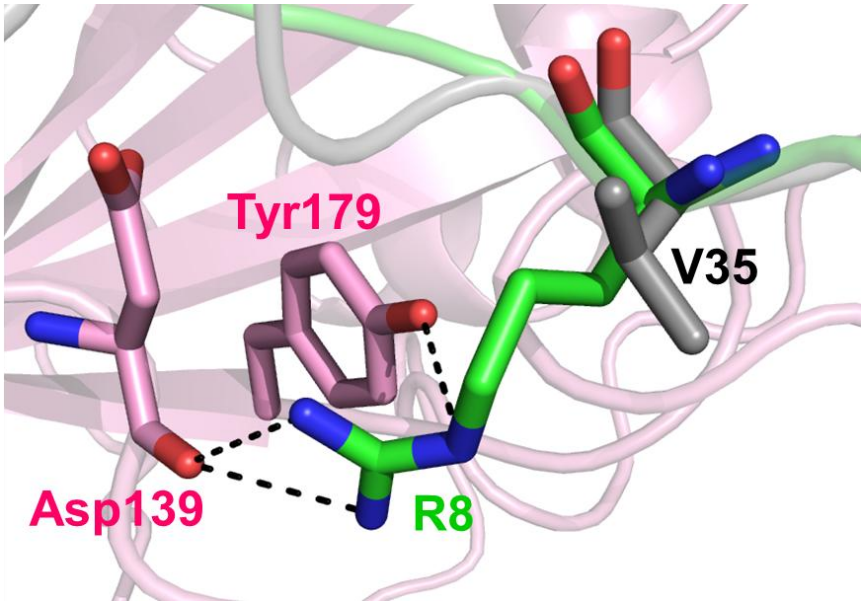

Figure 4.16: Rationale for the H3K36K9_V35R substrate. Overlay of the H3K9me3 (green) and H3K36me3 (grey) peptide on JMJD2D (pink) showing that R8 and V35 are superimposable.

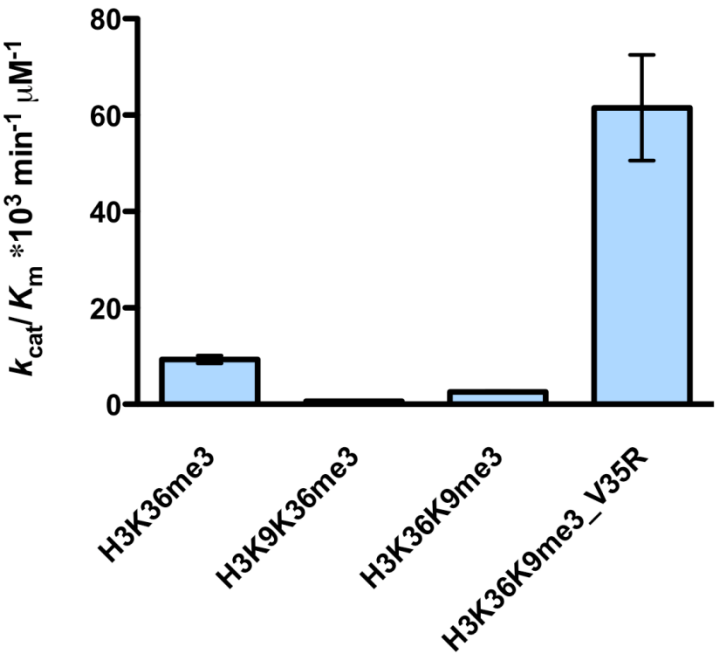

Figure 4.17: Activity of JMJD2A toward hybrid peptides.

of productive enzyme-substrate interactions contribute to the discrimination against H3K36me3 demethylation by JMJD2D.

DISCUSSION

Mode of H3K9me3 Recognition and H3K36me3 Occlusion by JMJD2 KDMs

Members of the JMJD2 family of KDMs have been implicated in numerous genomic and developmental functions [8-12]. The functional diversity within this family has been attributed in part to their differential substrate specificities. JMJD2A, JMJD2B and JMJD2C efficiently demethylate H3K9me3 and H3K36me3, whereas JMJD2D is an H3K9me2/3-specific demethylase. Our structural studies reveal that JMJD2A and JMJD2D employ similar modes of recognition of the H3K9me3 site at the -1 position through hydrogen bonding to R8 (Figure 4.1). However, these enzymes display unexpected differences in the recognition of residues S10 and T11 at the +1 and +2 positions of the H3K9me3 site, despite the overall structural homology of the H3K9me3 peptide binding mode and the S10-T11 binding clefts (Figure 4.3). S10 is pivotal for the recognition of H3K9me3 site by JMJD2A, whereas in JMJD2D, this requirement is more flexible owing to a compensatory interaction formed between T11 and Asp139 in JMJD2D. In addition, our structural and kinetic results also illustrate that phosphorylation of T11 impedes demethylation of H3K9me3 by JMJD2D KDMs, contrary to previous reports [6]. These findings correlate with prior studies illustrating that S10ph abrogates demethylation of H3K9me3 by JMJD2A [5] and are consistent with the overall acidic character of the S10-T11 binding clefts in JMJD2A and JMJD2D (Figure 4.6) that are electrostatically incompatible with the binding of S10ph and T11ph in histone H3.

Our structural and biochemical studies highlight key interactions at the -1, +1, +2 and +3

positions in the H3K9me3 sequence that are important for substrate recognition by JMJD2A and JMJD2D. These 'signature' residues are also conserved in other known substrates of JMJD2 KDMs, most notably K26me3 of linker histone H1.4 (H1.4K26me3) that has shown to be efficiently demethylated by all members of the JMJD2 family [13]. This site bears strong sequence similarity to H3K9me3, including R25 (at the -1 position), S27 (at the +1 position), A28 (at the +2 position) and G29 (at the +3 position), suggesting a conserved mode of recognition of these sites by the JMJD2 family (Figure 4.18). In contrast to H3K9me3 and H1.4K26me3, JMJD2 homologs display distinct preferences for H3K36me3, which is efficiently demethylated by JMJD2A, JMJD2B and JMJD2C but is not recognized by JMJD2D. The structural comparisons of JMJD2A and JMJD2D and docking studies reveal that steric and electrostatic clashes combined with lack of productive interactions with the H3K36me3 substrate contribute to the inability of JMJD2D to demethylate this site. Consistent with these findings, the residues that can favorably accommodate H3K36me3 recognition, are conserved among JMJD2A, JMJD2B, and JMJD2C, but are divergent in JMJD2D (Figure 4.19).

Comparing the JMJD2 and UTX Enzyme Families

Despite their ability to demethylate H3K9me3, JMJD2 KDMs are inactive toward the H3K27me3, a methylation site that mediates Polycomb group silencing [14-16]. Although the H3K9 and H3K27 sequences harbor a conserved ARKS motif (where K is the methylated lysine), sequence variations outside this ARKS motif, such as P30 in the +3 position, preclude recognition of H3K27me3 site by the JMJD2 enzymes [1, 3, 5]. A recently reported crystal structure of the H3K27me3-specific KDM UTX bound to an H3K27me3 peptide illustrates key differences in histone substrate recognition by UTX and the JMJD2 KDMs [17]. In JMJD2A and

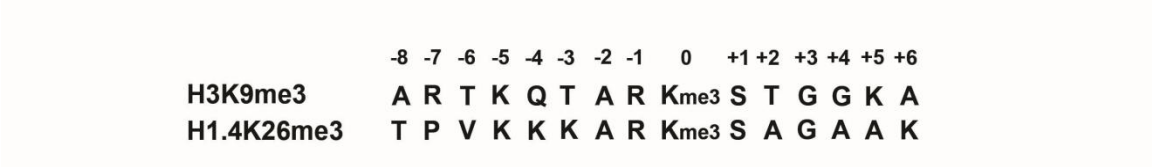

Figure 4.18: Similarities in the H3K9me3 and H1.4K26me3 sites. Alignment of the amino acid sequences of H3K9me3 and H1.4K26me3 illustrating the sequence identity at the -2,-1,+1 and +3 positions of these methylation sites. Both sites have been reported to be demethylated by all JMJD2 KDMs.

Figure 4.19: Divergence of residues involved in H3K36me3 discrimination. The residues in different domains are colored: Purple: JmjN domain; Orange: Mixed domain; Red: JmjC domain and Green: C-terminal domain. Residues in JMJD2A, JMJD2B and JMJD2C that permit favorable recognition of H3K36me3 are highlighted in black and they are not conserved in JMJD2D.

JMJD2D, the H3K9me3 peptide adopts a "W"-shaped conformation that is stabilized by interactions from residue R8-G12 (the –1 to +3 positions) in the H3K9 site. Conversely, UTX binds to an H3K27me3 peptide in an extended conformation through an extensive network of interactions involving hydrogen bonds, hydrophobic interactions, and van der Waals contacts spanning residues R17 to G33 in histone H3, corresponding to the -10 to +6 positions in the H3K27 site (Figure 4.20). Thus, UTX requires an H3K27me3 peptide sequence approximately twice as long as that observed for JMJD2 KDMs with H3K9me3 for optimal substrate recognition. Despite these differences, these enzymes share certain similarities in their substrate binding modes. For example, UTX recognizes R26 in the -1 position of the H3K27me3 site through multiple hydrogen bonds. Moreover, an R26A mutation abolishes H3K27me3 demethylation by UTX, in agreement with the recognition of R8 in the -1 position of H3K9me3 site by JMJD2A and JMJD2D (Figure 4.1 and Table 4.2). Similarly, phosphorylation of S28 at the +1 position abrogates demethylation of H3K27me3 by UTX, consistent with the mutual exclusivity of S10ph and K9me3 for demethylation by the JMJD2 enzymes. In summary, the differential conformations adopted by the H3K9me3 and H3K27me3 sequences facilitate distinct recognition modes for the demethylation of these sites by their cognate JmjC KDMs.

ACKNOWLEDGEMENTS

I thank Dr. Henriette Remmer at the Protein Structure Facility for help with peptide ordering. I also thank Douglas Jacobsen for trying out MD simulations with JMJD2D and H3K36me3.

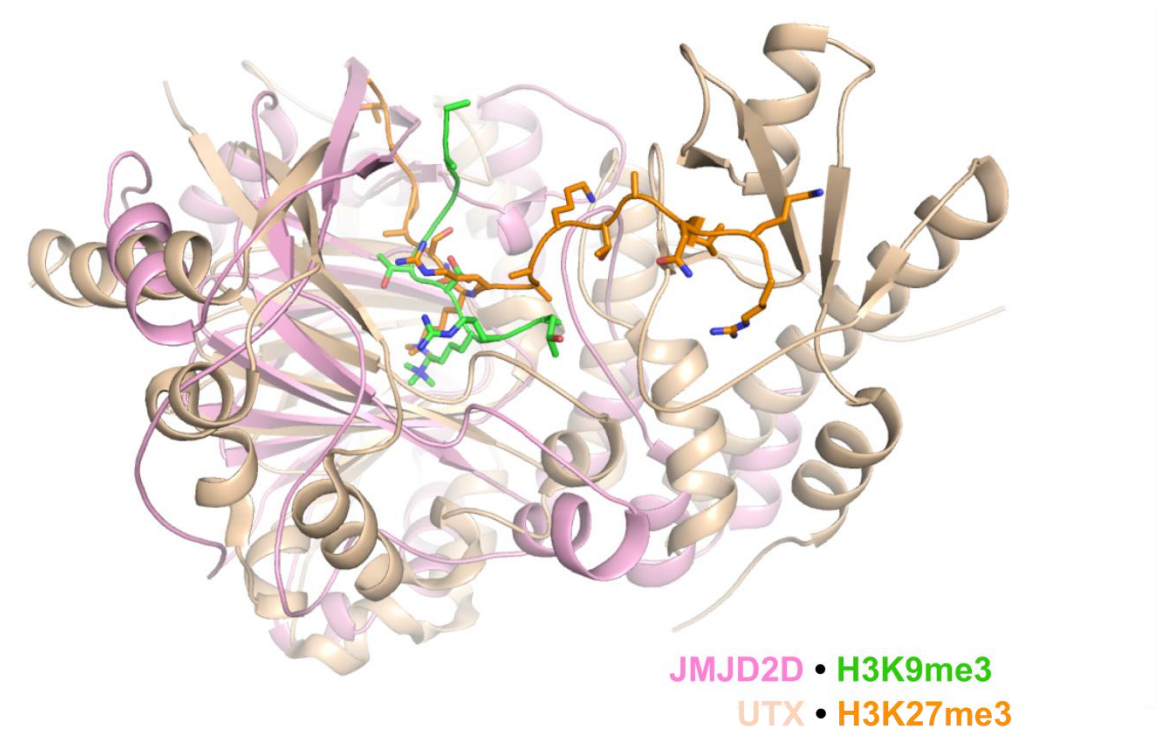

Figure 4.20: Structural alignment of the ternary complexes of JMJD2D (pink) and UTX (light brown). The H3K27me3 peptide adopts a more extended conformation and is recognized at many regions distal to K27me3. The H3K9me3 peptide, in contrast adopts tight, 'W' shaped conformation.

REFERENCES

1. Chen, Z., et al., Structural basis of the recognition of a methylated histone tail by JMJD2A. Proc Natl Acad Sci U S A, 2007. 104(26): p. 10818-23.

2. Whetstine, J.R., et al., Reversal of histone lysine trimethylation by the JMJD2 family of histone demethylases. Cell, 2006. 125(3): p. 467-81.

3. Couture, J.F., et al., Specificity and mechanism of JMJD2A, a trimethyllysine-specific histone demethylase. Nat Struct Mol Biol, 2007. 14(8): p. 689-95.

4. Hillringhaus, L., et al., Structural and evolutionary basis for the dual substrate selectivity of human KDM4 histone demethylase family. J Biol Chem, 2011. 286(48): p. 41616-25.

5. Ng, S.S., et al., Crystal structures of histone demethylase JMJD2A reveal basis for substrate specificity. Nature, 2007. 448(7149): p. 87-91.

6. Metzger, E., et al., Phosphorylation of histone H3 at threonine 11 establishes a novel chromatin mark for transcriptional regulation. Nat Cell Biol, 2008. 10(1): p. 53-60.

7. Shimada, M., et al., Chk1 is a histone H3 threonine 11 kinase that regulates DNA damage-induced transcriptional repression. Cell, 2008. 132(2): p. 221-32.

8. Cloos, P.A., et al., Erasing the methyl mark: histone demethylases at the center of cellular differentiation and disease. Genes Dev, 2008. 22(9): p. 1115-40.

9. Mosammaparast, N. and Y. Shi, Reversal of histone methylation: biochemical and molecular mechanisms of histone demethylases. Annu Rev Biochem, 2010. 79: p. 155-79.

10. Nottke, A., M.P. Colaiacovo, and Y. Shi, Developmental roles of the histone lysine demethylases. Development, 2009. 136(6): p. 879-89.

11. Shi, Y., Histone lysine demethylases: emerging roles in development, physiology and disease. Nat Rev Genet, 2007. 8(11): p. 829-33.

12. Shi, Y. and J.R. Whetstine, Dynamic regulation of histone lysine methylation by demethylases. Mol Cell, 2007. 25(1): p. 1-14.

13. Trojer, P., et al., Dynamic Histone H1 Isotype 4 Methylation and Demethylation by Histone Lysine Methyltransferase G9a/KMT1C and the Jumonji Domain-containing JMJD2/KDM4 Proteins. J Biol Chem, 2009. 284(13): p. 8395-405.

14. Cao, R., et al., Role of histone H3 lysine 27 methylation in Polycomb-group silencing. Science, 2002. 298(5595): p. 1039-43.

15. Kouzarides, T., Chromatin modifications and their function. Cell, 2007. 128(4): p. 693-705.

16. Min, J., Y. Zhang, and R.M. Xu, Structural basis for specific binding of Polycomb chromodomain to histone H3 methylated at Lys 27. Genes Dev, 2003. 17(15): p. 1823-8.

17. Sengoku, T. and S. Yokoyama, Structural basis for histone H3 Lys 27 demethylation by UTX/KDM6A. Genes Dev, 2011. 25(21): p. 2266-77.

CHAPTER 5

SUMMARY, CONCLUSIONS AND FUTURE DIRECTIONS

Since their discovery in 2006 [1], a large number of JmjC histone lysine demethylases have been biochemically, structurally and functionally characterized [2, 3]. An emerging common theme from these studies is that these KDMs are highly specific for various methylation sites and states and this specificity often dictates the biological functions of these enzymes. The structures of JMJD2A [4-6], JMJD2D (this study), PHF8 [7] and UTX [8] have been solved in complex with their cognate histone substrates, and these studies highlight specific structural elements in the enzymes that allow efficient recognition of their corresponding substrates. Interestingly, these enzymes are also structurally predisposed to occlude recognition of other methylation sites and are hence, highly site specific.

The JMJD2 family of enzymes is unique because most JMJD2 KDMs exhibit dual specificity for two methylation sites that bear no sequence or structural similarities. JMJD2A, JMJD2B and JMJD2C can demethylate both H3K9me3 and H3K36me3 (Table 4.4 from Chapter 4 and [9]). These methylation sites are linked to distinct functions: H3K9me3 is associated with heterochromatin and transcriptionally repressed regions. H3K36me3, on the other hand has been shown to associate with the elongating form of RNA Polymerase II and also play a role in gene splicing [3, 10-17]. Of the JMJD2 homologs, JMJD2D is an exception because, while it is highly efficient in recognizing H3K9me3 and H3K9me2, JMJD2D completely lacks specificity for the H3K36me3 site [9]. The goal of this study was to understand the molecular mechanisms by

which JMJD2 enzymes recognized H3K9me3 and the mechanisms of H3K36me3 occlusion by JMJD2D. This study provides insights into the mechanisms of site specific demethylation in the JMJD2 family, and the results of this study can also be used to uncover the biological functions of these enzymes- particularly those that pertain to H3K36me3 demethylation, which is not fully understood. In addition, the identification of mutant substrates that bind with higher affinity than the cognate H3K9me3 (eg: H3K9me3_T11S) substrate will be highly valuable in the design of peptido-mimetic inhibitors for a number of JMJD2 KDMs that are overexpressed in gastric, breast and prostate cancers and in certain heart diseases [18-34].

Methods for Purifying and Assaying Fe(II)-dependent Dioxygenases

In order to biochemically characterize the JMJD2 enzymes, we developed a purification and assay scheme that would aid in the accurate measurement of kinetic parameters. A highly overlooked fact in the field is that all JmjC enzymes are Fe(II) dependent metalloenzymes and are highly susceptible to transition state metal inhibition. To circumvent this metal inhibition caused by the use of metal affinity columns, we adopted a metal-free Strep-Tactin purification system (Chapter 2). Our two step Strep-Tactin-Superdex 200 purification scheme resulted in highly pure enzyme and metal analysis of these samples revealed less than 15% total metal content (Table 2.3 from Chapter 2). We also optimized the FDH-coupled demethylase assay including the source and concentration of all reagents and substrate peptides. When we assayed Strep-Tactin column purified JMJD2A and JMJD2D with the optimized assay, we measured turnover numbers that were 50-100 fold greater than their Ni(II) column purified counterparts [5]. We have used the same purification and assay scheme to characterize other JmjC enzymes such as UTX and JMJD3. Moreover, using this assay (in combination with mass spectrometry

analysis), we showed that the JmjC protein JMJD5 is not a histone demethylase as reported by Hsia et al [35]. These biochemical data were further supported by our JMJD5 structural studies [36]. The purification scheme reported in Chapter 2 is not only applicable to the various families of KDMs but will be useful in the biochemical characterization of other Fe(II) dependent JmjC enzymes including protein hydroxylases such as hypoxia-inducible factors (HIFs) and factor inhibiting hypoxia-inducible factor 1 (FIH-1) , RNA hydroxylases such as tRNA wybutosine-synthesizing enzyme 5 (TYW5) and mRNA demethylases such as Fat-mass and obesity associated proteins (FTO). More recently 2-OG dependent dioxygenases including the J-binding proteins (JBPs) and Ten-eleven translocation (TET) enzymes have garnered attention due to their potential roles in DNA demethylation. The JBP proteins are thymidine hydroxylases [37] whereas the closely related TET proteins have been reported to catalyze the hydroxylation, formylation and carboxylation of 5-methylcytosine [38-40]. While most of the biochemical studies on TET enzymes have been performed using FLAG and HA affinity tags [38, 40], kinetic studies on the JBP enzymes were done using metal affinity columns [37]. These kinetic analyses may not reflect the optimal catalytic activity of the JBP enzymes due to potential metal contamination in the active site. In these cases, use of Strep(II)-tagged dioxygenases coupled with the Strep-Tactin affinity purification could yield highly pure apoenzymes that can be reconstituted with Fe(II) in enzymatic assays. This approach can aid in the reliable biochemical characterization of these enzymes and lead to a better understanding of their substrate specificities and biological functions.

Structural Basis for Methylation Site Specificity in JMJD2 KDMs

The JMJD2 family of demethylases is an excellent model system to study site specific

demethylation. Although all members of the JMJD2 family can demethylate H3K9me3 (and the closely related repressive mark-H1.4K26me3), only JMJD2A, JMJD2B and JMJD2C can efficiently demethylate H3K36me3 whereas JMJD2D lacks specificity for this site. To determine the molecular basis of this varied specificity, we determined the crystal structure of JMJD2D in the apoenzyme form and in complex with 2-OG and H3K9me3 (Chapter 3). Comparing the JMJD2D•H3K9me3 and JMJD2A•H3K9me3 structures, we observed unexpected differences in the recognition of H3K9me3 by these enzymes especially at S10 and T11. In addition, we showed that the presence of other histone post translational modifications such as T11ph abolishes JMJD2 demethylation contrasting previous studies that claimed T11ph enhances JMJD2 demethylation during AR signaling [41]. Additionally, docking studies, structural comparisons with a JMJD2A•H3K36me3 complex [4] and biochemical analysis with hybrid peptides revealed that steric and electrostatic clashes combined with lack of productive interactions resulted in the occlusion of H3K36me3 site by JMJD2D. Our structural and biochemical data highlights that the determinants of methylation site specificity in the JMJD2 KDMs are located primarily within the catalytic domain similar to the UTX family which is specific for H3K37me3 [8]. This is in stark contrast to other JmjC KDMs such as the PHF8 family, which require additional domains such the PHD domain for optimal recognition of their substrates [7]. It will be interesting to explore the structures of other less understood KDMs such as the JARID and JHDM1 families to understand the molecular determinants of their substrate specificities.

Separation of H3K9 and H3K36 Site Specificities of JMJD2 KDMs

The H3K9me3 and H3K36me3 sites are involved in divergent genomic and biological

functions. In humans, the JMJD2 enzymes are the only known family of demethylases that can demethylate these methylation marks [3, 9]. Although these enzymes have been structurally and biochemically characterized, their biological functions have not been extensively studied. In the cases where functional studies have been performed (Table 1.2 from Chapter 1), a vast majority of them report different functions for the JMJD2 homologs, implying that these enzymes are not functionally redundant. Black *et al* showed that JMJD2A regulates cell cycle progression by demethylating H3K9me3 and increasing chromatin accessibility by antagonizing HP1γ occupancy [42]. Similarly, JMJD2A, JMJD2C and JMJD2D have been shown to upregulate AR target genes by demethylating H3K9me3 at target loci such as PSA [29, 32]. JMJD2B has been show to play a pivotal role in ER signaling and in the regulation of cyclin-dependent kinases [23, 28, 31, 33]. More recently, JMJD2D has been shown to regulate cell-type specific gene expression in H3K9me3-associated enhancers [43]. Almost all the functions reported for JMJD2 enzymes pertain to H3K9me3 demethylation whereas their functions associated with H3K36me3 demethylation remains unexplored. In contrast to H3K9me3 which is associated with transcriptional repression and heterochromatin formation [44], H3K36me3 has been implicated in regulation of gene splicing and in transcriptional elongation because of its association with the elongating form of RNA Polymerase (II) [16, 17, 45, 46]. In addition, H3K36me3 has been shown to prevent aberrant transcriptional initiation within coding sequences by recruiting the reduced potassium dependency 3 small (Rpd3S) deacetylase complex [46-49]. Since H3K9me3 and H3K36me3 marks are associated with different functions, demethylation of these marks could be associated with non-overlapping functions. In contrast, it is also conceivable that dual-specificity enzymes like the JMJD2 KDMs could participate in genomic processes that rely on its ability to demethylate both H3K9me3 and H3K36me3. To delineate the functions of JMJD2

enzymes that rely on H3K9me3 demethylation or H3K36me3 demethylation or both, it would be useful to engineer mutations that perturb the specificities in a site specific manner. Using our studies on H3K9me3 recognition and H3K36me3 discrimination by JMJD2D, we designed a series of mutations in JMJD2A that would make the enzyme either H3K9me3 specific or H3K36me3 specific (for a list of mutations and rationale, see Table 5.1). Of the mutations listed, we tested the activity of JMJD2A_I71L mutation toward both H3K9me3 and H3K36me3. This mutation was based on our docking studies with JMJD2D and H3K36me3, where we showed that Leu75 in JMJD2D sterically clashes with R40, a residue critical for H3K36me3 recognition by JMJD2A. We hypothesized that mutation of the corresponding Ile71 in JMJD2A to Leu75 would mirror the steric clash observed in JMJD2D and could potentially impair H3K36me3 recognition by disrupting the salt bridge formed between R40 and Asp135 in JMJD2A (Figure 4.9 and 4.10 in Chapter 4). Indeed, a JMJD2A_I71L mutation resulted in ~16 fold decrease in catalytic efficiency toward H3K36me3 compared to the WT enzyme (Figure 4.11 and Table 4.4 in Chapter 4). And, as predicted, H3K9me3 recognition by this mutant was essentially unaffected (Figure 4.11 and Table 4.4 in Chapter 4). Hence, a JMJD2A_171L mutant would selectively perturb H3K36me3 demethylation and could aid in the understanding of JMJD2A functions that pertain to demethylation of this site. In a similar manner, mutations in residues involved in the recognition of R8 (such as Y175Q) could impair H3K9me3 demethylation by JMJD2A while preserving H3K36me3 activity. These mutations can be expanded to *in vivo* and cell based assays to understand the effects of altered specificity on biological functions. We predict that a number of these mutations listed in Table 5.1 will be applicable to other JMJD2 enzymes (due to highly conserve nature of these residues) and these studies will furnish a better understanding of the functions associated with H3K9me3 and H3K36me3 demethylation by the JMJD2 KDMs.

Table 5.1: Mutations in JMJD2A that can potentially enable separation of specificity

MUTATION	RATIONALE	EXPECTED SPECIFICITY
I71L*	Introduces steric clash at R40 of H3K36me3 (Figure 4.9 and 4.10 from Chapter 4)	H3K9me3
I87K;Q88K	Introduces electrostatic clashes at residues C-terminal to H3K36me3 (Figure 4.12 from Chapter 4)	H3K9me3
I71L; N86H; I87K;Q88K	Introduces steric and electrostatic clashes at residues C-terminal to H3K36me3 (Figure 4.9 and 4.12 from Chapter 4)	H3K9me3
Y175Q	Disrupts hydrogen bonding at R8 of H3K9me3 (Figure 4.1 from Chapter 4)	H3K36me3
E169R; N137E	Disrupts hydrogen bonding and introduces electrostatic clash with R8 of H3K9me3 (Figure 4.1 from Chapter 4)	H3K36me3
E169Q; N137D	Disrupts hydrogen bonding at R8 of H3K9me3 (Figure 4.1 from Chapter 4)	H3K36me3

*The kinetic data for the I71L mutation is shown in Figure 4.11 and Table 4.4 in Chapter 4.

Implications of This Study in Drug Design and Therapy

Aberrant expression of specific JMJD2 homologs contributes to the onset or progression of breast, prostate, colon, gastric and squamous cell cancers, rendering these enzymes attractive targets for chemotherapeutic drug design [18-24, 26-33]. In addition, JMJD2A has been shown to upregulate the expression of four-and-a-half LIM domains 1 (FHL1), and promote cardiac hypertrophy [34]. A number of research groups have focused on the development of JMJD2 specific inhibitors to not only probe these enzymes *in vivo* but also use these compounds as lead molecules in drug design [50-55]. As mentioned above, a number of JMJD2 cellular functions are non-redundant and there is an impetus on developing inhibitors selective for specific JMJD2 homologs. Many groups have initiated the development of peptido-mimetic inhibitors based on the crystal structures of JMJD2A in complex with H3K9me3 and H3K36me3 [51, 55]. Woon *et al* designed a bi-substrate analog that spans both the 2-OG and peptide binding clefts of JMJD2A. These inhibitors were potent for the JMJD2 family with IC_{50} values of 1.5 μM for JMJD2A and 91.0 μM for JMJD2E and exhibited very low affinity (IC_{50} >1000 μM) for the FIH or PHF8 family of enzymes [55]. But these inhibitors displayed some cross-reactivity with other KDM families such as JMJD1A and FBX11 with IC50 values ranging from 50.0-60.0 μM. Luo *et al* fused a 2-OG analog with a trimethyllysine mimic and the resultant compound was called 'Methylstat'. This cell permeable compound exhibited much broader specificity in inhibiting the JMJD2 and UTX families with IC_{50} values in the range of 5.0-10.0 μM [51]. The major caveats with the bi-substrate analogs reported by Woon *et al* and Luo *et al* are their lack of specificity for specific JMJD2 homologs. Our structural studies revealed that the mutation of T11 to a serine increased JMJD2 recognition by 6-10 fold compared to WT H3K9me3 substrate (Figure 4.4 from Chapter 4), suggesting that the incorporation of serine-like moieties in these peptido-

mimetic inhibitors could substantially improve inhibitor affinity. Moreover, certain structural differences within the JMJD2 family-such as the GEAR motif in JMJD2D versus the RKDM motif in JMJD2A (Figure 4.13 from Chapter 4) could be exploited in the design of inhibitor scaffolds that interact with these specific regions thereby achieving high selectivity for specific JMJD2 homologs.

REFERENCES

1. Tsukada, Y., et al., Histone demethylation by a family of JmjC domain-containing proteins. Nature, 2006. 439(7078): p. 811-6.

2. Cloos, P.A., et al., Erasing the methyl mark: histone demethylases at the center of cellular differentiation and disease. Genes Dev, 2008. 22(9): p. 1115-40.

3. Mosammaparast, N. and Y. Shi, Reversal of histone methylation: biochemical and molecular mechanisms of histone demethylases. Annu Rev Biochem, 2010. 79: p. 155-79.

4. Chen, Z., et al., Structural basis of the recognition of a methylated histone tail by JMJD2A. Proc Natl Acad Sci U S A, 2007. 104(26): p. 10818-23.

5. Couture, J.F., et al., Specificity and mechanism of JMJD2A, a trimethyllysine-specific histone demethylase. Nat Struct Mol Biol, 2007. 14(8): p. 689-95.

6. Ng, S.S., et al., Crystal structures of histone demethylase JMJD2A reveal basis for substrate specificity. Nature, 2007. 448(7149): p. 87-91.

7. Horton, J.R., et al., Enzymatic and structural insights for substrate specificity of a family of jumonji histone lysine demethylases. Nat Struct Mol Biol, 2010. 17(1): p. 38-43.

8. Sengoku, T. and S. Yokoyama, Structural basis for histone H3 Lys 27 demethylation by UTX/KDM6A. Genes Dev, 2011. 25(21): p. 2266-77.

9. Whetstine, J.R., et al., Reversal of histone lysine trimethylation by the JMJD2 family of histone demethylases. Cell, 2006. 125(3): p. 467-81.

10. Guenther, M.G., et al., A chromatin landmark and transcription initiation at most promoters in human cells. Cell, 2007. 130(1): p. 77-88.

11. Li, J.X., D. Moazed, and S.P. Gygi, Association of the histone methyltransferase Set2 with RNA polymerase II plays a role in transcription elongation. Journal of Biological Chemistry, 2002. 277(51): p. 49383-49388.

12. Nimura, K., et al., A histone H3 lysine 36 trimethyltransferase links Nkx2-5 to Wolf-Hirschhorn syndrome. Nature, 2009. 460(7252): p. 287-U157.

13. Shilatifard, A., Chromatin modifications by methylation and ubiquitination: implications in the regulation of gene expression. Annu Rev Biochem, 2006. 75: p. 243-69.

14. Xiao, T.J., et al., Phosphorylation of RNA polymerase II CTD regulates H3 methylation in yeast. Genes Dev, 2003. 17(5): p. 654-663.

15. Yoh, S.M., J.S. Lucas, and K.A. Jones, The Iws1:Spt6:CTD complex controls cotranscriptional mRNA biosynthesis and HYPB/Setd2-mediated histone H3K36 methylation. Genes Dev, 2008. 22(24): p. 3422-3434.

16. de Almeida, S.F., et al., Splicing enhances recruitment of methyltransferase HYPB/Setd2 and methylation of histone H3 Lys36. Nat Struct Mol Biol, 2011. 18(9): p. 977-U1501.

17. Kolasinska-Zwierz, P., et al., Differential chromatin marking of introns and expressed exons by H3K36me3. Nature Genetics, 2009. 41(3): p. 376-381.

18. Cloos, P.A., et al., The putative oncogene GASC1 demethylates tri- and dimethylated lysine 9 on histone H3. Nature, 2006. 442(7100): p. 307-11.

19. Fodor, B.D., et al., Jmjd2b antagonizes H3K9 trimethylation at pericentric heterochromatin in mammalian cells. Genes Dev, 2006. 20(12): p. 1557-62.

20. Fu, L., et al., HIF-1alpha-induced histone demethylase JMJD2B contributes to the malignant phenotype of colorectal cancer cells via an epigenetic mechanism. Carcinogenesis, 2012.

21. Ishimura, A., et al., Jmjd2c histone demethylase enhances the expression of Mdm2 oncogene. Biochem Biophys Res Commun, 2009. 389(2): p. 366-71.

22. Kauffman, E.C., et al., Role of androgen receptor and associated lysine-demethylase coregulators, LSD1 and JMJD2A, in localized and advanced human bladder cancer. Mol Carcinog, 2011. 50(12): p. 931-44.

23. Kawazu, M., et al., Histone demethylase JMJD2B functions as a co-factor of estrogen receptor in breast cancer proliferation and mammary gland development. PLoS One, 2011. 6(3): p. e17830.

24. Kim, T.D., et al., Regulation of tumor suppressor p53 and HCT116 cell physiology by histone demethylase JMJD2D/KDM4D. PLoS One, 2012. 7(4): p. e34618.

25. Kim, T.D., et al., The JMJD2A demethylase regulates apoptosis and proliferation in colon cancer cells. J Cell Biochem, 2012. 113(4): p. 1368-76.

26. Li, B.X., et al., Effects of RNA interference-mediated gene silencing of JMJD2A on human breast cancer cell line MDA-MB-231 in vitro. J Exp Clin Cancer Res, 2011. 30: p. 90.

27. Li, W., et al., Histone demethylase JMJD2B is required for tumor cell proliferation and survival and is overexpressed in gastric cancer. Biochem Biophys Res Commun, 2011. 416(3-4): p. 372-8.

28. Shi, L., et al., Histone demethylase JMJD2B coordinates H3K4/H3K9 methylation and promotes hormonally responsive breast carcinogenesis. Proc Natl Acad Sci U S A, 2011. 108(18): p. 7541-6.

29. Shin, S. and R. Janknecht, Activation of androgen receptor by histone demethylases JMJD2A and JMJD2D. Biochem Biophys Res Commun, 2007. 359(3): p. 742-6.

30. Tan, M.K., H.J. Lim, and J.W. Harper, SCF(FBXO22) regulates histone H3 lysine 9 and 36 methylation levels by targeting histone demethylase KDM4A for ubiquitin-mediated proteasomal degradation. Mol Cell Biol, 2011. 31(18): p. 3687-99.

31. Toyokawa, G., et al., The histone demethylase JMJD2B plays an essential role in human carcinogenesis through positive regulation of cyclin-dependent kinase 6. Cancer Prev Res (Phila), 2011. 4(12): p. 2051-61.

32. Wissmann, M., et al., Cooperative demethylation by JMJD2C and LSD1 promotes androgen receptor-dependent gene expression. Nat Cell Biol, 2007. 9(3): p. 347-53.

33. Yang, J., et al., The histone demethylase JMJD2B is regulated by estrogen receptor alpha and hypoxia, and is a key mediator of estrogen induced growth. Cancer Res, 2010. 70(16): p. 6456-66.

34. Zhang, Q.J., et al., The histone trimethyllysine demethylase JMJD2A promotes cardiac hypertrophy in response to hypertrophic stimuli in mice. J Clin Invest, 2011. 121(6): p. 2447-56.

35. Hsia, D.A., et al., KDM8, a H3K36me2 histone demethylase that acts in the cyclin A1 coding region to regulate cancer cell proliferation. Proc Natl Acad Sci U S A, 2010. 107(21): p. 9671-6.

36. Del Rizzo, P.A., S. Krishnan, and R.C. Trievel, Crystal Structure and Functional Analysis of JMJD5 Indicate an Alternate Specificity and Function. Mol Cell Biol, 2012. 32(19): p. 4044-52.

37. Cliffe, L.J., et al., JBP1 and JBP2 Proteins Are Fe2+/2-Oxoglutarate-dependent Dioxygenases Regulating Hydroxylation of Thymidine Residues in Trypanosome DNA. Journal of Biological Chemistry, 2012. 287(24): p. 19886-19895.

38. Ito, S., et al., Tet Proteins Can Convert 5-Methylcytosine to 5-Formylcytosine and 5-Carboxylcytosine. Science, 2011. 333(6047): p. 1300-1303.

39. Wu, H. and Y. Zhang, Mechanisms and functions of Tet protein-mediated 5-methylcytosine oxidation. Genes Dev, 2011. 25(23): p. 2436-2452.

40. Tahiliani, M., et al., Conversion of 5-Methylcytosine to 5-Hydroxymethylcytosine in Mammalian DNA by MLL Partner TET1. Science, 2009. 324(5929): p. 930-935.

41. Metzger, E., et al., Phosphorylation of histone H3 at threonine 11 establishes a novel chromatin mark for transcriptional regulation. Nat Cell Biol, 2008. 10(1): p. 53-60.

42. Black, J.C., et al., Conserved antagonism between JMJD2A/KDM4A and HP1gamma during cell cycle progression. Mol Cell, 2010. 40(5): p. 736-48.

43. Zhu, Y., D. van Essen, and S. Saccani, Cell-type-specific control of enhancer activity by H3K9 trimethylation. Mol Cell, 2012. 46(4): p. 408-23.

44. Nakayama, J., et al., Role of histone H3 lysine 9 methylation in epigenetic control of heterochromatin assembly. Science, 2001. 292(5514): p. 110-3.

45. Butler, J.S. and S.Y.R. Dent, Chromatin 'resetting' during transcription elongation: a central role for methylated H3K36. Nat Struct Mol Biol, 2012. 19(9): p. 863-864.

46. Wagner, E.J. and P.B. Carpenter, Understanding the language of Lys36 methylation at histone H3. Nature Reviews Molecular Cell Biology, 2012. 13(2): p. 115-126.

47. Carrozza, M.J., et al., Histone H3 methylation by Set2 directs deacetylation of coding regions by Rpd3S to suppress spurious intragenic transcription. Cell, 2005. 123(4): p. 581-592.

48. Joshi, A.A. and K. Struhl, Eaf3 chromodomain interaction with methylated H3-K36 links histone deacetylation to Pol II elongation. Mol Cell, 2005. 20(6): p. 971-978.

49. Keogh, M.C., et al., Cotranscriptional Set2 methylation of histone H3 lysine 36 recruits a repressive Rpd3 complex. Cell, 2005. 123(4): p. 593-605.

50. King, O.N., et al., Quantitative high-throughput screening identifies 8-hydroxyquinolines as cell-active histone demethylase inhibitors. PLoS One, 2010. 5(11): p. e15535.

51. Luo, X., et al., A selective inhibitor and probe of the cellular functions of Jumonji C domain-containing histone demethylases. J Am Chem Soc, 2011. 133(24): p. 9451-6.

52. Rose, N.R., et al., Inhibitor scaffolds for 2-oxoglutarate-dependent histone lysine demethylases. J Med Chem, 2008. 51(22): p. 7053-6.

53. Rose, N.R., et al., Selective inhibitors of the JMJD2 histone demethylases: combined nondenaturing mass spectrometric screening and crystallographic approaches. J Med Chem, 2010. 53(4): p. 1810-8.

54. Thalhammer, A., et al., Inhibition of the histone demethylase JMJD2E by 3-substituted pyridine 2,4-dicarboxylates. Org Biomol Chem, 2011. 9(1): p. 127-35.

55. Woon, E.C., et al., Linking of 2-oxoglutarate and substrate binding sites enables potent and highly selective inhibition of JmjC histone demethylases. Angew Chem Int Ed Engl, 2012. 51(7): p. 1631-4.

APPENDIX A

METHYLATION STATE SPECIFICITY STUDIES USING JMJD2A AND JMJD2D

In addition to displaying striking variations in site specificities, the JMJD2 enzymes are also an ideal model system to study methylation state specificities. JMJD2A, JMJD2B and JMJD2C can demethylate trimethylated lysines and exhibit weak activity for dimethylated lysines [1]. JMJD2D on the other hand is highly efficient in demethylating both tri and dimethylated lysine. Similar to methylation sites, different methylation states can also signal for diverse genomic functions. A genome wide high resolution ChIP-seq analysis revealed that H3K9me3 and H3K9me2 are highly prevalent in heterochromatin regions while H3K9me1 was reported to be abundant in active promoters near the Transcription Start Sites (TSS) [2]. In addition, H3K9 monomethylation is prevalent in the cytosolic histones [3] and its subsequent methylation to H3K9me3 in the nucleus is vital for the formation of heterochromatin [4]. The mechanisms of state specific demethylation by JMJD2 KDMs have not been studied in detail. Using JMJD2A and JMJD2D, we performed structure-function analysis on active site residues (JMJD2A_Ser288 and JMJD2D_Ala292) to understand the molecular basis of state specific demethylation and explore the role of the unconventional carbon–oxygen (CH•••O) hydrogen bonds formed by JMJD2A_Tyr177 in substrate recognition and catalysis. Our studies provide a fundamental understanding of how JMJD2 KDMs achieve methylation state specificity and these mechanisms most likely hold true for other families of JmjC KDMs.

MATERIALS AND METHODS

Cloning, Expression and Purification of JMJD2A and JMJD2D Mutants

Mutations in JMJD2A Ser288 and JMJD2D Ala292 were made using the Quikchange Mutagenensis method (Stratagene) [Primer sequences are listed in Table A.1]. The mutations were verified by DNA sequencing and the Strep(II) tagged JMJD2A and JMJD2D mutants were purified as described in Chapter 2.

Incorporation of para-aminophenylalanine (pAF) in JMJD2A

The unnatural amino acid pAF was incorporated in JMJD2A using a modified version of the protocol reported by Hammill et al [5]. This method is based on the amber stop codon (TAG) encoded genetic incorporation of pAF. BL-21 AI cells (Invitrogen) were double transformed with 1.5µl each of two plasmids- the first was a plasmid encoding Strep(II) tagged (or his tagged for crystallography) JMJD2A in which the codon for Tyr177 was mutated to an amber stop codon by Quikchange mutagenesis (see Table A.1 for primer sequences); the second plasmid was a pDule2-pAF vector that encodes the tRNA synthetase for pAF incorporation [5]. The double transformation reaction was plated on Ampicillin (for the Strep(II) vector) and Spectinomycin (for the pDule2-pAF vector) agar plates. After 24 h, the double transformants were grown in 150ml of 2XYT media supplemented with 0.1% glucose, 100 µg/ml Ampicillin and 100 µg/ml spectinomycin. When the OD of the starter culture was ~1, 10 ml was transferred to 500 ml 2XYT media supplemented with the same reagents as mentioned above and the cells were grown at 37ºC until the OD reached 0.3-0.4. Subsequently, the temperature was reduced to 18ºC. After 30 min (when the temperature of the shaker was ~ 20ºC), Arabinose and IPTG were added to the media to a final concentration of 0.2% and 1 mM respectively. 30 min after the

Table A.1: Primer sequences for Site-Directed Mutagenesis of JMJD2A and JMJD2D

MUTANT	[a]PRIMER SEQUENCE FROM 5' to 3'
JMJD2A_S288A	GGTTTTAACTGTGCGGAGGCCACCAATTTTGCTACCCGTCGGTGG
JMJD2A_S288V	GGTTTTAACTGTGCGGAGGTTACCAATTTTGCTACCCGTCGGTGG
JMJD2A_S288T	GGTTTTAACTGTGCGGAGACTACCAATTTTGCTACCCGTCGGTGG
JMJD2A_S288C	GGTTTTAACTGTGCGGAGTGTACCAATTTTGCTACCCGTCGGTGG
JMJD2A_Y177Amber	GGTGTGAACACCCCATACCTGTAGTTTGGCATGTGGAAGACATCCTTTGC
JMJD2D_A292S	CCATGGTTTCAACTGCGCAGAGTCCATCAATTTTGCCACTCCGCG

[a]Listed in the table is the forward primer. The reverse complement of these sequences were used as the reverse primer. Mutation in the codon is highlighted in yellow.

addition of IPTG and arabinose, 1 mM (final concentration) pAF was added to the media (pAF was dissolved freshly in autoclaved water and used immediately in the culture). Protein expression was allowed to continue for ~48 h (Figure A.1). Cells were centrifuged and the pellets were suspended in 100 mM Tris (pH 7.5) and 500 mM NaCl and stored at -20ºC. Strep-Tactin affinity purification (for enzyme assays) or Ni(II) affinity purification (for crystallography) was performed as described in Chapters 2 and 3 respectively. The protein expression levels and hence the yield were much lower in the His-tagged JMJD2A Y177pAF and protein samples from multiple purifications (at least 3) were used for setting up crystallization trials.

Crystallization and Structure Determination of JMJD2A_Y177pAF

Crystallization trails were performed as described in Chapter 3. The crystallization mix was prepared with 7 mg/ml protein and 1 mM 2-OG. Initial hits were obtained in the PEGs I screen (Qiagen) where a number of conditions containing different salts and PEG 3350 produced crystals. Rod-clusters from the condition 0.2M sodium fluoride and 20% PEG 3350 were crushed in the 96 well plate and used directly for streak seeding using the hanging drop method. Seeding into the condition 0.3M sodium fluoride and 14% PEG 3350 resulted in the formation of rod clusters and a few individual rods (Figure A.2). These crystals were harvested by serial transfer into the crystallization solution supplemented with 5%, 15% and 25% 1,2-propanediol and subsequently flash frozen in liquid nitrogen. Diffraction data were collected at the Life Sciences-Collaborative Access Team (LS-CAT) beamline 21-ID-G at the Advanced Photon Source Synchrotron (Argonne, IL). The JMJD2A_Y177pAF crystals diffracted to 3.2 Å and the crystallographic statistics are listed in Table A.2. Although 2-OG was added during

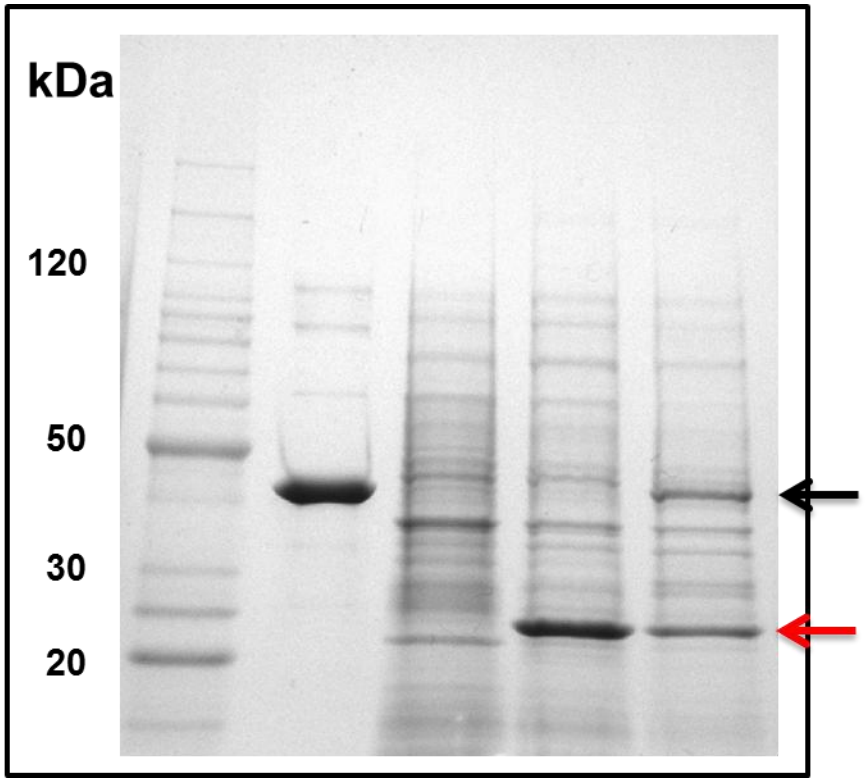

Figure A.1; Expression analysis of JMJD2A_Y177pAF. Lane 1: Molecular weight standards; Lane 2: Strep(II) tagged JMJD2A (WT); Lane 3: Uninduced culture; Lane 4: Culture induced with IPTG; Lane 5: Culture induced with IPTG and pAF for 48 h. Black and red arrows indicate full length and truncated protein respectively.

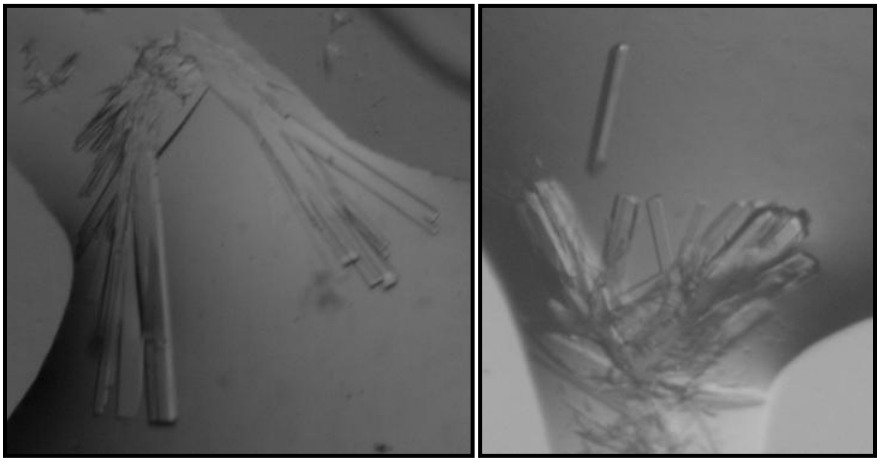

Figure A.2: Crystals of JMJD2A_Y177pAF obtained by streak seeding. These crystals were obtained using 0.3M sodium fluoride and 14% PEG 3350.

Table A.2: Crystallographic Data and Refinement Statistics of JMJD2A_Y177pAF

		JMJD2A_Y177pAF
Data Collection		
Beamline		APS 21-ID-G
Wavelength (Å)		0.9786
Space Group		$P2_12_12$
Cell Dimensions *a*,*b*,*c* (Å)		101.0, 148.9, 57.34
Resolution Range (Å)[a]		83.6-3.25 (3.36-3.25)
$I/\sigma I$ [a]		20.7 (6.87)
Completeness (%)[a]		99.75 (97.77)
Refinement & Validation[b]		
No. of Reflections		13,469
No. of Atoms		5392
Protein Atoms		5344
Ligand Atoms		4
Solvent Atoms		44
R_{work}/R_{free} [c]		0.20/ 0.30
B-factors (Å^2)		
Overall		45.3
Protein		45.4
Ligands		34.0
Waters		30.0
Root mean square deviation		
Bond Length (Å)		0.012
Bond Angles (°)		1.36
MolProbity Scores		
Clashscore (all atoms)[d]		16.12 (97th percentile N=37)
Molprobity Score		2.7 (94th percentile N=1581)
Resolution Range (Å)		3.25 ± 0.25
Ramachandran		
Favored (%)		94.4
Allowed (%)		5.2
Outliers (%)		0.4

[a] Values in parentheses correspond to the highest-resolution shell. [b] Structures were refined in Refmac [6] using overall temperature-factor refinement [c] $R_{work} = \Sigma \, ||F_o|-|F_c|| \, / \, \Sigma \, |F_o|$; R_{free} = 5% of the total reflections. [d] Clashscore is the number of serious steric overlaps (> 0.4 Å) per 1000 atoms.

crystallization, there was no discernible electron density for 2-OG in our structure. Data was processed and scaled using HKL2000 [7]. Molecular replacement was performed using MOLREP [8] with a JMJD2A structure (PDB entry: 2Q8C) used as the search model. Model building and refinement were conducted using Coot and Refmac, respectively [6, 9]. There was significant deviation between the R_{work} and R_{free} values (Table A.2) potentially due to the poor data quality and model bias. Refinement was done using overall B factors. After refinement, structures were validated using MOLPROBITY [10]. Structural figures were rendered using PyMOL (Schrödinger, LLC).

Histone Substrate Peptides and FDH-Coupled Demethylase Assay

Tri-, di- and monomethylated histone H3 peptide substrates used in the kinetic analyses of JMJD2A and JMJD2D and the various mutants were purchased from Anaspec Inc., and were purified with a chloride counter ion. Peptide concentrations were quantified by amino acid analysis. The FDH-coupled demethylase assay was performed as described in Chapter 2 and Chapter 4.

RESULTS

Active Site Residues Determine Methylation State Specificity

The active sites of JMJD2A and JMJD2D are highly conserved with the exception of a single amino acid difference. In JMJD2A, the side chain hydroxyl of Ser288 in the active site forms critical CH•••O hydrogen bonds to the substrate methyl groups (Figure A.3). These set of interactions are absent in JMJD2D where Ser288 is substituted by Ala292. This single amino acid difference between the enzymes manifests in differential state specificity among JMJD2

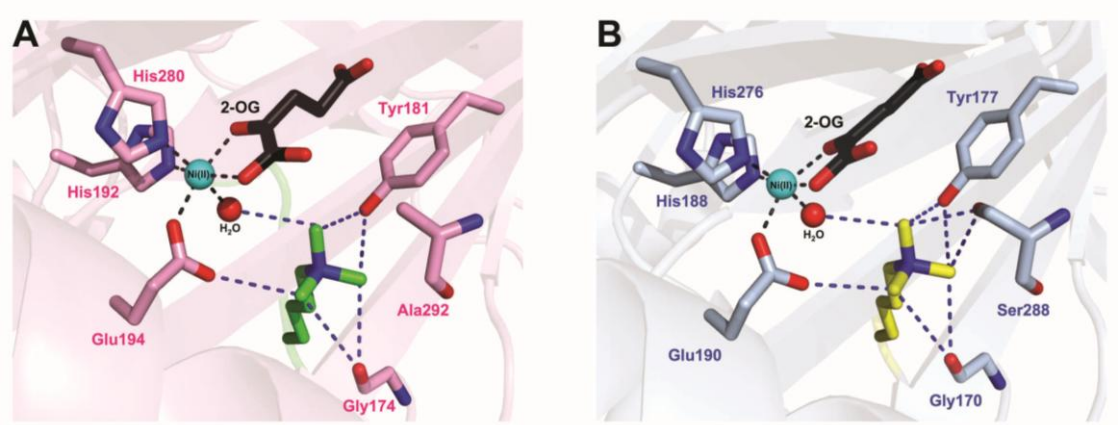

Figure A.3: Comparison of the active sites of JMJD2D and JMJD2A. Active site structures of (A) JMJD2D (pink) bound to 2-OG (black) and K9me3 in histone H3 (green) and (B) JMJD2A (blue) in complex with 2-OG and K9me3 (yellow). CH•••O hydrogen bonding between the K9me3 methyl groups and active site atoms are represented by dark blue dashed lines. Co-ordination to the active site metal (Ni(II)) is represented in black dashed lines.

enzymes. It was shown by Couture *et al.*, that an S288A mutation in JMJD2A imparted the enzyme with activity toward dimethyllysines but a A292S mutation in JMJD2D had lower catalytic activity for both tri and dimethyllysines [11]. These analyses were performed using Ni(II) column purified enzymes and reported very low turnover numbers. We performed kinetic analysis on Strep-Tactin column purified JMJD2A_S288A and JMJD2D_A292S mutants. We observed a similar change in substrate specificity in JMJD2A albeit with much higher turnover numbers (Figure A.4 and Table A.3). The JMJD2A_S288A mutant displayed a 10-fold increase in catalytic efficiency for H3K9me2 compared to WT JMJD2A. Similar to previous reports by Couture *et al* [11], a JMJD2D_A292S mutant had a 10-fold decrease in catalytic efficiency toward both H3K9me2 and H3K9me3. Interestingly however, for H3K9me2, the k_{cat} was reduced 10-fold while for H3K9me3, the K_m was increased by 10-fold. These results show that the active site Ala292 in JMJD2D might play different roles in the demethylation of H3K9me2 and H3K9me3. When we tested the activity of the JMJD2A_S288A and JMJD2D_A292S mutants and the WT enzymes for H3K9me1, we were unable to detect any measurable activity corroborating previous studies that the JMJD2 enzymes do not display activity toward monomethyllysines [1, 11]. To test the effects of other substitutions at JMJD2A Ser288, we mutated it to Cys, Thr and Val. Even though the mutants were stable after purification, they lacked catalytic activity toward all three methylation states suggesting that these residues sterically occlude the binding of methylated substrates (data not shown).

JMJD2A_Y177pAF is Catalytically Inactive

In addition to Ser288, Tyr177 also forms CH•••O hydrogen bonds with the substrate methyl groups (Figure A.3). To analyze the role of the CH•••O hydrogen bonds formed by this

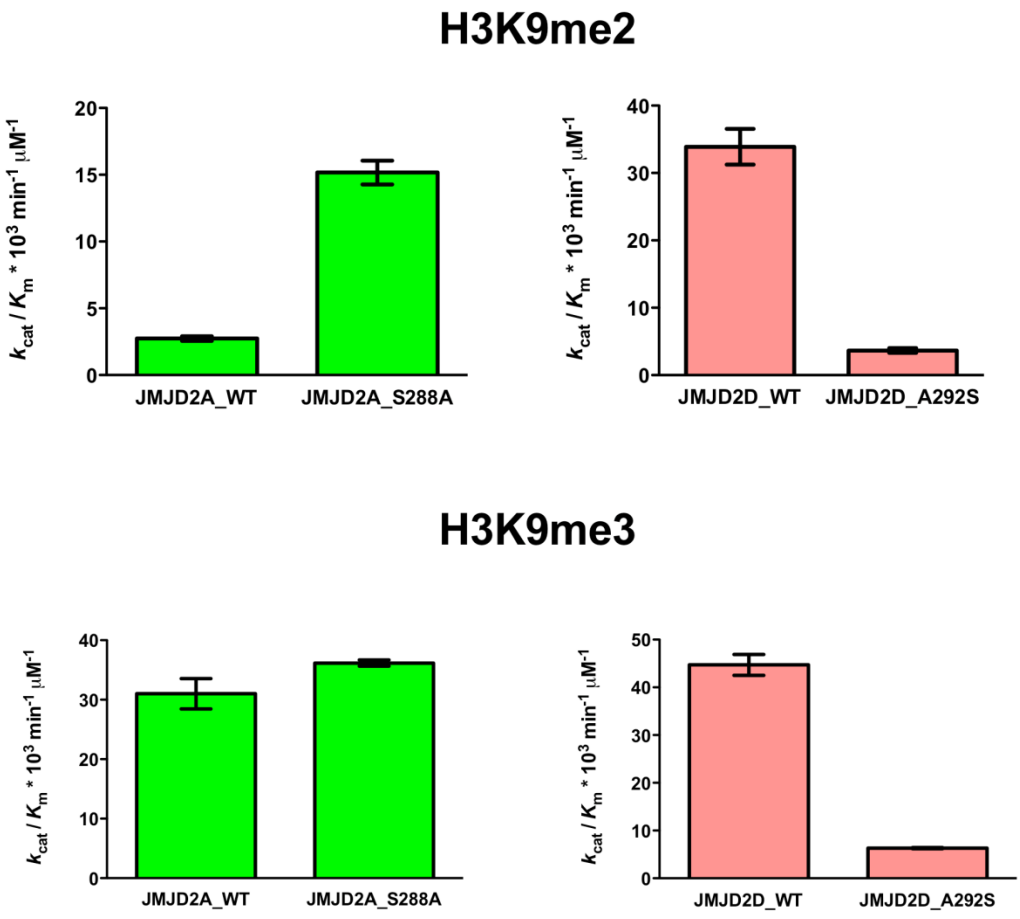

Figure A.4: Activity of JMJD2A, JMJD2D and their state specificity mutants. The kinetic parameters are listed in Table A.3.

Table A.3: Kinetic analysis of JMJD2A, JMJD2D, JMJD2A_S288A and JMJD2D_A292S with H3K9me2 and H3K9me3

H3K9me2 kinetics			
	k_{cat} **min^{-1}**	K_m **µM**	k_{cat} **/** K_m *** 10^3 min^{-1} µM^{-1}**
JMJD2A_WT	0.29 ± 0.01	110 ± 11	2.7 ± 0.3
JMJD2A_S288A	1.3 ± 0.1	83 ± 1	15 ± 1
JMJD2D_WT	1.0 ± 0.1	31 ± 5	34 ± 5
JMJD2D_A292S	0.10 ± 0.01	28 ± 3	3.7 ± 0.6
H3K9me3 kinetics			
JMJD2A_WT	1.7 ± 0.1	56 ± 9	31 ± 4
JMJD2A_S288A	1.3 ± 0.1	37 ± 3	36 ± 1
JMJD2D_WT	2.3 ± 0.2	53 ± 9	45 ± 4
JMJD2D_A292S	1.3 ± 0.1	200 ± 7	6.3 ± 0.2

No activity was detected for H3K9me1.

residue, we mutated Tyr177 to the unnatural amino acid, para-aminophenylalanine (pAF). A phenylalanine mutation at Tyr177 could potentially disrupt critical structural hydrogen bonds in addition to the active site CH•••O bonds. A pAF mutation however, would preserve the structural hydrogen bonds and hence enabled us to selectively perturb only the active site CH•••O hydrogen bonds. Our kinetic analyses of JMJD2A_Y177pAF mutant revealed that the enzyme was inactive toward H3K9me3, H3K9me2 and H3K9me1 suggesting that CH•••O bonds formed by Tyr177 are pivotal for catalysis. We also determined a 3.2 Å crystal structure of JMJD2A_Y177pAF with Ni(II) in the active site to verify that the protein was folded and the pAF substitution did not alter the structure. The mutation of Y177 to pAF resulted in no major structural deviations compared to WT JMJD2A (RMSD Cα= 0.32Å) (Figure A.5).

DISCUSSION

In contrast to methylation site specificity which is determined by residues distal to the active site, our studies reveal that the active site residues largely determine methylation state specificity of JMJD2 lysine demethylases. In particular, the active site Ser288 in JMJD2A and Ala292 in JMJD2D are the state specificity determinants which dictate the preference of different methylation states for these enzymes. Although the biochemical effects of these mutants has been explored, studying the effects of varied state specificities, in particular, the JMJD2A_S288A mutant *in vivo* would be instrumental in understanding the biological significance of state specific demethylation by JMJD2 KDMs.

Our studies on the JMJD2A_Y177pAF revealed that the CH•••O hydrogen bonds formed at this position are indispensable for catalysis. To our knowledge this is the first time, an unnatural amino acid has been incorporated in a JmjC KDM and has been biochemically and

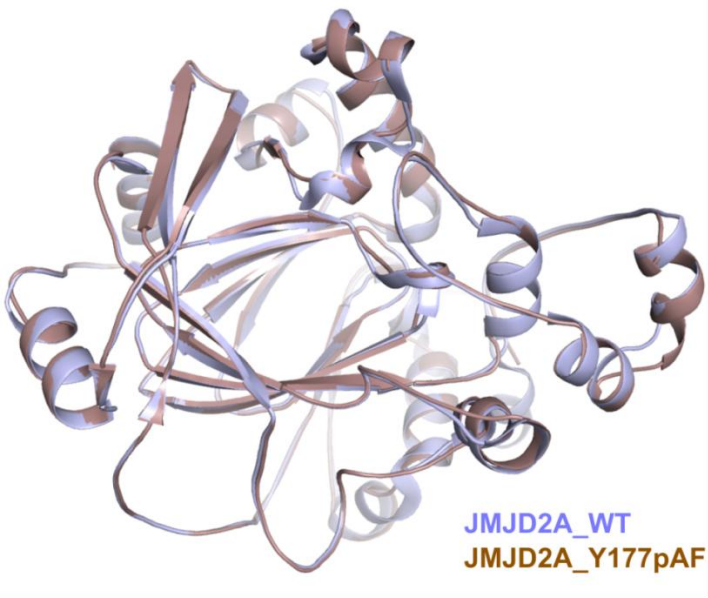

Figure A.5: Alignment of the JMJD2A_WT and JMJD2A_Y177pAF structures. Incorporation of the unnatural amino acid pAF at position 177 did not result in major structural deviations compared to the wild type enzyme (RMSD Cα=0.3Å).

structurally characterized. These studies open the platform for the use of unnatural amino acids as viable tools to understanding the biochemical and physiological functions of these enzymes.

ACKNOWLEDGEMENTS

I thank Dr. Henriette Remmer for assistance in peptide ordering. I thank Scott Horowitz for cloning pDule2-pAF and Rob Fick for cloning JMJD2D_A292S and performing the kinetic analysis of JMJD2A_Y177pAF.

REFERENCES

1. Whetstine, J.R., et al., Reversal of histone lysine trimethylation by the JMJD2 family of histone demethylases. Cell, 2006. 125(3): p. 467-81.

2. Barski, A., et al., High-resolution profiling of histone methylations in the human genome. Cell, 2007. 129(4): p. 823-37.

3. Campos, E.I., et al., The program for processing newly synthesized histones H3.1 and H4. Nat Struct Mol Biol, 2010. 17(11): p. 1343-51.

4. Pinheiro, I., et al., Prdm3 and Prdm16 are H3K9me1 Methyltransferases Required for Mammalian Heterochromatin Integrity. Cell, 2012. 150(5): p. 948-60.

5. Hammill, J.T., et al., Preparation of site-specifically labeled fluorinated proteins for 19F-NMR structural characterization. Nat Protoc, 2007. 2(10): p. 2601-7.

6. Murshudov, G.N., A.A. Vagin, and E.J. Dodson, Refinement of macromolecular structures by the maximum-likelihood method. Acta Crystallographica Section D-Biological Crystallography, 1997. 53: p. 240-255.

7. Otwinowski, Z. and W. Minor, Processing of X-ray diffraction data collected in oscillation mode. Macromolecular Crystallography, Pt A, 1997. 276: p. 307-326.

8. Vagin, A. and A. Teplyakov, MOLREP: an automated program for molecular replacement. Journal of Applied Crystallography, 1997. 30: p. 1022-1025.

9. Emsley, P. and K. Cowtan, Coot: model-building tools for molecular graphics. Acta Crystallographica Section D-Biological Crystallography, 2004. 60: p. 2126-2132.

10. Chen, V.B., et al., MolProbity: all-atom structure validation for macromolecular crystallography. Acta Crystallographica Section D-Biological Crystallography, 2010. 66: p. 12-21.

11. Couture, J.F., et al., Specificity and mechanism of JMJD2A, a trimethyllysine-specific histone demethylase. Nat Struct Mol Biol, 2007. 14(8): p. 689-95.